Plasma versus thermal activation of the Phillips catalyst

Victoria Jane Ruddick

PLASMA VERSUS THERMAL ACTIVATION OF THE PHILLIPS CATALYST

Ph.D. Thesis

by

Victoria Jane Ruddick

University of Durham

Department of Chemistry

1996

For Mum and Dad

Statement of Copyright

Declaration

The work described in this thesis was carried out in the Chemistry Department at the University of Durham between October 1993 and September 1996. It is the original work of the author except where otherwise acknowledged, and has not been submitted previously for a degree at this or any other University.

Publication

The results from this work have been published as follows:

Ruddick, V.J.; Dyer, P.W.; Bell, G.; Gibson, V.C.G.; Badyal, J.P.S. *J. Phys. Chem.* **1996**, *100*, 11062.

Acknowledgements

I would like to thank my supervisor, Prof. J.P.S. Badyal, for his continued support and encouragement throughout the preparation of this thesis. Many thanks also to my colleagues in CG98, both past and present, for all the laughs, the Friday evenings and "intellectual discussions". A special thank you goes to Sam for all the proof-reading and criticism during the final thesis preparation - I'll leave you my address for next year!

I would like to thank Crosfield Limited for providing the catalyst precursors used in the work reported here, particularly Bob Parker for his helpful discussions.

There are many people in the chemistry department without whom none of this work would have been possible. In particular the glassblowers, Ray and Gordon, thanks for all the repairs and for not laughing at my drawings. Thanks also to Neil and Jim in the mechanical workshop, and to Kelvin and Barry in the electrical workshop. George Rowe needs a special thank you for all the hours spent studying the electronics of my mass spec. and plasma reactors.

Thank you Angela for giving me a home, helping me to wind down in the evenings, and of course for all the shopping trips! Thank you also to Mum and Dad for all your support throughout the last six years. Finally, thank you Ian for being so patient, for all the weekend "holidays" and for continuing to believe in me, even when I didn't believe in myself.

Abstract

Silica supported chromium oxide catalysts, known as Phillips catalysts, are used in the production of over 40% of the world's high-density polyethylene. The original catalyst comprised CrO_3 impregnated onto silica. Due to the carcinogenic nature of chromium(VI), chromium(III) catalyst precursors which are oxidised during calcination are now preferred. Two such precursors have been employed throughout the studies reported in this thesis; one is prepared by the aqueous impregnation of a silica support with basic chromium(III) acetate, whilst the other comprises a dry-blended mixture of chromium(III) acetylacetonate with silica.

Calcination of the two precursors has been studied using a combination of temperature-programmed quadrupole mass spectrometry and infrared spectroscopy. The chromium(III) acetylacetonate precursor is postulated to disperse near its melting point and react via an acetate intermediate. Both precursors may therefore be expected to produce the same catalyst following calcination. The study of subsequent CO reduction of these calcined catalysts by quadrupole mass spectrometry supports this observation. The reduction is found to proceed via a Langmuir-Hinshelwood mechanism, both precursors demonstrating the same behaviour. Activation energies for the catalyst reduction have been determined from the corresponding Arrhenius plots.

Quadrupole mass spectrometry techniques have identified 1-hexene production during the early stages of polymerization using the CO reduced catalysts. This indicates the formation of a chromacyclopentane intermediate species which may also be involved in the initiation of polymerization.

The continuous fragmentation of the catalyst support and polymer growth have been investigated using contact mode and phase-imaging atomic force microscopy.

Non-equilibrium plasma oxidation of the two catalyst precursors has been studied by quadrupole mass spectrometry. An active catalyst is obtained from the chromium(III) acetate catalyst, however the dry-blended chromium(III) acetylacetonate precursor is unable to achieve the dispersion required, and the oxidised species are inactive for ethylene polymerization.

CONTENTS

CHAPTER 1.

CHAPTER 1. AN INTRODUCTION TO ETHYLENE POLYMERIZATION CATALYSTS, ANALYTICAL TECHNIQUES AND NON-EQUILIBRIUM PLASMAS

1.1 Polyethylene

There are three major classes of polyethylene, each of which is prepared in a different way to produce polymer with varying extents of chain branching, which in turn has a major effect on the polymer properties. The three grades all contain the same repeat unit, $(-CH_2-CH_2-)$, and are known as low density polyethylene (LDPE), linear low density polyethylene (LLDPE) and high density polyethylene (HDPE). A comparison of these three grades is shown in Table 1.[1,2]

Property	LDPE	LLDPE	HDPE
Melting Point (K)	383	393-403	>403
Density (g/cm^3)	0.92	0.92-0.94	0.94-0.97
Film tensile strength (MPa)	24	37	43
Uses	Packaging films, wire and cable coverings	Film blowing and casting applications	Bottles, crates, pipes and fittings, toys

Table 1: A comparison of the properties of LDPE, LLDPE and HDPE, and some uses of these materials.

Increasing the polymer density increases stiffness, tensile strength, hardness, heat and chemical resistance, opacity and barrier properties, but also decreases impact strength and stress-crack resistance.[1]

1.1.1 Low Density Polyethylene (LDPE)

Low density polyethylene is a highly branched polymer, with approximately 60 branch points per 1000 carbon atoms.[2] It is manufactured by a high pressure, radical initiated process and has a high amorphous content (crystallinity can be as low as 50%).[1] The excellent film-forming properties which are demonstrated by LDPE have meant that its largest application is as a film for packaging and cable coatings. The more amorphous nature of LDPE leads to a relatively higher gas permeability than that demonstrated by HDPE.[2]

1.1.2 High Density Polyethylene (HDPE)

High density polyethylene is prepared by Ziegler-Natta or supported-metal-oxide catalysed chain polymerization. The catalyst systems are described in section 1.2. The resulting polymer chains are structurally regular, possessing very few branch points (< 7 per 1000 carbon atoms).[2] This enables efficient packing of the polymer chains to give a highly crystalline material (up to 90% crystallinity),[1] with a corresponding high density.

1.1.3 Linear Low Density Polyethylene (LLDPE)

The property gap between LDPE and HDPE has been filled by LLDPE. It may be prepared using solution- or gas-phase processes, and is now used to replace blends of HDPE and LDPE. LLDPE is actually a copolymer of ethylene with 8-10 % of an α-olefin such as 1-butene, 1-pentene, 1-hexene or 1-octene. This allows the manufacturer to control the number of short chain branches, and hence the polymer density, by controlling the amount and type of co-monomer.[2] For example, incorporation of 1-octene will produce a lower density product than 1-butene incorporation, since the longer (hexyl) branch in the former will push the chains further apart than the ethyl branch of the latter, hence lowering the packing efficiency of the chains.

1.2 Alkene Polymerization Catalysts

Two major groups of catalysts are responsible for the production of high density polyethylene: Ziegler-Natta catalysts and supported transition metal catalysts.[3] Both classes of catalyst are capable of producing a range of polymer products with well defined properties depending upon the exact catalyst and conditions employed.

1.2.1 Ziegler-Natta Catalysts

Ziegler-Natta catalysts comprise mixtures of a base metal alkyl promoter and a group IV to VIII metal salt,[4, 5] although a small number may work in the absence of a promoter. The promoter creates the active species, thought to be a cationic transition metal salt,[6] by alkylation, ligand abstraction and counter-ion complexation. Reactions are performed under inert conditions in an inert solvent or diluent.[5] Ziegler-Natta catalysts may be further classified as heterogeneous or homogeneous depending upon whether the active site formed by reaction of the two components is present as an insoluble precipitate or is itself soluble in the reaction medium used.

The accepted polymerization mechanism was first suggested by Cossee,[7] and involves the coordination of the alkene across its double bond to the vacant metal site, followed by a migratory insertion step with the growing polymer chain to generate another vacant site. This is repeated until termination occurs either by spontaneous β-elimination, or by the addition of hydrogen to the system, which allows control of the molecular weight distribution of the resulting polymer.

1.2.1.1 Heterogeneous Ziegler-Natta Catalysts

The best known example of this type of catalyst is probably $TiCl_3/Et_2AlCl$, which demonstrates high ethylene polymerization activity at 25°C and 1 atm.[6] Thermal polymerization, which was the only method available for the production of polyethylene prior to the discovery of these catalysts, required much harsher

conditions (200°C, 1000 atm.) and produced highly branched polymer.[6] Ziegler-Natta catalysts generally form highly linear polymer products.[4, 8, 9] In the polymerization of propene and higher α-alkenes or dienes, many insoluble combinations of metal alkyls and transition metal salts exhibit stereospecific control; therefore, by careful selection of catalyst and solvent, it is possible to produce either highly isotactic or syndiotactic polymer.[4-6, 8, 9]

1.2.1.2 Homogeneous Ziegler-Natta Catalysts

Although soluble catalysts are nominally classed as homogeneous, the polymer formed is very often, if not always, precipitated as it forms. This means that the system is not truly homogeneous.[10] Current interest appears to be centered around soluble metallocene catalysts. This interest was fuelled in the early 1980's by the discovery that catalysts such as Cp_2ZrMe_2 or Cp_2ZrCl_2 in toluene solution could be activated by an excess of methylaluminoxane (MAO) to produce polyethylene with activities greater than 25 x 10^6 g PE (g Zr)$^{-1}$ hr^{-1}.[5, 11] Polyethylene produced using these zirconocene/MAO catalysts shows relatively narrow molecular weight distributions with respect to heterogeneous systems.[10] The MAO must be present in excess ([Al]:[Metallocene] = 500-10000) and has a dual role - to alkylate metallocenes and create the active cationic species by abstracting and complexing the counter-ion, as well as scavenging catalyst poisons.[12] Some researchers have observed the existence of an optimum MAO concentration.[12] This has been explained by considering that at concentrations below the optimum, there is insufficient initiator to scavenge Lewis base impurities and to convert all of the metallocenes to active, cationic metallocenes. When neutral metallocenes remain present, the active site concentration is decreased further by complexation between neutral and cationic metallocenes. At concentrations above the optimum, oligomers of aluminoxane which are free of trimethylaluminium compete with the alkene for the vacant site by coordination via alkyl groups or oxygen.

Only atactic polypropene is formed using non-chiral metallocenes such as Cp_2TiCl_2; however, the use of cyclopentadienyl-based indenyl ligands allows the

formation of chiral metallocene catalysts.[5] Using stable chiral transition metal compounds, isotactic polypropene may be prepared in homogeneous systems.[3, 5, 10]

1.2.2 Supported Catalysts

Supported catalysts are highly active for the polymerization of ethylene. There are two broad families of supported catalysts:[13] using a) organometallic catalysts, and b) Phillips catalysts. Suitable supports for both types of catalyst include silica, alumina, aluminophosphates or silica-titania.[13]

1.2.2.1 Organometallic Catalysts

This family of catalysts is prepared by dehydrating a high surface area support material and then anhydrously depositing an organometallic compound onto it. There has been considerable interest in supporting metallocene catalysts to prepare alkene polymerization catalysts, since heterogeneous metallocene catalysts have been shown to have many advantages over the corresponding homogeneous catalysts,[14] including significantly decreasing the optimal methylaluminoxane/metallocene ratio.[15] Recently, aluminoxane incorporation into the support has been proposed, with polymethylaluminoxane-treated silica[16] and cyclodextrin[17] being successfully used as supports for metallocene polymerization catalysts.

Supported organochromium complexes show particularly high activity, and have been known for some time. Suitable organochromium compounds include chromocene,[13, 18, 19, 20] bis(arene)-chromium(0), allyl-chromium(II) or -chromium(III) and various alkyls of chromium(II) and chromium(IV).[13]

Chromocene is thought to react with surface hydroxyl groups on the support and to lose a cyclopentadienyl (Cp) ligand to form the active site, a CpCr complex.[18] The catalysts formed are highly active for ethylene polymerization, but are not very thermally stable.[13, 19] At temperatures below 363 K, the catalysts demonstrate a high chain-transfer response to hydrogen and form linear, highly saturated polyethylene containing terminal methyl groups with relatively narrow

molecular weight distributions. Above 363 K, removal of the remaining ligand will occur, leading to a reduced activity catalyst which forms polymer with an increasing vinyl content with temperature.[19]

1.2.2.2 Phillips Catalysts

Industrially, the Phillips catalyst is used exclusively to make high-density polyethylene, although comonomers are occasionally incorporated in order to reduce the crystallinity of polymers formed.[4] The catalyst is responsible for the production of approximately 40% of the worlds HDPE,[13] the remainder being formed using the methods discussed previously.

It was almost by accident that Hogan and Banks of the Phillips Petroleum company discovered this commercially important catalyst in the early 1950's.[21] They were attempting to improve upon an earlier discovery at Phillips that ethylene could be converted to liquid fuels by passage over a nickel oxide-silica-alumina catalyst.[4, 22, 23] In an effort to reduce the 1-butene formation by replacing NiO with CrO_3, they found that their catalyst beds became blocked by a white powder.[4, 13, 23] The system was developed into a commercial process within five years,[23] and has been operating and diversifying ever since.

The Phillips catalyst is prepared by the impregnation or dry-blending of a wide-pore, high surface area oxide support with a chromium compound and then calcining to 673-1073 K under a dry oxygen or air atmosphere. Originally CrO_3 was impregnated onto a wide-pore silica;[21] however the chromium may take almost any form, and more recently trivalent chromium salts are preferred due to the carcinogenic nature of Cr(VI). Following calcination these catalysts appear to be identical regardless of the nature of the chromium species adsorbed on the support during preparation of the precursor.[24] Calcination leaves hexavalent chromium monodispersed on the surface of the support in the form of chromate or dichromate esters.[25] Many studies have been performed in attempts to verify the precise nature of these species,[25-29] and the indications are that, at chromium loadings below 5%, the chromium species are initially bound to the support as chromate esters. Increasing the activation temperature brings about a conversion to dichromate or even polychromate species. This calcination procedure is

remarkable since, in the absence of the support, bulk CrO_3 decomposes above 473 K to form Cr_2O_3 and O_2.[25] The stabilization of the chromium species by the support is possible up to loadings of 5 wt%, above which Cr_2O_3 crystallites are observed upon calcination.[30, 31] In order to avoid this decomposition, catalyst precursors are usually prepared with a chromium loading of 1 wt%.[25]

The hexavalent catalyst resulting from the calcination procedure outlined above demonstrates a dormant period upon exposure to ethylene at the polymerization temperature, after which polyethylene production begins. The dormant period is believed to be due to reduction of the hexavalent chromium species to a lower, active oxidation state. The nature of this active species is, however, the subject of much debate, with every valence from 2+ to 6+ having been proposed over the years.[25] The observation that only a small percentage of the chromium is involved in the active centres (estimates vary from between 3.2-7.3%[32] to between 6 and 30%[33]) has not helped, since it means that the direct observation of a particular oxidation state is not enough to say that it is an active valence.

The majority of the early work performed to address the question of the active site concentrated on the study of a γ-phase resonance ESR signal which was attributed to a Cr^{5+} species.[25, 34, 35] This signal was very weak and some researchers even argued that it was due to a combination of Cr^{6+} and Cr^{3+}.[36]

Direct evidence has been obtained to show Cr^{2+} as an active valence. Reduction of the hexavalent catalyst with CO at 623 K leads to a quantitative reduction of the Cr^{6+} to Cr^{2+} species.[37] The resulting catalyst polymerizes ethylene (with no induction period) to produce polymer possessing virtually identical properties to that formed by direct reaction of ethylene with the Cr^{6+} catalyst.[25] This is a very strong endorsement for Cr^{2+} being an active valence since the polymer properties are strongly dependent on the catalyst pretreatment. The reaction of ethylene with supported hexavalent catalyst has also been observed to yield Cr^{2+} in a concerted process during which formaldehyde is formed.[38] Evidence of Cr^{2+} species has also been obtained by XPS following reduction by either CO or ethylene.[39] It should be noted that when the active valence is discussed, this is the valence prior to alkylation since the formal

oxidation state may be altered by the addition of ethylene, as observed by UV-Vis diffuse reflectance spectroscopy.[40] The issue has been further complicated by IR studies which have shown the presence of a variety of Cr(II) species on the surface of the catalyst, some of which are claimed to be active and others which are not.[41-45] These different species may be mononuclear or dinuclear, differing only in their degree of coordinative unsaturation, and are given the labels Cr(II)-A, Cr(II)-B and Cr(II)-C.

Despite the direct evidence of Cr(II), the controversy has not ended. Trivalent catalysts have been prepared by the impregnation of chromium(III) salts such as $CrCl_3$ onto silica and calcining under vacuum,[46] which are claimed to demonstrate a higher activity than the Cr(II) catalysts.[41, 42] Of course it is possible that there are a variety of active species, and no one particular valence is responsible for the polymerization activity of the Phillips catalyst.

Polymerization may be performed using any one of three processes: solution, slurry or gas phase. The solution phase polymerization route was the first to be commercialized,[47] and uses a hydrocarbon solvent at 398-443 K which dissolves the polyethylene as it is formed.[25] The variation of reaction temperature allows control of the polymer melt index;[47, 48] however the requirement of solvent evaporation by this route means that the energy consumption is quite high.

The slurry polymerization is used commercially in a system known as the Phillips particle-form process.[47, 48] A poor solvent is used at temperatures between 333 and 383 K in order that the polymer does not swell or dissolve.[25] The liquid phase acts as a heat transfer agent and allows efficient monomer transport to the catalyst particle.

The gas-phase ethylene polymerization reaction occurs at similar temperatures to those employed in the slurry polymerization.[25, 49] A bed of catalyst is fluidized by ethylene which usually contains an inert gas to improve the heat transfer efficiency.[49] The absence of any liquid phase means that the gas-phase process is not constrained by solubility and viscosity, and can produce polymer with a wide range of melt-indexes.[49]

The mechanism of ethylene polymerization using the Phillips catalyst is the subject of yet more controversy. Numerous suggestions have been put forward

over the years, but there is still no one accepted route. This subject is discussed in chapter 4.

The diversity of the Phillips catalyst has contributed greatly to its continued success. Polymer properties are strongly dependent upon the precise conditions used for the catalyst activation, as well as the composition and structure of the catalyst support and the overall catalyst composition.

The support material chosen for the catalyst is critical. In order to produce an active catalyst it is necessary that the support is strong enough to withstand the high temperature activation procedure, yet able to fragment and allow continued monomer access to the active sites within the pores.[50] The friability of the catalyst is strongly related to the porosity of the support material. Catalysts which have a low pore volume are unable to fragment efficiently, and therefore polymerization will cease due to the internal pores becoming blocked by polymer. On the other hand, if the support is highly porous, sintering is liable to occur during catalyst activation. The pore size distribution is also important. A variety of techniques have been used to demonstrate that optimum activity is obtained from pores of diameters between 100 and 1000 Å.[25]

There is a very strong connection between the porosity of Phillips catalysts and the molecular weight of polyethylene formed using them. As the average pore diameter of the support is increased, the polymer formed using identical activation and polymerization conditions demonstrates decreasing molecular weight.[25] This observation is opposite to that expected, and has not been fully explained. The polymer molecular weight is also strongly influenced by the catalyst activation temperature. Increasing the activation temperature both increases the catalyst activity and decreases the molecular weight of the polymer formed up to ~1073 K, where silica support materials sinter. This phenomenon has been explained as being a result of the degree of dehydroxylation of the support material.[50] Above 1073 K, the activity decreases and the molecular weight of the polymer formed increases, probably due to the decrease in pore volume caused by sintering of the support.[47]

The properties of polyethylene formed using the Phillips catalyst are strongly influenced by the chemical composition of the catalyst. The incorporation of various modifying species including titanium,[25, 51-55] magnesium,[51]

or aluminium,[56-58] has been reported to have a promotional effect on the activity of the catalyst, whilst influencing properties such as the molecular weight distribution. For example, the incorporation of small amounts of titania on Cr/silica catalysts enhances both the activity and the termination rate, leading to a lower molecular weight distribution.[25] The modifiers may be added by impregnation of the catalyst precursor, or by incorporation into the support material.

An alternative method of altering the polymer properties is to substitute the silica support for another oxide. Suitable alumina supports typically contain 50-100% more hydroxyl groups than corresponding silica materials and can therefore stabilize more Cr(VI) species on their surfaces. The resulting catalysts form very high molecular weight polymer, since the termination rate is low, as is the activity compared to that of silica supported catalysts.[25] An interesting effect is seen if the chromium compound is deposited on an aluminophosphate support. Aluminophosphates are isoelectronic with silica, and catalysts prepared using them are highly active. The polymer formed always shows a bimodal molecular weight distribution, attributed to the presence of two types of chromium sites - one attached by reaction with an Al-OH bond, and the other by reaction with a P-OH bond.[13] The bimodal polymers produced by these catalysts have been found to be particularly good for film applications.

The commercial success of the Phillips catalyst owes much to its diversity and the ability to tailor the properties of the polymer formed. Many questions regarding its activity remain unanswered, despite 40 years of study. The work reported in this thesis attempts to answer some of these questions.

1.3 Mass Spectrometry

Mass spectrometry involves the separation and measurement of ions according to their mass-to charge ratio.[59-63] The sample is normally introduced as either a gas or a volatile liquid. If the sample is in the solid form it must be vapourised by, for example, heating or irradiation before ionization can occur. Ionization is commonly performed by bombarding the sample with a perpendicular beam of electrons in a process known as Electron Impact (EI).[59-63] Experience has shown that an electron beam energy of 70 eV produces a reproducible and maximised ion current, therefore this energy is routinely used.[59, 61] EI does, however, produce ions with a large excess of internal energy and causes a high extent of fragmentation, which can be problematic with some samples.[61] Alternative 'soft ionization' techniques such as chemical ionization (CI) and Fast-atom Bombardment (FAB) have been developed which fragment the ions less and can therefore provide molecular ion information when electron bombardment fails.[59, 61]

Once the ions are formed, they pass through a mass analyser which separates them on the basis of mass-to-charge. Mass analysers may be separated into three main types by the method used to separate the charged particles:[59, 61]

1) **Magnetic field deflection**

The ions are accelerated through a large potential (V) and are then fired into a magnetic field (B). A radial path of radius r, which is governed by both B and V, is then described by these particles before they are detected.

a) Single-focusing (Magnetic field only)

b) Double-focusing (An electrostatic field is introduced either before or after the magnetic field to improve the focusing of ions onto the detector. This method produces high resolution spectra.)

2) **Time of Flight (TOF)**

The ions are separated on the basis of the time taken to reach the detector. Higher masses move slower, and therefore are detected later.

3) **Quadrupole**

Here only the last of these three classes, the quadrupole mass spectrometer (QMS) will be considered.

1.3.1 The Quadrupole Mass Spectrometer

The quadrupole mass spectrometer is summarised in Figure 1.

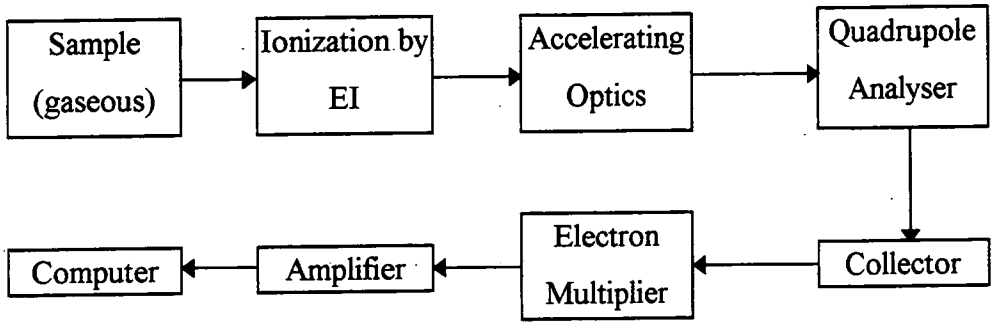

Figure 1: A Schematic Representation of the Operation of a Quadrupole Mass Spectrometer

The gas enters the spectrometer and is ionized by bombardment at right angles using an electron beam which is emitted by a hot filament (often Tungsten).[61] The positive ions produced are then accelerated by electrostatic forces between a series of slits, and focused into the quadrupole analyser.[59]

1.3.1.1 The Quadrupole Mass Analyser

The quadrupole mass analyser comprises four parallel electrically conducting rods, which have hyperbolic cylindrical surfaces described by the equation:

$$x^2 + y^2 = \pm C$$

where C is a constant and x and y are the diameters of the poles in the x and y directions respectively.[62]

A combination of dc and rf electric fields are applied to these rods.[59, 60, 62, 63] Opposite rods in the quadrupole arrangement are connected to the same potential, given by:

$$P(t) = \pm[U + V\cos(2\pi ft)]$$

where U is a dc voltage and V is the peak amplitude of a radio-frequency voltage at frequency f.[62] A potential of the opposite sign is applied to the other pair of electrodes. Under these conditions the equipotential surfaces are symmetrically hyperbolic cylinders, and the potential on the z-axis is zero.[62] This is shown schematically in Figure 2.

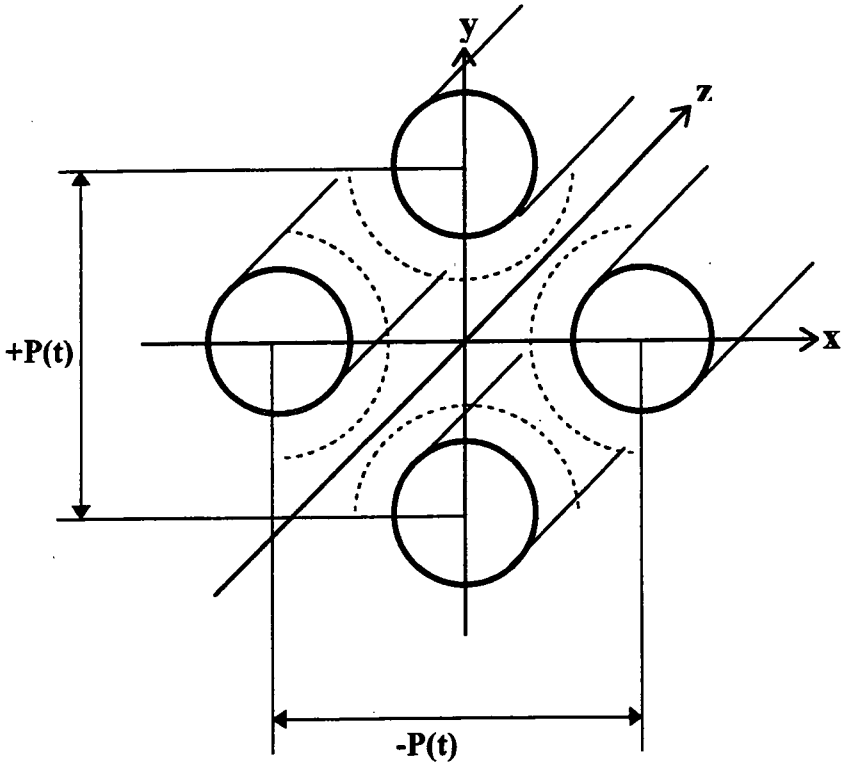

Figure 2: A Schematic Representation of a Quadrupole Mass Analyser

An ion entering the assembly with a constant velocity in the z-direction (parallel to the poles) will acquire oscillations in the x- and y-directions due to the action of the perpendicular rf and dc fields.[59, 62, 63] With proper selection of dc and rf peak voltages, ions of a given mass-to-charge ratio will have a stable trajectory, and will oscillate about the z-axis to emerge at the opposite end of the mass filter assembly for detection. Ions with other mass-to-charge ratios will have unstable oscillations, which means that they will move away from the z-axis and eventually strike an electrode or the assembly supporting structure, thus being removed from the system.[59, 62, 63]

The mass-to-charge ratio to be transmitted can be altered by either varying U or V, or by changing f. Keeping the ratio between U and V constant will mean that the resolution of the quadrupole remains constant, as may be seen by:[62]

$$m/\Delta m = 0.126/(0.16784-U/V)$$

From this equation, it can be seen that (a) infinite resolution is, in theory at least, possible by fixing U/V at 0.16784; and (b) the resolution can be changed by variations in U/V. In practice most systems operate by keeping f constant, and simultaneously varying U and V.[62]

Since the operation of the quadrupole mass filter is dependent on very precise rf and dc fields along its entire length, for good resolution both stable applied voltages and a high degree of dimensional precision are necessary. The dimensional precision may be achieved more readily if the hyperbolic cylinders are replaced by circular cylindrical rods; therefore most mass filters are designed and manufactured in this way. If the radius of the cylindrical rods is 1.145 times the radius of the circle inscribed by the poles, a good approximation of the ideal hyperbolic field is achieved.[62]

Quadrupole mass analysers have the advantage of passing positive and negative ions simultaneously. The paths of these ions are identical except for the direction of rotation for any given magnitude of m/e, therefore ions of both polarities may be monitored with near simultaneity by appropriate source voltage switching and the use of a dual detector system.[63]

1.3.1.2 Detection Systems

After passing through the quadrupole mass analyser, ions are most commonly detected using a standard electron multiplier. These are secondary electron multipliers containing a series of dynodes. The positive or negative ions are accelerated into the surface of the first dynode, which is held at the appropriate high voltage. The impact releases several electrons which then initiate a cascade. This is amplified through the multiplier to yield a measurable current which is taken as a signal and fed into a recorder or a data system.[63]

1.4 Infrared Spectroscopy

Infrared radiation refers to the region of the electromagnetic spectrum between the microwave and the visible regions.[64] The region between 4000 and 400 cm^{-1} is of the most practical use, since it is absorbed by organic molecules and converted into molecular vibrational energy.[64-66] At normal temperatures the bonds within a molecule vibrate as a result of exchanges with other molecules in the immediate environment.[66, 67] The absorption of energy at the appropriate wavenumber from an IR source acts so as to increase the amplitude of these vibrations in a quantized process.[64-68] Collisions between these excited molecules and their less active neighbours dissipate the extra energy, ensuring that the system does not become saturated with energy. The quantized absorption results in spectra which consist of a series of bands rather than lines, since a single vibrational energy change is accompanied by a number of rotational energy changes.[64]

Within a bond, two types of vibration are possible: it may stretch along its axis, or it may bend. As a rule, less energy is required to bend a bond than to stretch it, therefore bending vibrations are observed at lower wavenumbers than stretching modes.[64, 66]

In a molecule containing N atoms, there are 3N degrees of freedom. Three of these degrees of freedom describe translation, and in a non-linear molecule three describe rotation leaving 3N-6 vibrational degrees of freedom.

Linear molecules have 3N-5 vibrational degrees of freedom, since they lack a rotational degree of freedom about the internuclear axis.[64, 65] These theoretical numbers of absorption frequencies are seldom observed. The number of bands observed are increased by the appearance of overtones (multiples of a given frequency) and combination tones (the sum of two other vibrations). A variety of factors serve to decrease the number of bands observed, including:[64, 66, 67]

1) The fundamental vibration does not involve a change in dipole moment. IR can only observe vibrations which lead to a rhythmical change in the dipole moment of a molecule. This is because the alternating electric field produced by the changing charge distribution accompanying such a vibration acts to couple the molecular vibration with the oscillating electric field of the electromagnetic radiation. This means that homonuclear diatomic molecules such as Cl_2 or N_2, as well as the symmetric stretches of linear molecules such as CO_2, are infrared inactive.
2) The fundamental frequency lies outside the 400 - 4000 cm^{-1} range.
3) The fundamental band is too weak to observe. Generally, a strong absorption in the IR region is related to a strong dipole moment change.
4) Fundamental vibrations are so close that they coalesce.
5) In highly symmetrical molecules, a degenerate band can be produced by several absorptions of the same frequency.

An approximation of the stretching frequency of a bond may be obtained by application of Hooke's law:[64, 66-68]

$$\nu = 1/2\pi\ (k/\mu)^{1/2}$$

where ν = frequency

k = force constant of bond

μ = reduced mass, $(M_xM_y/(M_x+M_y))$, if M_x and M_y are the masses of atoms x and y respectively.

The application of Hooke's law also allows calculation of the shift in absorption of a C-H bond following deuteration.

1.4.1 Instrumentation

In the spectrometer, light from the infrared source (a Nernst filament or rare-earth oxides) is split into a reference beam and an identical beam which passes through the sample.[64, 66, 68] If a Nernst filament is used as the radiation source, a grating monochromator is required in order to give a smooth emission in the infrared region. The sample may be a solid, liquid or vapour, but cells must be made from NaCl, KBr etc. since glasses absorb in the infrared region.[66] These cells have the disadvantage that they are easily damaged by moisture, either in the atmosphere or the sample. A solid sample may be in the form of a mull in a medium such as paraffin wax (Nujol); in solution using chloroform or carbon disulphide as solvents; or as a thin disc of sample ground up very finely with potassium bromide and compressed. This latter method has the advantage of producing a spectrum free from solvent bands.

The intensities of the reference beam and the beam which has passed through the sample are compared electronically, and a plot is produced of the percentage of light transmitted through the sample against wavenumber (or wavelength depending upon the chart paper).[64, 66, 68] This process is limited by the time taken for the pen of the recorder to scan the wavelengths.

The application of Fourier-Transform techniques overcomes this limitation by subjecting the compound to a broadband of energies, and thus electronically collecting the complete IR spectrum at each broadband pass. This technique provides several advantages including:[64, 66]

1) Much of time is saved by simultaneously passing the entire radiation range through the sample.
2) High resolution spectra are obtained.
3) The data undergoes Analogue→Digital conversion, therefore the results are easily manipulated,
4) Combining the results of several scans acts to average out random artefacts, therefore even very small samples may give excellent spectra.

1.5 Atomic Force Microscopy

The Atomic Force Microscope (AFM) was developed by Binnig, Quate and Gerber in 1986 to overcome the requirement of conducting surfaces for imaging by Scanning Tunnelling Microscopy (STM).[69] Using the AFM, surface topography of both non-conductive and conductive samples can be examined at scales ranging from micrometers to sub-nanometers, thus making atomic resolution possible.[70]

1.5.1 Forces

The AFM operates by measuring the forces between the sample and a probe tip which is attached to a cantilever. The sample is mounted on an xyz piezoelectric translator, which rasters the sample under the probe tip.[71] Force changes between the two surfaces cause a measurable deflection of the cantilever, allowing an image of the surface topography of the sample to be built up.[70, 72]

As the probe tip is approached by the sample, it is first attracted to the sample surface by long range interactions such as van der Waals forces. As the probe-sample distance is decreased further, the electron orbitals of atoms on the sample surface start to interact with those on the surface of the probe, and the two surfaces start to repel one another. Upon bringing the sample closer still, attractive forces first neutralise, and then dominate the repulsive forces.[73]

Any surface under ambient conditions will have a thin (25-500 Å) contamination layer, comprising water and other ambient species.[74] This produces capillary action within the contamination layer, which acts to increase the attractive forces between the probe tip and the surface. These effects are observed to a greater extent on a retracting probe tip because it will be held more firmly to the surface, therefore the forces observed at a given sample-tip distance may be greater when moving the tip away from than when approaching the surface.[73] These capillary effects may be greatly reduced by taking advantage of the ability of the AFM to image under a variety of environmental conditions, including liquids.[75]

These forces are responsible for the force curve obtained during an oscillation of the tip, moving towards the surface and then away. The force curve may be used during imaging to ensure that the tip has engaged properly on the surface.

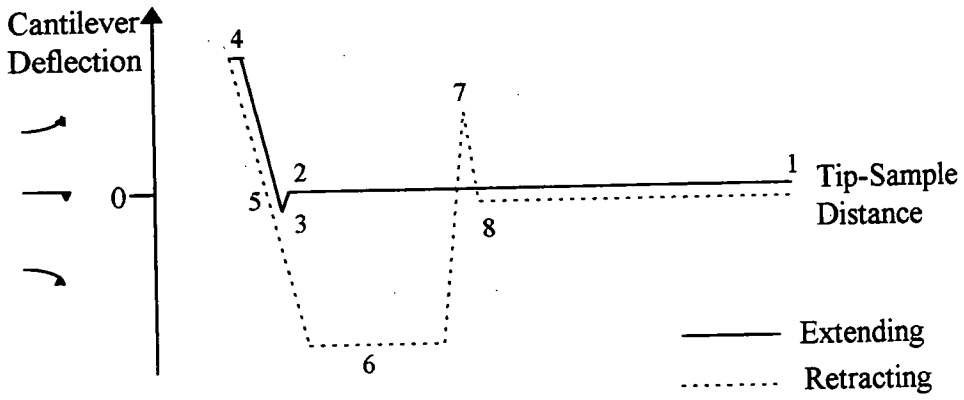

Figure 3: A Typical Force Curve

Figure 3 shows a typical force curve obtained during AFM. At point 1, the tip is fully retracted and no forces are operating between the tip and the surface. Upon moving from 1 to 2, there is no change in the deflection signal as the piezo extends and the sample approaches the tip because there is still no contact between the surfaces. A dip is evident at 3 because attractive forces cause the cantilever to bend towards the surface, prior to the repulsive forces becoming dominant forcing the tip away from the sample (3-4). Maximum piezo extension is observed at point 4, after which the sample is retracted from the tip once more, and the cantilever deflection decreases. Typically the deflection signal continues to decrease after the zero deflection point of the force curve, (5). This is due to attractive forces between the tip and the cantilever which cause the tip to "stick" to the sample, which in turn causes the cantilever to bend down as the piezo continues to retract. The plateau 6 represents the region where the spring force of the cantilever is equal to the attractive forces between the tip and the sample. When the spring force of the cantilever overcomes these attractive forces, the cantilever deflection returns to zero (6-8). Occasionally the tip "flicks" off the sample due to overcoming the capillary forces which act to hold it to the surface

more firmly. This phenomenon demonstrates itself as a peak (7) in the force curve.[76]

1.5.2 Measuring Forces

There are two main techniques of force measurement used in AFM, known as non-modulated and modulation techniques.[73] Both classes of technique require a measurement of the deflection of the cantilever. In early AFM systems, this deflection was measured using a STM stylus in contact with the conductive rear surface of the cantilever in order to measure the tunnelling current between the two. The most common method in use today involves focusing the light beam from a laser diode or a HeNe laser onto the end of the cantilever. Reflection of this beam off the back of the cantilever is picked up by a segmented photodiode. Amplification of the difference signal between the upper and lower photodiodes produces a sensitive measure of the cantilever deflection.[71] The basic operation of the AFM using this type of sensor system is shown in Figure 4.

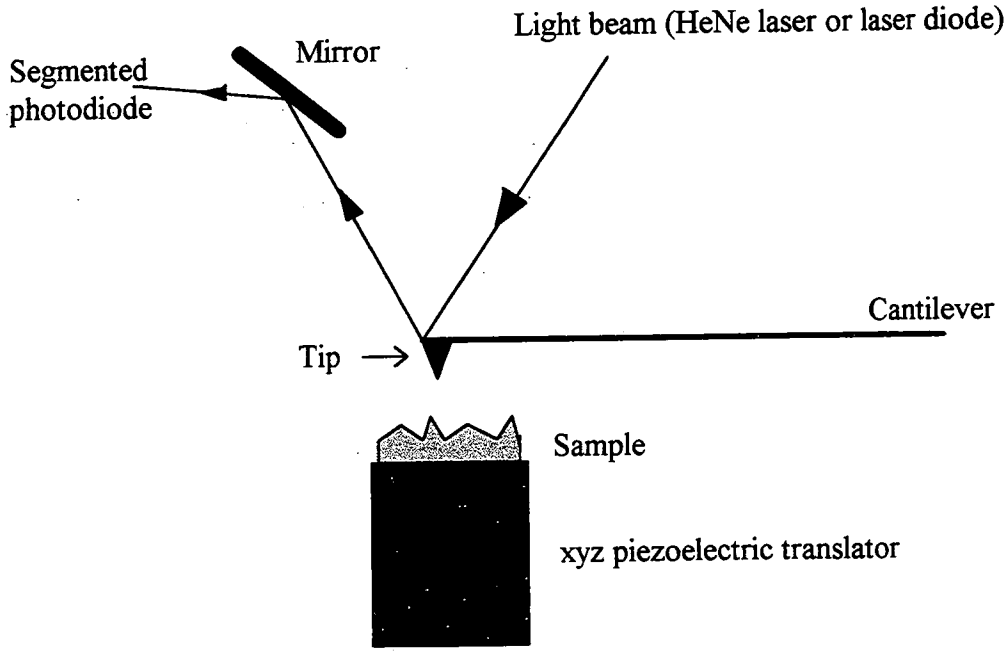

Figure 4: Schematic Diagram of the Atomic Force Microscope

1.5.2.1 Non-Modulated Techniques

Non-modulated techniques are used in "contact mode" AFM. The sample is brought very close to the tip and operates in the region where repulsive forces are dominant. The force exerted on the tip by the sample causes the cantilever to deflect as the sample is rastered beneath the tip. This deflection is detected using the methods described previously. The standard operation of contact mode AFM involves the use of the photodiode difference signal by a feedback loop to adjust a z-piezoelectric ceramic in order that the force between the probe and the sample remains constant. The voltage required to do this is used as the z-data for imaging - this is the "constant" force mode. If the scan is performed very fast, or the feedback loop is slowed, then the z-piezoelectric ceramic will be unable to keep up with the surface features of the sample. In such cases, the sensor output is used directly as the z-data in "variable force" mode. Which of these two force modes is used depends upon the surface of the sample. If there is a significant change in surface feature height over the scan area, then the "constant force" mode is preferred, whereas for areas of very flat samples, "variable force" mode is used.[73]

Probe tip and cantilever design are critical in contact AFM. Sharp tips are favourable, since this will reduce capillary action within the contamination layer.[71] In order to produce the maximum deflection for a given force (a larger deflection will be easier to detect), a low spring constant cantilever is required.[73] This may be rationalised if we consider Hookes law; $F=k\Delta x$, where F is force, k is the cantilever spring constant and Δx is the cantilever displacement.

One disadvantage of contact AFM is that although the contact forces between the tip and the sample are small, soft samples may be damaged by the tip.[76] One method of overcoming this problem is to use modulation techniques.

1.5.2.2 Modulation Techniques

If the cantilever is moved away from its equilibrium position and then released, it will oscillate at a "resonant frequency" determined by the mechanical

properties of the cantilever. In modulation techniques, such as non-contact or TappingMode™, the cantilever is made to oscillate by mounting its base on a piezoelectric ceramic driven by an alternating voltage. When a force acts on the probe, it behaves as though the mass of the cantilever has been altered, thus modifying the resonant frequency and amplitude of the oscillations.[73] By measuring the RMS value of the deflection detector signal, the change in oscillation amplitude may be determined, and the feedback signal used to overcome this change. Modulation techniques are ideal for studying the surfaces of very soft samples which are susceptible to tip damage.[77]

In non-contact AFM the tip undergoes small-amplitude (<5 nm) oscillations near the sample surface. These oscillations are low-energy since the short-range van der Waals forces which they are probing are relatively weak. There is, however, only a very narrow region in which the oscillation amplitude is affected by the short-range van der Waals interaction before the tip becomes trapped within the water layer which contaminates all samples under ambient conditions. This constraint means that non-contact AFM has found limited applications, and has led to the development of TappingMode™ AFM.[76, 77]

TappingMode™ involves higher amplitude (20-100 nm) oscillations of the cantilever at frequencies close to the resonant frequency (~300 kHz). The tip strikes the sample surface on each oscillation, but has enough energy to overcome the surface tension of the adsorbed contamination layer due to the large oscillation amplitude and the high spring constant of the cantilever. Very high resolution may be achieved using TappingMode™ AFM, since the tip strikes the surface many times before being laterally displaced by a tip diameter.[77]

1.6 Plasmas

A plasma is basically a partially ionized gas containing ions, electrons and neutral species, which is produced by a gaseous electric discharge.[78] The gas must be quasi-neutral, that is to say it should contain roughly equal numbers of ions and electrons, in order that it may be classified as a plasma. This requirement is satisfied when the dimensions of the discharged gas volume are significantly

greater than the Debye length. The Debye length, λ_D, is defined as the distance over which a small potential or charge imbalance can exist within the conductive plasma, and is given by:[78-80]

$$\lambda_D = \sqrt{[\varepsilon_o k T_e / n_e e^2]}$$

where ε_o is the permittivity of free space, k is the Boltzmann constant, n_e is the number density of free electrons and e is the electronic charge. The term plasma was first used to describe this, the fourth state of matter, in the 1920's by Irving Langmuir, who was studying types of mercury vapour discharges.[81]

1.6.1 Classification of Plasmas

There are two major types of plasma, known as "equilibrium" (or "hot") plasmas, or "non-equilibrium" ("cold") plasmas.[78, 82-85]

Equilibrium plasmas have $T_e \approx T_g > 5x10^3$ K, where T_e is the electron temperature and T_g is the gas temperature. This type of plasma is usually produced by arcs or plasma jets, and is suitable for processing inorganic materials and organic compounds with very simple structures. Under these conditions it is impossible to treat more complex molecules and polymeric materials since they would degrade rapidly. Equilibrium plasmas are usually produced at higher pressures, at which charged particles are unable to move very far between collisions, or at very low fields where the kinetic energy of the charged particles tends towards the kinetic energy of the neutrals.

Non-equilibrium plasmas have $T_e >> T_g$. Typically T_e/T_g is of the order 10 to 100, therefore, although the gas temperature is near ambient, the electrons are sufficiently energetic to cause molecular bonds to rupture. This makes plasmas of this type ideal for the promotion of chemical reactions involving thermally sensitive materials. Examples of non-equilibrium discharges include glow, corona, silent, RF and microwave discharges.

The temperatures of electrons in a plasma may be calculated using the Boltzmann relationship:[86]

$$\varepsilon = 3/2(kT)$$

where ε is the average kinetic energy of electrons (1-10 eV for non-equilibrium plasmas). This means that 1 eV has an equivalent temperature of 7739 K. The electron energy distribution in a plasma is often assumed to be Maxwellian, however this assumes that $T_e=T_g$.[85] For non-equilibrium plasmas a better approximation is given by a Druyvesteyn distribution, which makes the assumption that $T_e >> T_i$, where T_i is the ion temperature.[85] Both approximations are shown in Figure 5, where the solid line represents the Maxwellian distribution and the dashed line represents the Druyvesteyn distribution.

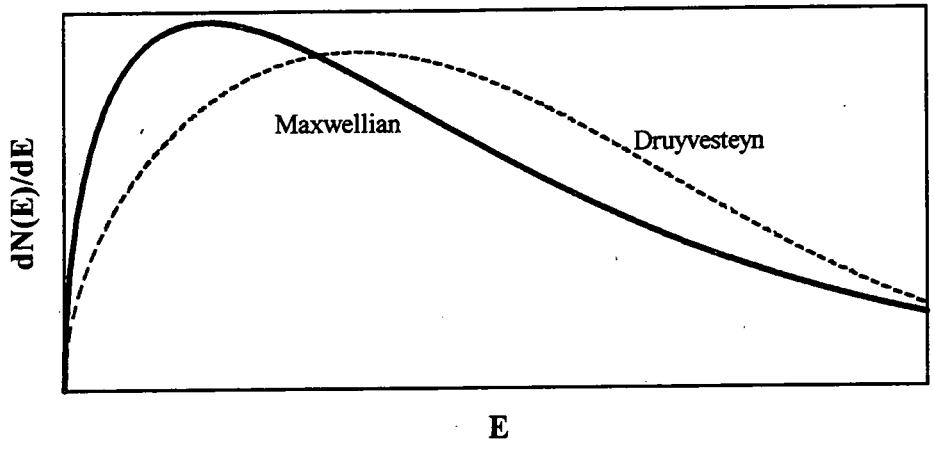

Figure 5: Maxwellian and Druyvesteyn distributions

Both distributions exhibit a high energy tail in which the electrons possess energies significantly higher than the average electron energy. These electrons are important since they are responsible for the ionization processes which occur in the plasma.

For the purposes of this thesis only rf non-equilibrium plasmas are considered.

1.6.2 RF Discharges

In any gas there are always a small number of free electrons available as a result of ionization by naturally occurring radiation or cosmic rays. As the voltage applied to the gas gradually increases these electrons are accelerated into the electric field, resulting in an increase in their kinetic energy. Concomitantly

electron energy is lost through collision processes with atoms or molecules in the gas, leading to ionization and ignition of the plasma.[85] If an alternating frequency above 1 MHz is used to create the discharge the electrodes do not need to be in direct contact with the plasma; a necessity in dc or silent discharges.[78] This avoids contamination problems introduced by sputtering and decomposition of the electrodes, and eliminates the presence of very large or high voltage sheaths (section 1.6.3.4). Instead, for plasmas operating at radio-frequencies (2-60 MHz), the energy may be fed into the reactor using capacitive or inductive coupling. Capacitive coupling employs two conductive bands which are wrapped around the discharge volume and act as the two plates of a capacitor. One of the bands is earthed, and the other has an rf discharge applied to it. For inductive coupling, the discharge is placed within the magnetic field of an induction coil.[78] The most common frequency used is the industrial frequency of 13.56 MHz, since this does not interfere with radio or other equipment.

One problem with using external electrodes is the presence of various impedances within the plasma, transmission lines and power supply. In order that these impedances may be overcome, and the highest power fraction is coupled into the plasma, a matching network containing two tunable capacitors and an inductor is used between the rf generator and the glow discharge.[80] This "matchbox" is adjusted so that the impedance between the generator and the matchbox is the same as that between the matchbox and the plasma.

1.6.3 Concepts of Plasma Physics

1.6.3.1 Plasma Frequency

The concept of the Debye length being the distance over which a small potential may disturb a plasma has already been discussed, however, the electrons in the plasma do not move instantaneously in order to counter these variations. The time taken to do this is the Debye length divided by the electron velocity. This motion may not be damped, therefore the electrons will move in an oscillatory manner with a frequency (the plasma frequency) which is the inverse of the time taken to move one Debye length.[79] This is given by:

$$\omega_p = \sqrt{(ne^2/(\varepsilon_o m))}$$

Applied electric fields at frequencies below the plasma frequency will be filtered out since the electrons are able to move and shield the charge or potential imbalance induced by the applied field. At higher frequencies the electrons are too slow to respond.

1.6.3.2 Plasma Potential

The much higher kinetic energy of electrons in a plasma compared with ions means that the electrons reach the edges of the plasma at a higher rate than the ions. A negative charge therefore builds up at the chamber walls, and the bulk of the plasma acquires a net positive charge.[79, 80] A steady state condition is eventually reached in which the rate of electron loss to the walls decreases due to this charging effect to the same level as the loss rate of ions. At this point the average potential of the bulk plasma with respect to the chamber is defined as the plasma potential, which will be several volts more positive than the most positive surface in contact with the plasma.[79, 80] It should be noted that since the loss rates of ions and electrons are equal under these conditions, the plasma retains overall neutrality.

1.6.3.3 Floating Potential

The same explanation may be applied to the concept of floating potential at an electrically isolated substrate. The more mobile electrons reach the substrate faster than the ions do, and eventually a steady-state is established where the substrate has a negative potential associated with it with respect to the plasma.[79] This negative potential makes ion bombardment of the substrate possible.

1.6.3.4 Sheath Formation and the Plasma Dark Space

Since the chamber walls and the surface of anything within the plasma has a negative potential with respect to the plasma potential, there is a net repulsion of

electrons from the areas immediately adjacent to these surfaces. These surfaces have acquired a net positive charge around them in a region known as the sheath.[79, 80] Since the sheath has a very low electron density, and in a plasma it is the electrons which excite the neutral species, which in turn relax to produce the glow, this region will appear relatively dark and is often referred to as a dark space. The plasma is a region of uniform potential, and virtually all the voltage change from the plasma to a surface in contact with the plasma occurs within the sheath.

1.6.3.5 Reduced Field

The reduced field ultimately determines the electron energy in a plasma. It is given by E/n, i.e. electric field/neutral gas density, and has its own unit, the Townsend (Td), where 1 Td=10^{-17} V cm^2.[83] The reduced field is also a measure of the breakdown strength of a plasma. For a typical gas such as O_2, N_2 or air, breakdown occurs at 100 Td.

Whether a plasma is in equilibrium or not is determined by the reduced field. Equilibrium conditions are expected only at very low values of E/n (<1 Td), where the electron energy is similar to the kinetic energy of heavy particles. Non-equilibrium plasmas have higher values of E/n.

1.6.4 Uses of Plasmas

Plasmas are widely used in a variety of processes ranging from the production of ozone in a silent discharge[87] to the fabrication of semiconductor devices[88] and modifications to the wettability of surfaces.[78, 82]

1.7 References

1. Ulrich, H.; *Introduction to Industrial Polymers*; Hanser: Munich, 1982
2. Cowie, J.M.G.; *Polymers: Chemistry and Physics of Modern Materials*; 2nd Ed., Blackie: Glasgow, 1991
3. Jordan, RF, *J. Chem. Educ.* **1988**, *65*, 285
4. Boor, J. Jr.; *Ziegler-Natta Catalysts and Polymerizations*; Academic Press: London, 1979
5. Tait, P.J.T.; *Comprehensive Polymer Science;* Ed. Allen, G., Bevington, J.C.; Vol. 4, Ch. 1; Pergamon Press: Oxford, 1989
6. Crabtree, R.H.; *The Organometallic Chemistry of the Transition Metals;* Wiley: Singapore, 1988
7. Cossee, P. *J. Catal.* **1964**, *3*, 80
8. Elsenbroich, C.; Salzer, A.; *Organometallics; A Concise Introduction;* Second Ed.; VCH: New York, 1992
9. Gates, B.C.; *Catalytic Chemistry;* Wiley: Singapore, 1992
10. Ciardelli, F.; Carlini, C.; *Comprehensive Polymer Science; First Supplement;* Eds. Aggarwal, S.L. and Russo, S.; Pergamon Press: Oxford, 1992
11. Kaminsky, W. *Stud. Surf. Sci. Catal.* **1986**, *25*, 293
12. Jüngling, S.; Mülhaupt, R. *J. Organomet. Chem.* **1995**, *497*, 27
13. McDaniel, M.P. *Ind. Eng. Chem. Res.* **1988**, *27*, 1559
14. Soga, K.; Arai, T.; Nazawa, H.; Uozumi, T. *Macromol. Symp.* **1995**, *97*, 53
15. Kaminsky, W. *Macromol. Symp.* **1995**, *97*, 79
16. Lee, D.; Shin, S.; Lee, D. *Macromol. Symp.* **1995**, *97*, 195
17. Lee, D.; Yoon, K.; Huh, W. *Macromol. Symp.* **1995**, *97*, 185
18. Fu, S.L.; Rosynek, M.P.; Lunsford, J.H. *Langmuir*, **1991**, *7*, 1179
19. Karol, F.J.; Wu, C. *J. Polym. Sci.: Polymer Chem. Ed.* **1974**, *12*, 1549
20. Karol, F.J.; Brown, G.L.; Davison, J.M. *J. Polym. Sci.: Polymer Chem. Ed.* **1973**, *11*, 413
21. Hogan, J.P.; Banks, R.L. U.S. Patent 2,825,721, **1958**
22. Bailey, G.C.; Reid, J.A. U.S. Patent 2,381,198, **1945**

23. Hogan, J.P.; *Applied Industrial Catalysis, Volume 1*; Academic, 1983, Chap. 6
24. Chudek, J.A.; Hunter, G.; McQuire, G.W.; Rochester, C.H.; Smith, T.F.S. *J. Chem. Soc., Faraday Trans.* **1996**, *92*, 453
25. McDaniel, M.P. *Adv, Catal.* **1985**, *33*, 47
26. McDaniel, M.P.; *Transition Metal Catalyzed Polymerization, Vol. 4, Part B*; MMI Press Symposium Series, 1983, pp713-735
27. Ellison, A.; Overton, T.L.; Bencze, L. *J. Chem. Soc., Faraday Trans.* **1993**, *89(5)*, 843
28. McDaniel, M.P. *J. Catal.* **1981**, *67*, 71
29. Hierl, G.; Krauss, H.L. *Z. Anorg. Allg. Chem.* **1975**, *415*, 57
30. Zecchina, A.; Garrone, E.; Ghiotti, G.; Morterra, C.E.; Borello, E. *J. Phys. Chem.* **1975**, *79*, 966
31. Hogan, J.P. *J. Polym. Sci.:A-1* **1970**, *8*, 2637
32. Wang, S.; Tait, P.J.T.; Marsden, C.E. *J. Molec. Catal.* **1991**, *65*, 237
33. McDaniel, M.P.; Martin, S.J. *J. Phys. Chem.* **1991**, *95*, 3289
34. Clark, A. *Catal. Rev.* **1969**, *3*, 145
35 Eley, D.D.; Rochester, C.H.; Scurrell, M.S. *J. Catal.* **1973**, *29*, 20
36. Spitz, R.; Revillon, A.; Guyot, A. *J. Catal.* **1974**, *35*, 355
37. Krauss, H.L.; Stach, H. *Inorg. Nucl. Chem. Lett.* **1968**, *4*, 393
38. Baker, L.M.; Carrick, W.L. *J. Org. Chem.* **1968**, *33*, 616
39. Merryfield, R.; McDaniel, M.; Parks, G. *J. Catal.* **1982**, *77*, 348
40. Rebenstorf, B. *Acta Chem. Scand.* **1985**, *A39*, 133
41. Rebenstorf, B. *Z. Anorg. Allg. Chem.* **1984**, *513*, 103
42. Zielinski, P.A.; Szymura, J.A.; Dalla Lana, I.G. *Catal. Lett.* **1992**, *13*, 331
43. Rebenstorf, B. *Acta Chem. Scand.* **1989**, *43*, 413
44. Rebenstorf, B. *Z. Anorg. Allg. Chem.* **1989**, *571*, 148
45. Zecchina, A.; Spoto, G.; Ghiotti, G.; Garrone, E. *J. Molec. Catal.* **1994**, *86*, 423
46. Beck, D.D.; Lunsford, J.H. *J. Catal.* **1981**, *68*, 121
47. Hogan, J.P.; Norwood, D.D.; Ayres, C.A. *J. Appl. Polym. Sci.: Appl. Polym. Symp.* **1981**, *36*, 49

48. Choi, K.Y.; Ray, W.H. *J.M.S.-Rev. Macromol. Chem. Phys.* **1985**, *C25(1)*, 1
49. Xie, T.; McAuley, K.B.; Hsu, J.C.C.; Bacon, D.W. *Ind. Eng. Chem. Res.* **1994**, *33*, 449
50. Marsden, C.E. *Plastics, Rubber and Composites Processing and Applications* **1994**, *21*, 193
51. Ellison, A.; Overton, T.L. *J. Chem. Soc. Faraday Trans.* **1993**, *89(24)*, 4393
52. Jehng, J.M.; Wachs, I.E.; Weckhuysen, B.M.; Schoonheydt, R.A. *J. Chem. Soc. Faraday Trans.* **1995**, *91(5)*, 953
53. Lichelli, J.A. U.K. Patent 2,098,228 A, **1982**
54. Chalfont, G.R.; Crump, R.A.; Thukral, P.S. U.K. Patent 1,429,174, **1976**
55. McDaniel, M.P. U.S. Patent 4,402,864, **1983**
56. Rekers, L.J.; French, R.J.; Mayhew, H.W. U.S. Patent 4,356,294, **1982**
57. Speca, A.N. U.S. Patent 4,119,773, **1978**
58. Rekers, L.J.; Katzen, S.J.; Krekeler, J.H. U.S. Patent 3,984,351, **1976**
59. Silverstein, R.M.; Bassler, G.C.; Morrill, T.C.; *Spectrometric Identification of Organic Compounds*; Fifth Edition; Wiley: Singapore, 1991, Ch. 2
60. Briggs, D.; Brown, A.; Vickerman, J.C.; *Handbook of Static Secondary Ion Mass Spectrometry*; Wiley: Chichester, 1989
61. Brown, D.W.; Floyd, A.J.; Sainsbury, M.; *Organic Spectroscopy*; Wiley: Bath, 1988, Ch. 5
62. Briggs, D.; Seah, M.P.; *Practical Surface Analysis, Volume 2 - Ion and Neutral Spectroscopy*; Second Edition; Wiley: Chichester, 1992
63. Busch, K.L.; in *Ion Spectroscopies for Surface Analysis (Methods of Characterization series, Volume 2)*; Czanderna, A.W.; Hercules, D.M. eds.; Plenum Press: New York, 1991
64. Silverstein, R.M.; Bassler, G.C.; Morrill, T.C.; *Spectrometric Identification of Organic Compounds*; Fifth Edition; Wiley: Singapore, 1991, Ch. 3
65. Nakamoto, K.; *Infrared and Raman Spectra of Inorganic and Coordination Compounds*; Third Edition; Wiley: New York, 1978
66 Brown, D.W.; Floyd, A.J.; Sainsbury, M.; *Organic Spectroscopy*; Wiley: Chichester, 1988, Ch. 3

67 . Banwell, C.N.; *Fundamentals of Molecular Spectroscopy*; McGraw-Hill: London, 1966

68 . Hollas, J.M.; *Modern Spectroscopy*; Wiley: Chichester, 1987

69. Binnig, G.; Quate, C.F.; Gerber, C. *Physical Review Letters* **1986**, *56(9)*, 930

70. Snyder, S.R.; White, H.S. *Anal. Chem.* **1992**, *64*, 116R

71. Gould, S.A.C.; Drake, B.; Prater, C.B.; Weisenhorn, A.L.; Manne, S.; Kelderman, G.L.; Butt, H-J.; Hansma, H.; Hansma, P.K.; Maganov, S.; Cantow, H-J. *Ultramicroscopy* **1990**, *33*, 93

72. Frommer, J.; Meyer, E. *J. Phys.: Condens. Matter* **1991**, *3*, S1

73. TopoMetrix Technical Report, *AFM Imaging Modes*, TopoMetrix Corporation, 1993

74. Quate, C.F. *Surf. Sci.* **1994**, *299/300*, 980

75. Maganov, S.N.; Qvarnström, K.; Elings, V.; Cantow, H-J. *Polymer Bulletin* **1991**, *25*, 689

76. MultiMode SPM Manual; Digital Instruments, Inc.

77. Zhang, Q.; Inniss, D.; Kjoller, K.; Elings, V.B. *Surface Science Letters* **1993**, *290*, L688

78. Hollahan, J.R.; Bell, A.T.; *Techniques and Applications of Plasma Chemistry*; Wiley: New York, 1974

79. Vossen, J.L.; Kern, W.; *Thin Film Processes II;* Academic: London, 1991

80. Chapman, B.N.; *Glow Discharge Processes;* Wiley: New York, 1980

81. Langmuir, I. *Phys. Rev.* **1929**, *33*, 954

82. Shohet, J.L. *IEEE Transactions on Plasma Science* **1991**, *19(5)*, 725

83. Eliasson, B.; Kogelschatz, U. *IEEE Transactions on Plasma Science* **1991**, *19(6)*, 1063

84. National Research Council *Plasma Processing of Materials - Scientific Opportunities and Technological Challenges*; National Academy Press: Washington DC, 1991

85. Grill, A.; *Cold Plasma in Materials Fabrication-From Fundamentals to Applications;* IEEE Press: New York, 1994

86. Atkins, P.W.; *Physical Chemistry;* Oxford: Oxford, 1990

87. Eliasson, B.; Kogelschatz, U. *IEEE Transactions on Plasma Science* **1991**, *19(2)*, 309

88. Coburn, J.W. *IEEE Transactions on Plasma Science* **1991**, *19(6)*, 1048

CHAPTER 2. A MECHANISTIC STUDY OF THE CALCINATION OF SUPPORTED CHROMIUM(III) PRECURSORS FOR ETHYLENE POLYMERIZATION CATALYSTS

2.1 Introduction

Supported transition metal oxide catalysts are usually prepared by the impregnation or adsorption of a precursor compound onto a carrier substrate from solution.[1-10] Monolayer coverages may be reliably obtained by using a stoichiometric reaction between the support hydroxyls and the precursor species,[1, 11, 12] followed by a calcination step to produce a dispersed metal oxide phase.[1, 7, 8, 13, 14] Occasionally an alternative preparative method can be employed which comprises heating a physical mixture of the transition metal oxide and support material to generate the highly dispersed oxide species.[1, 9] Supported metal oxides tend to exhibit better thermal stability;[1, 13] for instance, bulk CrO_3 begins to decompose into O_2 and Cr_2O_3 above 473 K, whereas CrO_3 supported on silica is stabilized up to temperatures as high as 1173 K.[8, 13, 14] Such supported metal oxide systems are used for a wide variety of catalytic reactions, including: SO_2 oxidation (e.g. K_2O-V_2O_5/SiO_2), selective oxidation and ammoxidation of aromatics (e.g. V_5O_5/TiO_2), selective reduction of NO by NH_3 (e.g. V_2O_5/TiO_2), alkene polymerization (e.g. Phillips CrO_x/SiO_2 catalyst) and hydrodesulphurization (e.g. promoted MoO_3/Al_2O_3, WO_3/Al_2O_3).[1]

One of the most commercially important examples of this type of catalyst is the Phillips CrO_x/SiO_2 ethylene polymerization catalyst.[13] Silica supported chromium catalysts are used for the production of over four million tonnes of high-density polyethylene every year.[15] Catalytic activity as well as the polymer structure and properties are critically dependent upon the preparation and calcination procedures adopted [13, 15, 16, 17] since the active site profiles and the pore structures of the supports are related to these conditions.[15] These materials are usually prepared by impregnating a chromium complex in almost any valence onto a wide pore silica substrate and then calcining in dry air or oxygen at 673-1073 K[8, 10, 13, 14] to generate chromium(VI) centres dispersed on the support surface. These centres take the form of either mono-, di- or even poly-chromate

species,[13, 18] the proportion of each being dependent on the activation temperature.[19] As the activation temperature increases, the proportion of dichromate species on the surface increases.[10, 13, 20] Calcination above 1073 K causes sintering of the support and therefore reduces the surface area which is available for stabilization of the Cr(VI) species leading to a deactivation of the catalyst.[10] Catalytic activity is observed to increase with calcination temperature up to this limit.[15] Following calcination the catalyst is cooled to 333-383 K, where, upon exposure to ethylene, the chromium centres are reduced to generate active sites for ethylene polymerization. Alternatively the activated chromium(VI) centres can be pre-reduced by either exposing the calcined catalyst to carbon monoxide at 573-623 K, or by the addition of reducing agents such as the alkyls of aluminium, boron or zinc to the catalyst at the polymerization stage.[13, 21]

There are inherent environmental and health hazards associated with the use of hexavalent chromium species as precursors for the CrO_x/SiO_2 catalyst;[13, 22] therefore lower valence chromium compounds are becoming more prominent on the industrial scale. In this chapter, the thermal activation of bulk chromium(III) acetate, chromium(III) acetate supported on high surface area silica, and chromium(III) acetylacetonate dry-blended with silica has been studied with oxygen as the carrier gas.

2.2 Experimental

Bulk basic chromium(III) acetate, $Cr_3(OH)_2(CH_3CO_2)_7$ (Aldrich, 24% Cr content) and high surface area silica (Crosfield Limited, surface area = 323 m^2g^{-1}, pore volume = 1.81 cm^3g^{-1}) were used as control samples. Bulk chromium(III) acetylacetonate, $Cr(C_5H_7O_2)_3$ was not studied since it melts at 489 K prior to its decomposition above 613 K.[23] The CrO_x/SiO_2 catalyst precursors (Crosfield Limited) were prepared by either impregnating silica with an aqueous solution of basic chromium(III) acetate and then drying, or alternatively chromium(III) acetylacetonate was dry-blended with high surface area silica. Both supported catalysts contained 1% chromium loading. 1 g of material was loaded into a quartz microreactor tube. Oxygen carrier gas (BOC, 99.9% purity) was dried

through a conc. H_2SO_4 bubbler, followed by a P_2O_5 drying column, and then a 3A molecular sieve (Aldrich) at a flow rate of 1.5 dm^3hr^{-1}. The reactor tube was heated at 1 K min^{-1} up to 1053 K using a Eurotherm temperature controller and then held at this high temperature for 5 hours prior to cooling at 5 K min^{-1} back down to room temperature. A Vacuum Generators SX200 quadrupole mass spectrometer was connected via a heated fine capillary tube to the microreactor outlet; this was multiplexed to a PC computer, thereby allowing the simultaneous acquisition of up to 50 mass profiles. Figure 1 shows a schematic representation of the apparatus. For each set of experiments, the whole background mass spectrum (0-200 amu) was recorded as a function of furnace temperature, facilitating the identification of all of the desorbing species. Subsequently, each experiment was repeated with fresh material, but this time actual temperature programmed decomposition profiles were obtained by tuning into the most intense fragments evolved during temperature ramping, and these were assigned from literature spectra.[24] The fragmentation patterns for methane, carbon monoxide and carbon dioxide were also measured independently using the respective gases, and normalised using the appropriate ion gauge sensitivity factors, Table 1.[25, 26] The respective mass fragmentation patterns have been taken into consideration during peak assignment; for instance, where the carbon monoxide and carbon dioxide profiles coincide, the mass 28 contribution from CO_2 has been subtracted from the overall mass 28 profile to yield the true CO profile. For overlapping peaks, the mass intensity versus temperature profiles were deconvoluted assuming Gaussian peak fits[10] from which the integrated areas and peak temperatures (± 2 K) could be determined.

Molecule	m/e	Correction factor
CH_4	16 (100%), **15** (88%), 14 (14%), 13 (6%)	x 0.89
H_2O †	**18** (100%)	†
CO	**28** (100%), 12 (3%), 16 (0.7%)	x 0.70
CO_2	**44** (100%), 28 (15%), 16 (12%), 12 (7%)	x 1.00

† Uncorrected for sensitivity factor.

Table 1: Fragmentation patterns for major masses evolved (± 0.5 %).

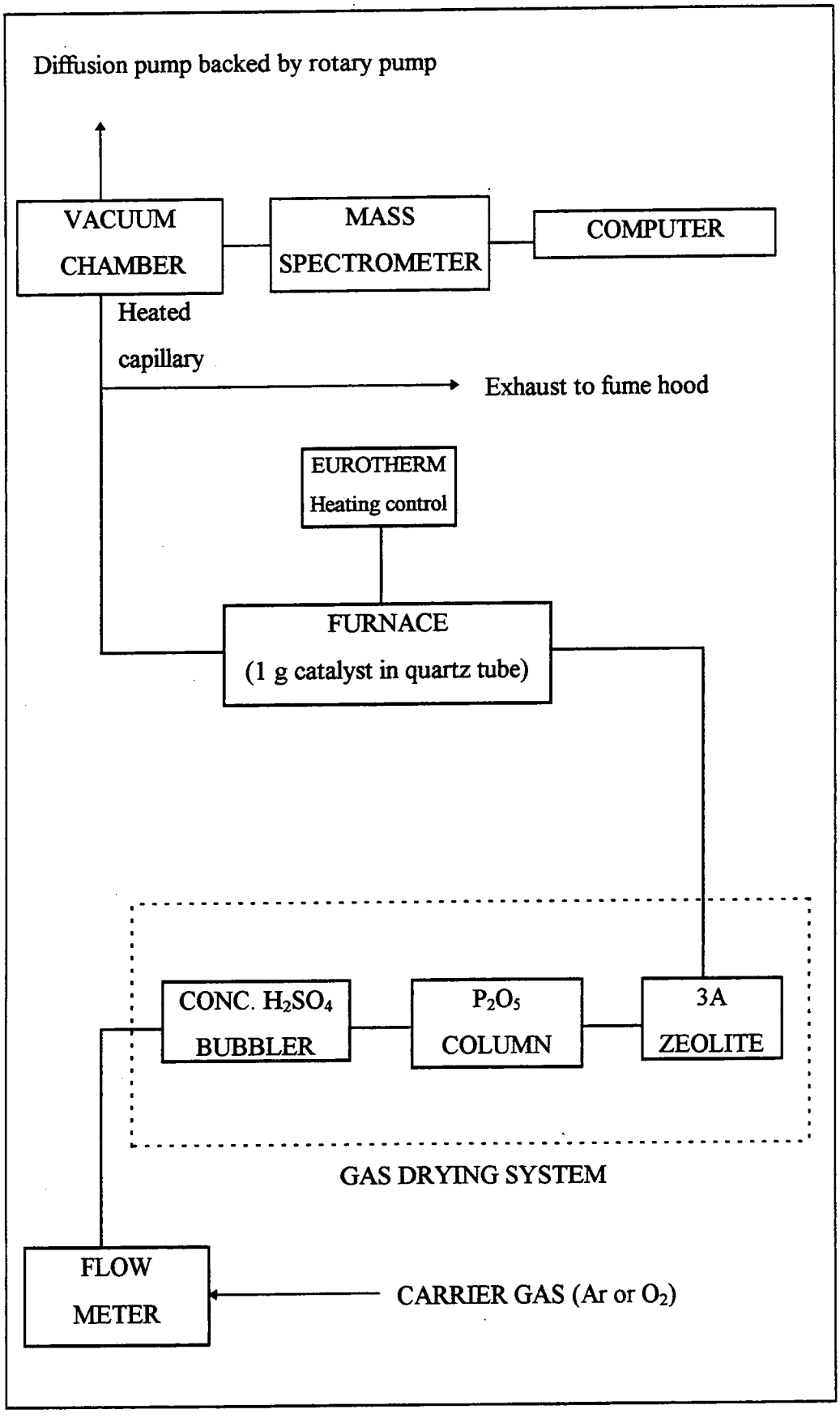

Figure 1: Schematic diagram of the TPA apparatus.

Fourier transform infrared spectroscopy was used to confirm the formation of intermediate acetate-like species during the activation of chromium(III) acetylacetonate dry-blended with silica. The catalyst precursor was heated at 1 K min^{-1} up to 543 K under an oxygen flow of 1.5 dm^3hr^{-1} (this temperature corresponds to completion of the first stage of precursor decomposition). The product was then mixed with potassium bromide and pressed into a disk for characterization by transmission infrared spectroscopy. Reference samples were prepared by mixing potassium bromide with chromium(III) acetylacetonate/silica, chromium(III) acetate/silica, bulk chromium(III) acetylacetonate, bulk chromium(III) acetate, and the silica support material. A FTIR Mattson Polaris instrument was used for infrared analysis. Typically, 100 scans were acquired at a resolution of 4 cm^{-1}.

Finally, the oxidized CrO_x/SiO_2 catalysts were screened for ethylene polymerization activity by pre-reducing under carbon monoxide at 623 K for 15 minutes followed by exposure to high purity ethylene (99.8%, Scott Speciality Gases) at 383 K. The formation of white polyethylene granules was taken as being indicative of an active catalyst, as studied in chapter 4.

2.3 Results

2.3.1 Silica Support

Temperature programmed desorption of just the silica support using oxygen feed gas resulted in the evolution of water over two well defined temperature regimes, Figure 2. Loss of weakly physisorbed water (44%) occurs at low temperatures (~351 K); further heating to higher temperatures (~757 K) causes the elimination of water molecules from adjacent surface silanol groups (56%).[27, 28]

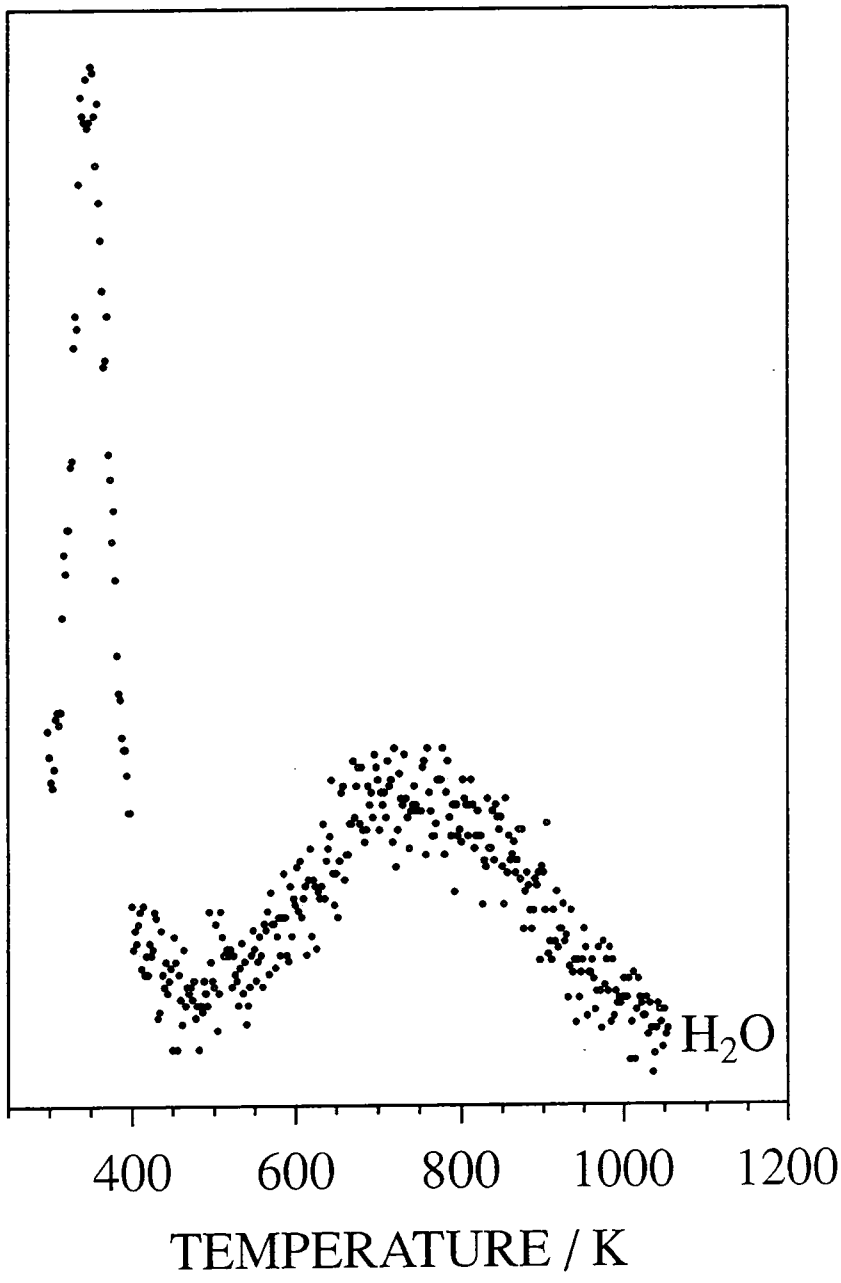

Figure 2: Thermal desorption spectra of H_2O from silica with oxygen carrier gas.

2.3.2 Bulk $Cr_3(OH)_2(Ac)_7$ Decomposition Under Oxygen

Basic chromium(III) acetate is a dark green solid which changed to a black / dark green material during heating under oxygen up to 1053 K. All of the decomposition peaks are very sharp coinciding at 563 K, except for the water profile which displays two broad features with a superimposed sharp peak at 563 K, Figure 3 and Table 2. The sharp dip in the m/e = 32 oxygen profile at 563 K corresponds to straightforward combustion of the chromium acetate to form predominantly water and carbon dioxide.

m/e	Area (Temperature)	Molecule
2†	3 (562 K)	H_2
15	20 (563 K)	CH_4
18 †	185 total area (spike at 563 K)	**H_2O**
28(CO)	29 (563 K)	CO
32 †	-221 (563 K)	O_2
44	280 (563 K)	**CO_2**

† Uncorrected for sensitivity factor.

Table 2: Summary of temperature programmed decomposition peak areas for bulk $Cr_3(OH)_2(Ac)_7$ under flowing oxygen (± 2 K).

2.3.3 Thermal Activation of Chromium(III) Acetate/Silica

Since the chromium(III) acetate/silica catalyst was prepared by aqueous impregnation, it must contain some trapped water ligands around the coordination sphere of the chromium centre. Heating this material up to 503 K in order to drive off any physisorbed water results in the catalyst precursor changing from a pale blue colour to green without any variation in the characteristic C=O (~1635 cm^{-1}) and C-O (~1454 cm^{-1}) infrared stretching bands from the acetate ligand. Complete calcination transformed the material to a bright orange appearance, which is similar in colour to the conventional activated CrO_x/SiO_2 Phillips catalyst

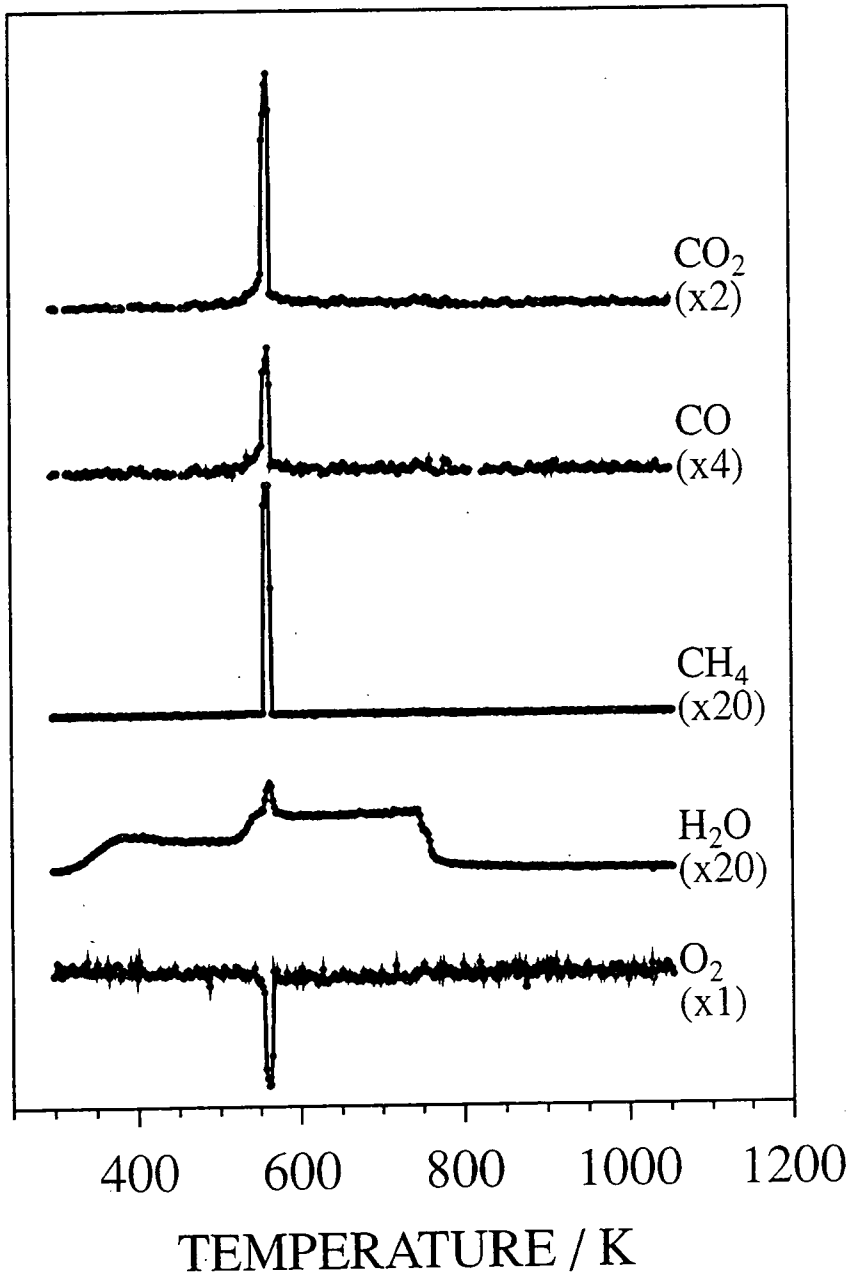

Figure 3: Temperature programmed decomposition profiles for bulk basic chromium(III) acetate under flowing oxygen.

prepared by impregnating silica with aqueous CrO_3 solution.[29] The thermal decomposition of basic chromium(III) acetate supported on high surface area silica under oxygen occurs via a single step reaction pathway at 563 K following the loss of physisorbed water at 362 K, Figure 4 and Table 3. Carbon dioxide and water are the major reaction products during decomposition of the chromium(III) acetate species. This oxidation temperature (563 K) is identical to that observed during the calcination of bulk chromium(III) acetate. Silanol-type elimination to produce water on the silica support is still evident at higher temperatures (~ 716 K).

m/e	~362 K	~563 K	~716 K
18 †	7 (362 K)	5 (570 K)	10 (716 K)
28(CO)	-	2 (563 K)	-
44	-	11 (565 K)	-
Molecule	**H_2O**	**H_2O, CO, CO_2**	**H_2O**

† Uncorrected for sensitivity factor.

Table 3: Summary of temperature programmed activation peak areas for silica impregnated with chromium(III) acetate under flowing oxygen (± 2 K).

2.3.4 Thermal Activation of Chromium(III) Acetylacetonate/Silica

Dry-blended chromium(III) acetylacetonate/silica changed from a maroon colour to bright orange during calcination. Desorption of physisorbed water at 359 K is followed by two well-defined decomposition steps comprising water, carbon monoxide and carbon dioxide evolution, at both 485 K and 583 K, Figure 5 and Table 4. The ratio of carbon-containing fragments produced in the first stage to those produced in the second stage is ~3:2. Once again, the water profile exhibits a broad, high temperature peak which is characteristic of silanol-type elimination.

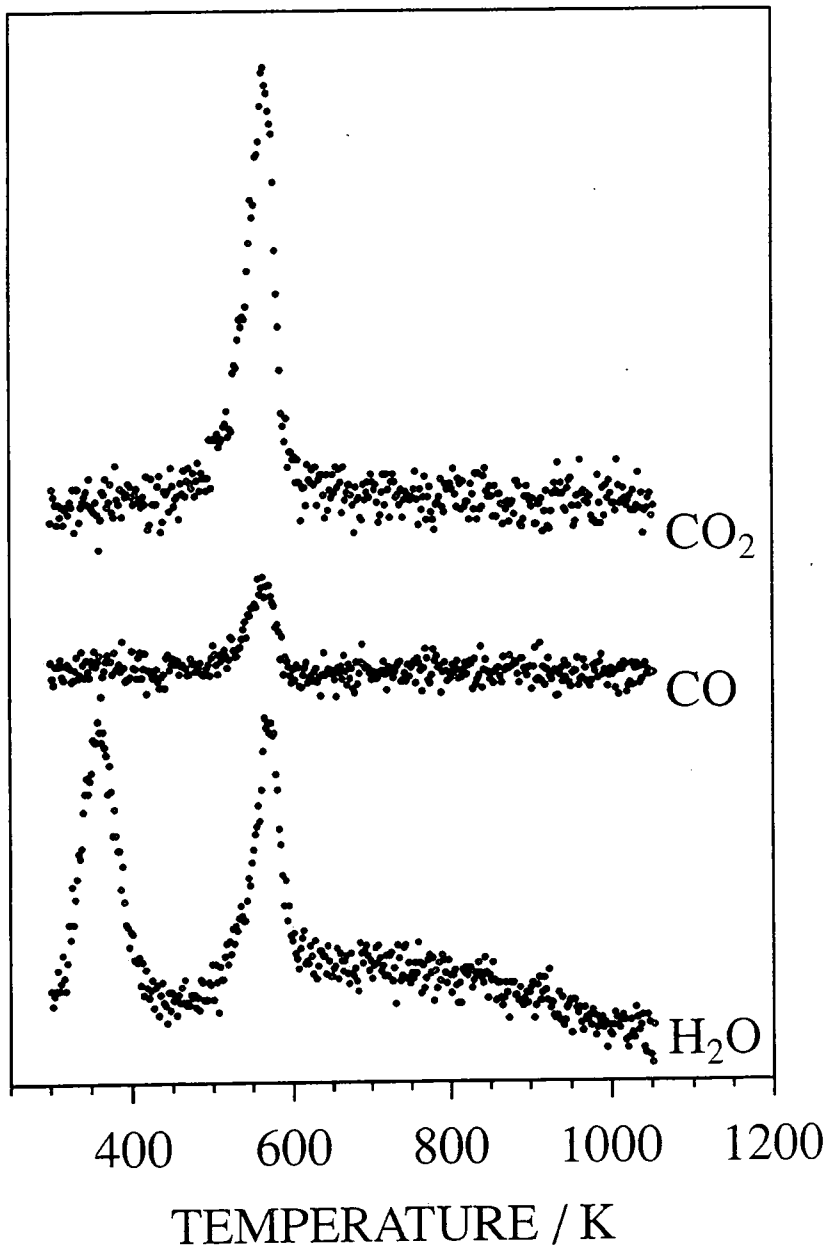

Figure 4: Temperature programmed activation profiles for silica impregnated with basic chromium(III) acetate under flowing oxygen.

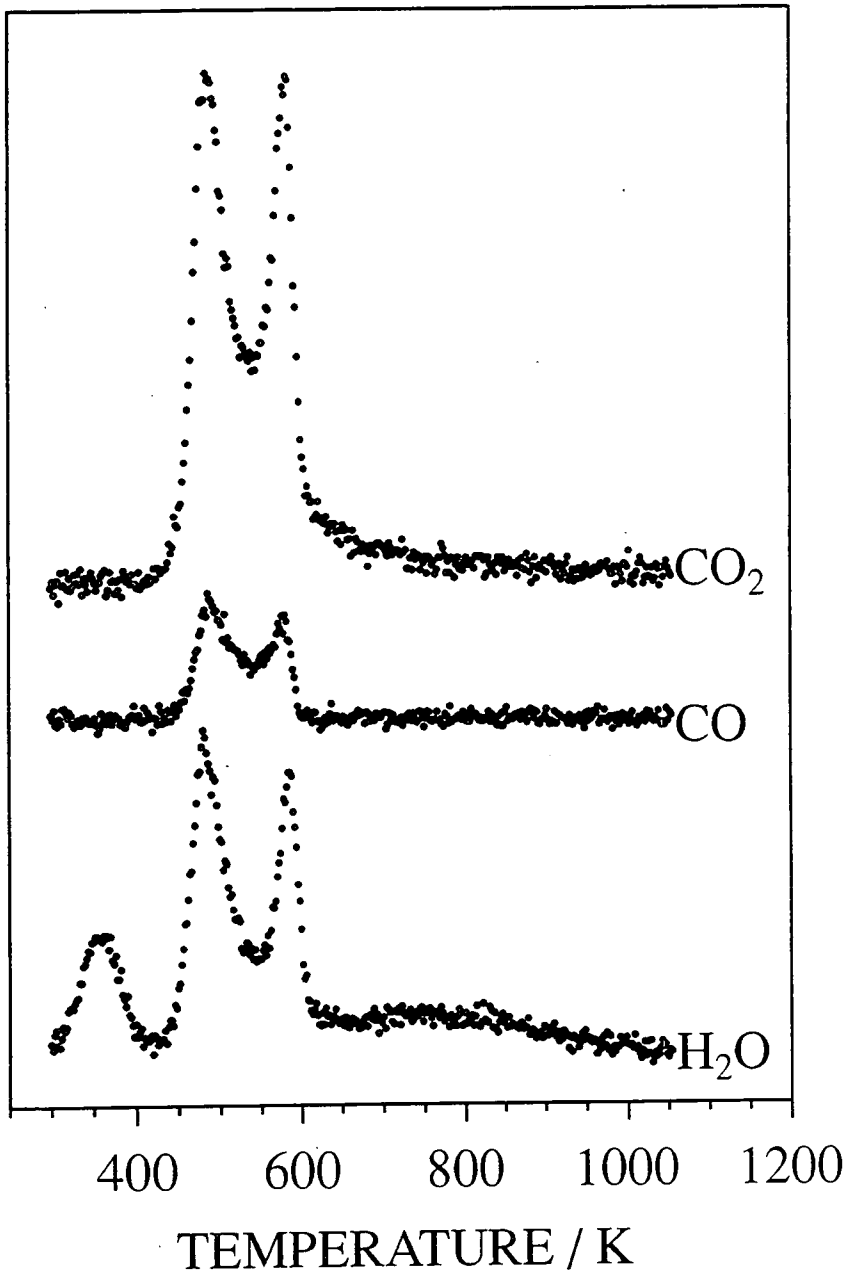

Figure 5: Temperature programmed activation profiles for silica dry-blended with chromium(III) acetylacetonate under flowing oxygen.

m/e	~359 K	~485 K	~583 K	~699 K
18†	7 (359 K)	19 (483 K)	7 (586 K)	15 (699 K)
28	-	8 (488 K)	3 (580 K)	-
44	-	34 (489 K)	25 (581 K)	-
Molecules	**H_2O**	**H_2O, CO, CO_2**	H_2O, CO, CO_2	**H_2O**

† Uncorrected for sensitivity factor

Table 4: Summary of temperature programmed activation peak areas for silica dry-blended with chromium(III) acetylacetonate under flowing oxygen (± 2 K).

The $Cr(acac)_3$/silica precursor material changed to a green colour upon heating under oxygen up to the end of the first stage of decomposition at 543 K. This is the same colour as previously noted following the loss of physisorbed water from chromium(III) acetate/silica. A comparison of the respective transmission infrared spectra of bulk silica, silica impregnated with chromium(III) acetate, silica dry-blended with chromium(III) acetylacetonate, and the product obtained following heating chromium(III) acetylacetonate/silica up to 543 K shows that the C=O and C-O infrared stretching bands at ~1635 and ~1454 cm^{-1} respectively from the acetate ligand[30] are present for both the chromium(III) acetate/silica and partially decomposed chromium(III) acetylacetonate/silica catalytic precursor materials, Figure 6. The other intense infrared absorption features can all be attributed to the silica support, along with an absorption band at ~1640 cm^{-1} due to entrained water which coincides with the C=O stretch found in the acetate samples.[31] Therefore along with the thermal decomposition data, it can be concluded that acetate species are formed on the silica surface during the first stage of oxidative activation of $Cr(acac)_3$ dry-blended with silica.

2.3.5 Ethylene Polymerization

Passage of ethylene over the calcined CrO_x/SiO_2 catalysts produced large white granules which were characterized by FTIR to consist of polyethylene

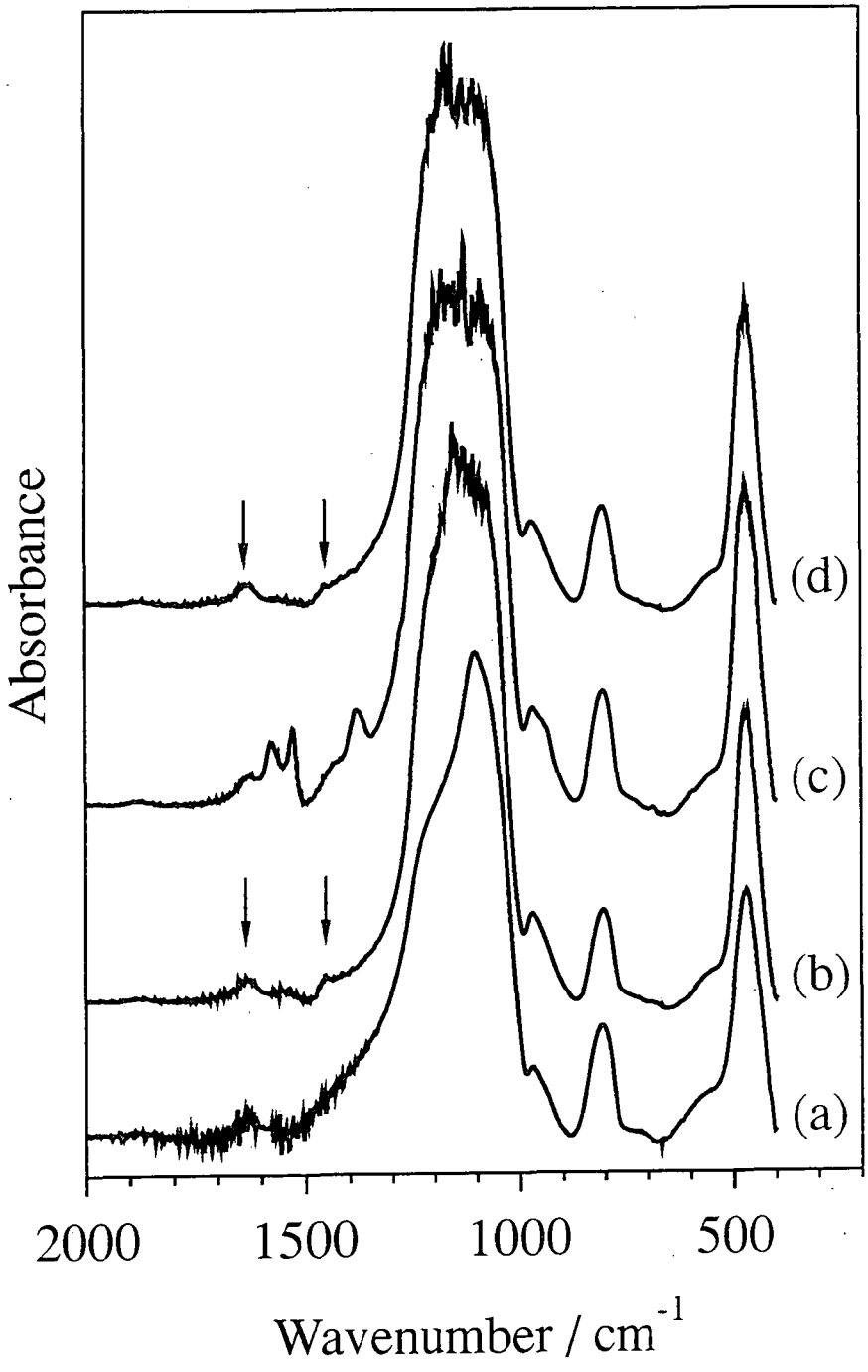

Figure 6: FTIR of (a) silica; (b) silica impregnated with chromium (III) acetate; (c) silica dry-blended with chromium(III) acetylacetonate; and (d) the product of the heating to 543 K of chromium(III) acetylacetonate dry-blended with silica.

polymer (methylene rocking mode band at 719 cm^{-1},[32] and C-H stretches in the 3000-2840cm^{-1} region[33]). The polymerization is discussed in chapter 4.

2.4. Discussion

2.4.1 Silica Support

The low temperature water peak evident in the silica experiments is characteristic of physisorbed water desorbing from the silica surface.[27] At higher temperatures water is evolved from the silica surface by the well established silanol condensation reaction which forms siloxane bridges in conjunction with the evolution of water molecules,[28] Scheme 1.

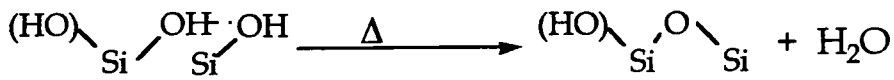

Scheme 1: Silanol condensation reaction.[28] This mechanism is valid with or without the geminal OH groups shown in brackets.

2.4.2 Bulk $Cr_3(OH)_2(Ac)_7$ Decomposition Under Oxygen

The structure of basic chromium(III) acetate[34-36] comprises complex ions of the type $[Cr_3(Ac)_6(OH)_2]^+$, Figure 7. The three carboxylate-bridged chromium(III) atoms form an equilateral triangle around a shared central oxygen atom which can be part of a hydroxyl ligand. The chromium(III) atoms all possess octahedral geometry, the vertex trans to the central oxygen atom being the only ligand which will readily undergo substitution.[36] It is these sites which may be occupied by extra acetate groups, hydroxyls, water molecules etc .

Acetate ligands may coordinate in several configurations, including. bridging, chelating or unidentate. Upon heating, changes may occur within the complex, making the actual bonding mode immediately prior to decomposition uncertain, but there should remain an exposed methyl group available for reaction.

Water evolution at low temperatures for the bulk compound can be accounted for in terms of water of crystallization. The sharp dip in the oxygen profile during calcination is indicative of the oxygen gas participating in the ongoing chemistry. The major products are carbon dioxide and water, i.e. combustion products. This can be explained in terms of oxygen attack at the acetate ligands initiating both C-H and C-C bond scission to release CO_2 and H_2O.[37, 38] Incomplete combustion leads to the additional loss of some carbon monoxide and methane.

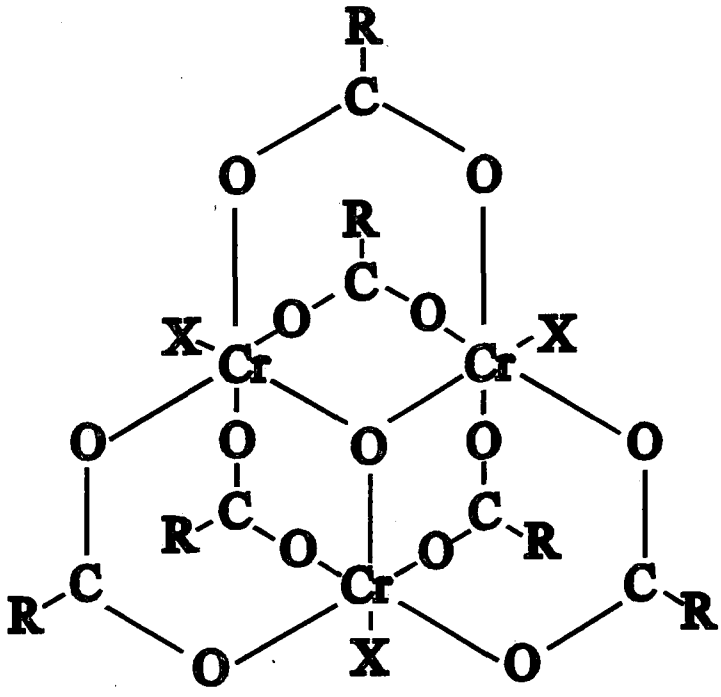

Figure 7: The structure of basic chromium(III) acetate.

2.4.3 Chromium Acetate/Silica Activation

Since there is no shift in decomposition temperature under oxygen between using bulk chromium acetate versus chromium acetate supported on silica, it can be concluded that the chromium acetate structure is retained in some form during aqueous impregnation, probably as small crystallites dispersed over the silica support. This description is consistent with previously reported infrared studies which concluded that the infrared absorption bands characteristic of basic

chromium(III) acetate are still present for basic chromium(III) acetate supported on silica.[39] This result could not be reproduced in the present study where two C=O stretches are observed in the supported sample at 1635 cm^{-1} and ~1560 cm^{-1}, i.e. higher and lower than in the bulk sample (1620 cm^{-1} with a shoulder at ~1560 cm^{-1}), whilst the C-O stretch is observed at 1454 cm^{-1} in both samples, Figure 8. The separation between the two CO stretches provides information on the bonding configuration of the acetate group.[30, 40] In a bridging acetate group, the two CO stretches are found to be close to the symmetric and antisymmetric COO^- stretch frequencies, but when the acetate is unidentate, the C=O and C-O stretches are more widely separated, and in a chelating ligand the separation is smaller than in a bridging configuration.[30] Since we know that six of the acetate groups in the bulk compound are bridging,[34-36] the results would suggest that the shoulder to lower wavenumber must correspond to a chelating seventh ligand, and that the supported species contains a mixture of unidentate and chelating ligands. The observation of decomposition at the same temperature for both the bulk and supported samples can be explained by a possible rearrangement of ligands to the same configuration in both materials during heating to the decomposition temperature. Heating the bulk sample under oxygen to 543 K, i.e. below the decomposition temperature, shows a change in the ligand configuration with a higher proportion of chelating acetate groups, Figure 8.

Oxidative decomposition occurs over a broader temperature range in the supported samples, which can be attributed to the stabilizing interactions between the chromium(III) acetate and the silica surface. Good agreement is found between the reported decomposition of acetate groups in the presence of adsorbed oxygen on metal single crystal surfaces[41-44] and the present bulk and supported chromium acetate results. In both cases, carbon dioxide and water are the major decomposition products, thereby signifying straightforward oxidation of the acetate functionalities. Nucleophilic attack by oxygen is suggested to occur at the methyl group to cause C-H scission which is immediately followed by C-C scission to release CO_2.[37, 38] The remaining methylene ($CH_{2(ads)}$) moieties must then undergo oxidation to produce CO_2 and H_2O.[37]

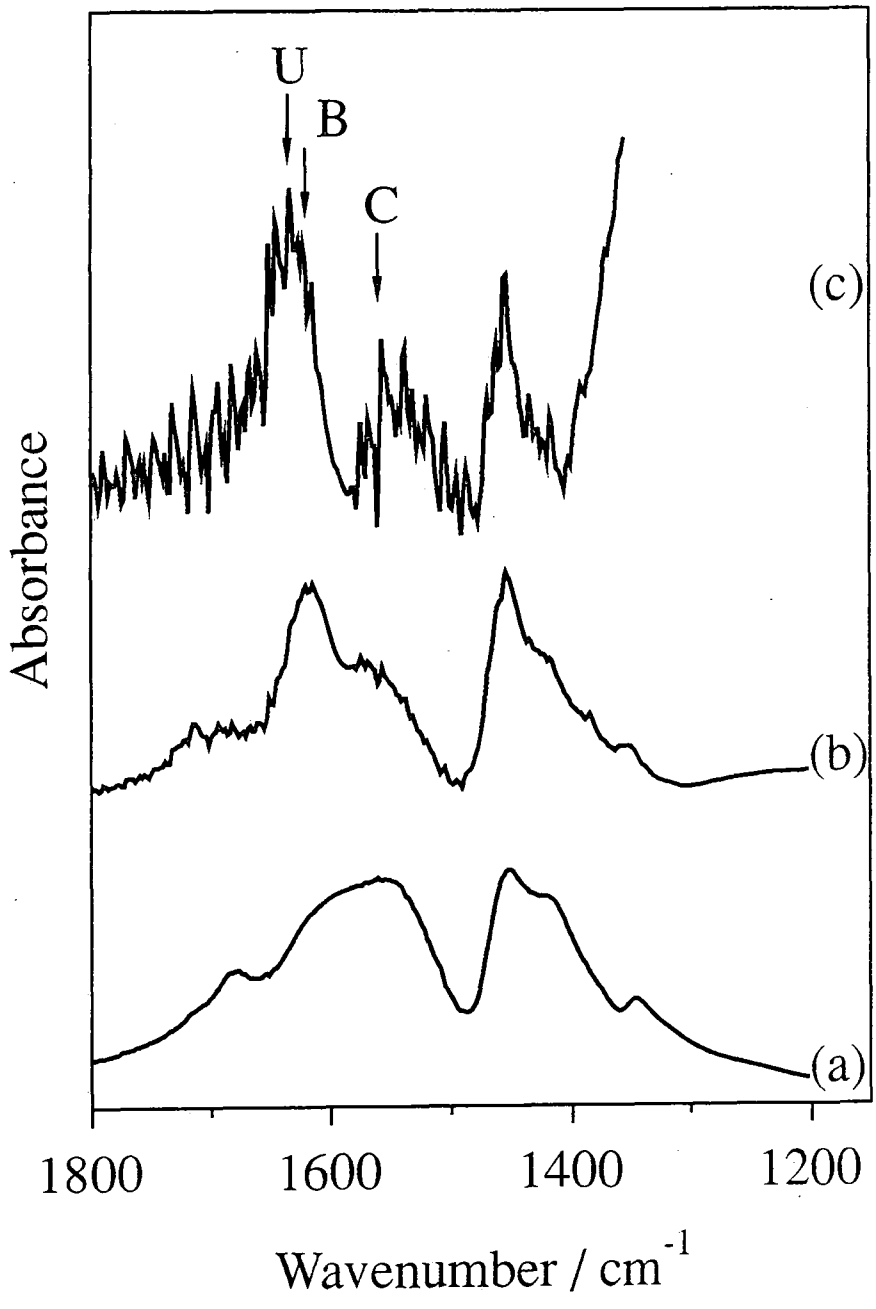

Figure 8: FTIR of (a) the product of heating bulk chromium(III) acetate to 543 K under a flow of oxygen; (b) bulk chromium(III) acetate; and (c) silica impregnated with chromium(III) acetate. U, B and C indicate the C=O stretches assigned to unidentate, bridging and chelating acetate ligands respectively.

2.4.4 Chromium(III) Acetylacetonate/Silica Activation

A variety of metal acetylacetonates, including $Cr(acac)_3$, have previously been impregnated onto silica for investigation as precursors for supported metal oxide catalysts.[45] The present study however uses a dry-blended precursor; therefore, initially there will be no bonding between the support and the chromium species. $Cr(acac)_3$ is an octahedral complex in which each acetylacetonate ligand is bonded through two oxygen atoms to a central chromium atom,[36] Figure 9.

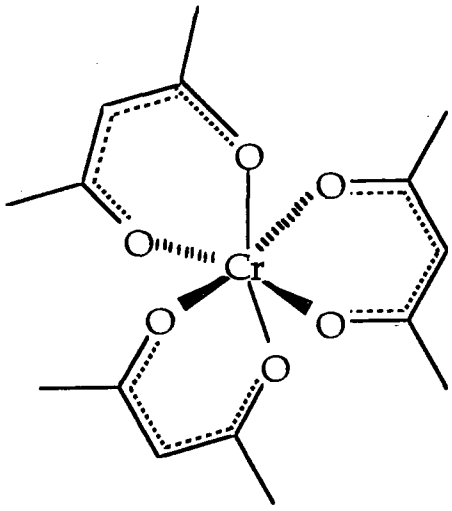

Figure 9: The structure of chromium(III) acetylacetonate.

The two-stage thermal activation of $Cr(acac)_3$ dry-blended with silica under oxygen exhibits a 3:2 ratio of C-containing fragments lost at ~485 K relative to those lost at ~ 583 K. Since each acetylacetonate ligand contains five carbons, this corresponds to the loss of three carbons from each acac ligand in the first stage to leave behind a two carbon atom ligand complexed to the metal centre. Chromium acetylacetonate melts at 489 K,[23] therefore it undergoes partial oxidation (~485 K) close to its melting point. It is of interest to note that the activation of chromium(III) acetate/silica produces activation profiles with a single peak, where the ratio of products and the decomposition temperatures are similar to the second stage of the supported chromium(III) acetylacetonate catalyst activation. The surfaces of solids become mobile at temperatures well below the melting point.[46] It is therefore reasonable to conclude that the first stage of the $Cr(acac)_3$/silica activation involves the diffusion of $Cr(acac)_3$ across

the support surface, followed by reaction with molecular oxygen leading to the formation of acetate-like species bonded to the silica support. These acetate-like species subsequently decompose during the second stage of calcination. The reported infrared studies are consistent with this description.

The formation of acetate-like species from acetylacetonate ligands has previously been observed during the aerobic photo-oxidation and C-C bond cleavage of the acac ligand induced by UV or long-wavelength visible light in (arylazo)aryl(acetylacetonato)palladium(II) complexes,[47] where the photon energy is absorbed by the long-wavelength transition of the azobenzene chromophore and intramolecularly transferred to the metal centre. The excited palladium ion then promotes the transfer of an electron within an acac ligand to produce a radical-like acetylacetonyl fragment which rapidly reacts with molecular oxygen to form acetate ligands with the concomitant loss of carbon dioxide, water and carbon monoxide. A similar, thermally induced, non-radical process is thought to be occurring in the system studied here, involving the cycloaddition of molecular oxygen to the acetylacetonate ligand, followed by C-C and O-O bond rupture to form acetate-like species at the surface, in conjunction with the loss of carbon dioxide, water and carbon monoxide. This is summarised in Scheme 2.

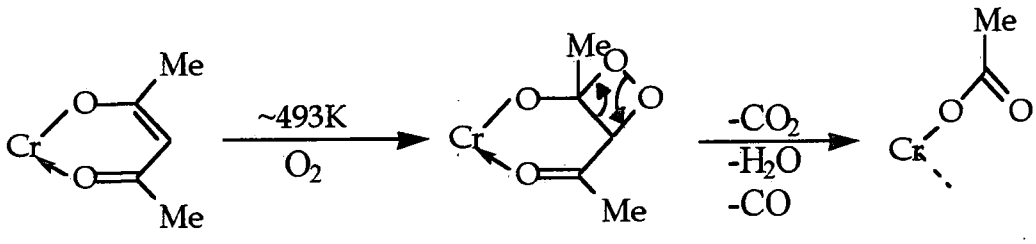

Scheme 2: Proposed mechanism for the first step of oxidative decomposition of $Cr(acac)_3$ / silica

In the second stage of oxidative decomposition, nucleophilic attack by oxygen at the methyl group in the acetate ligand causes C-H and C-C scission to produce carbon dioxide and methylene species (which oxidise to CO_2, H_2O, and a small amount of CO).[37, 38] The slightly higher temperature observed here compared to the chromium(III) acetate/silica investigation may be accounted for in terms of a

potentially different type of bonding/dispersion interaction between the partially decomposed chromium acetylacetonate species with the silica surface due to the different route of chromium acetate formation.

2.4.5 Heating Beyond the Chromium Acetate Decomposition Temperature

Decomposition of supported chromium(III) precursors on silica occurs well below the temperature required to generate an active ethylene polymerization catalyst. Heating beyond the chromium acetate decomposition threshold must be required for subsequent surface rearrangement reactions which includes water elimination via silanol-type condensation reactions at high temperatures. This produces an active ethylene polymerization catalyst.

2.5 Conclusions

Chromium(III) acetate supported on high surface area silica decomposes in a similar way to that observed for bulk chromium acetate under oxygen carrier gas. Therefore, the impregnation of silica with chromium acetate results in the dispersion of small chromium acetate crystallites over the silica surface. Nucleophilic attack by oxygen at the methyl group of the acetate ligand occurs under an oxygen atmosphere to produce carbon dioxide and water.

Chromium(III) acetylacetonate/silica concurrently melts and undergoes a cycloaddition reaction with molecular oxygen followed by bond cleavage to leave behind chromium acetate-like structures supported on silica. These moieties then undergo the same decomposition reaction pathway as observed for chromium(III) acetate/silica, where nucleophilic attack by oxygen at the methyl group of the acetate ligand causes C-C and C-H scission.

Both chromium(III) acetate and chromium(III) acetylacetonate salts supported on silica produce active CrO_x/SiO_2 ethylene polymerization catalysts.

2.6 References

1. Bond, G.C.; Flamerz, S.; Shukri, R. *Faraday Discuss. Chem. Soc.* **1989**, *87*, 225
2. McVicker, G.B; Ziemak, J.J. *J. Catal.* **1985**, *95*, 473
3. Kunimori, K.; Doi, Y.; Ho, K.; Uchijima, T. *J. Chem. Soc. Chem. Commun.* **1986,** 965
4. Hu, Z.; Maeda, A.; Kunimori, K.; Uchijima, T. *Chemistry Letters* **1986,** 2079
5. Beard, B.C.; Ross, P.N. *J. Phys. Chem.* **1986,** *90*, 6811
6. Lin, Y.J.; Resasco, D.E.; Haller, G.L. *J. Chem. Soc. Faraday Trans. 1.* **1987,** *83*, 2091
7. Hu, Z.; Nakamura, H.; Kunimori, K.; Uchijima, T. *Catalysis Letters* **1988,** *1*, 271
8. Clark, A. *Catalysis Reviews* **1969,** *3*, 145
9. Hogan, J.P. *J. Polym. Sci.* A **1970,** *8*, 2637
10. Ellison, A.; Overton, T.L.; Bencze, L. *J. Chem. Soc. Faraday Trans.* **1993,** *89*, 843
11. Bond, G.C.; König, P. *J. Catal.* **1982,** *77*, 309
12. Bond, G.C.; Brückman, K. *Faraday Discuss. Chem. Soc.* **1981,** *72*, 235
13. McDaniel, M.P. *Adv. Catal.* **1985,** *33*, 47
14. Benham, E.A.; Smith, P.D.; Hsieh, E.T.; McDaniel, M.P. *J. Macromol. Sci.-Chem.* **1988,** *A25*, 259
15. Marsden, C.E. *Plastics, Rubber and Composites Processing and Applications* **1994,** *21*, 193
16. Weist, E.L.; Ali, A.H.; Conner, W.C. *Macromolecules* **1987,** *20*, 689
17. Jehng, J.-M.; Wachs, I.E.; Weckhuysen, B.M.; Schoonheydt, R.A. *J. Chem. Soc. Faraday Trans.* **1995,** *91*, 953
18. Hierl, G.; Krauss, H.L. *Z. Anorg. Allg. Chem.* **1975,** *415*, 57
19. Kim, C.S.; Woo, S.I. *J. Mol. Catal.* **1992,** *73*, 249
20. M.P. McDaniel in *Transition Metal Catalyzed Polymerization*; Vol. 4, Part B; MMI Press Symposium Series: 1983; pp713-735

21. Wang, S.; Tait, P.J.T.; Marsden, C.E. *J. Mol. Catal.* **1991,** *65*, 237
22. Lenga, R.E.; *The Sigma-Aldrich Library of Chemical Safety Data* Edition II, Vol. 1; 1988
23. Von Hoene, J.; Charles, R.G.; Hickam, W.M. *J. Phys. Chem.* **1958,** *62*, 1098
24. Cornu, A.; Massot, R.; *Compilation of Mass Spectral Data;* Second Edition; Heydon and Son: London, 1975
25. Ko, E.I.; Benziger, J.B.; Madix, R.J. *J. Catal.* **1980,** *62*, 264
26. Barteau, M.A.; Bowker, M.; Madix, R.J. *Surf. Sci.* **1980,** *94*, 303
27. Iler, R.K.; *Chemistry of Silica;* Wiley: New York, 1979
28. Gallas, J.P.; Lavalley, J.C.; Burneau, A.; Barres, O. *Langmuir* **1991,** *7*, 1235
29. McDaniel, M.P.; Martin, S.J. *J. Phys. Chem.* **1991,** *95*, 3289
30. Nakamoto, K.; *Infrared and Raman Spectra of Inorganic and Coordination Compounds;* Third Edition; Wiley Interscience: New York, 1978
31. *The Polaris FT-IR Spectrometer Owners Guide;* Mattson Instruments Inc., 1986
32. Koenig, J.L.; *Chemical Microstructure of Polymer Chains.*; Wiley: New York, 1980
33. Silverstein, R.M.; Bassler; G.C.; Morrill, T.C.; *Spectrometric Identification of Organic Compounds*; Fifth Edition; John Wiley and Sons: New York, 1991
34. Orgel, L.E. *Nature* **1960,** *187*, 504
35. Figgis, B.N.; Robertson, G.B. *Nature* **1965,** *205*, 694
36. Wilkinson, G. Ed.; *Comprehensive Coordination Chemistry.*; Vol. 3; Pergamon Press: Oxford, 1987
37. Houtman, C.J.; Brown, N.F.; Barteau, M.A. *J. Catal.* **1994,** *145*, 37
38. Sault, A.G.; Madix, R.J. *Surf. Sci.* **1986,** *172*, 598
39. Chudek, J.A.; Hunter, G.; Rochester, C.H.; Smith, T.F.S. *J. Catal.* **1992,** *136*, 246
40. Cotton, F.A.; Lay, D.G. *Inorg. Chem.* **1981,** *20*, 935
41. Barteau, M.A.; Bowker, M.; Madix, R.J. *J. Catal.* **1981,** *67*, 118
42. Aas, N.; Bowker, M. *J. Chem. Soc. Faraday Trans.* **1993,** *89*, 1249

43. Li, Y.; Bowker, M. *Surf. Sci.* **1993,** *285*, 219

44. Li, Y.; Bowker, M. *J. Catal.* **1993,** *142*, 630

45. Kenvin, J.C.; White, M.G.; Mitchell. M.B. *Langmuir* **1991,** *7*, 1198

46. Spencer, M.S. *Nature* **1986,** *323*, 685

47. Vicente, J.; Arcas, A.; Bautista, D.; and Shul'pin, G.B. *J. Chem. Soc. Dalton Trans.* **1994,** 1505

CHAPTER 3. CO REDUCTION OF CALCINED CrO_x / SiO_2 ETHYLENE POLYMERIZATION CATALYSTS

3.1 Introduction

Following calcination under dry oxygen or air atmospheres up to 673-1073 K,[1-5] the Phillips catalyst is cooled to between 373-383 K. Contact with ethylene in the gas phase at this temperature leads to the reduction of the supported hexavalent chromium species[2, 6] in conjunction with methanal evolution[7] during an initiation period; this is followed by the onset of polymerization.[8] An alternative method is to prereduce the calcined catalyst at 623 K using CO, which produces similar polymer product upon ethylene exposure at 373-383 K to that obtained by straightforward ethylene reduction and polymerization[2] via a quantitative reduction to chromium(II).[9, 10] Previous CO reduction studies have been concerned with identifying the nature of the active chromium site using titrimetric [9-11] or adsorption and low-temperature FT-IR[12-16] methods. Krauss *et al.*[17] noted that variations in the activation and/or reduction temperatures result in products of different reactivity, whilst retaining equal Cr(II) content. This is ascribed to the variety of surface species remaining in the support following calcination, which means that neither the bonding of the Cr centre to the silica support, nor the arrangement of the Cr centres in relation to the surface silanol groups and dehydrated siloxane bridges are uniform. Later FT-IR studies[12-16] have identified at least three families of Cr(II) centres which differ in their degree of coordinative unsaturation.

The oxidation of CO over transition metal oxides is reported in the literature to proceed via two routes simultaneously. CO adsorbed on the surface can interact with two oxygen ligands bonded to the same metal centre to form a bridged carbonate species, as identified by IR.[18-20] This species subsequently decomposes to $CO_{2(ads)}$ and an oxygen ligand prior to desorption of the CO_2. Carbon monoxide adsorbed on a surface metal atom with only one oxygen ligand attached will concurrently undergo a straightforward Langmuir-Hinshelwood mechanism to eliminate CO_2.[21]

The activation energy for CO reduction of calcined Phillips-type catalysts has previously only been reported for the partially oxidised CrO_x/alumina system,[21] and not for the fully calcined CrO_x/silica catalyst. The calcination of two Phillips catalyst precursors has been investigated in the previous chapter. In the present chapter, the isothermal reaction of calcined CrO_x/silica material with CO gas has been monitored by quadrupole mass spectrometry in order to obtain activation energies for catalyst reduction.

3.2 Experimental

The two types of CrO_x/silica catalyst precursor (Crosfield Limited) described in the previous chapter were used. Briefly, these comprised silica impregnated with an aqueous solution of basic chromium(III) acetate followed by drying, and a dry-blended mixture of silica with chromium(III) acetylacetonate. Both starting materials contained 1 wt% chromium loading.

Oxygen, argon, and carbon monoxide (BOC; 99.5%, 99.998%, and 99.9% purity respectively) were dried through a conc. H_2SO_4 bubbler, followed by a P_2O_5 drying column and then a 3A molecular sieve (Aldrich) at a flow rate of 1.5 dm^3hr^{-1}. 1 g of catalyst precursor material was loaded into a quartz microreactor tube and heated under a flow of O_2 carrier gas at 1 K min^{-1} up to 1053 K using a Eurotherm temperature controller. The furnace was maintained at this high temperature under flowing O_2 for five hours, prior to switching to an argon gas flow and cooling at 5 K min^{-1} to the appropriate CO reduction temperature. This activation procedure produced a bright orange coloured catalyst.

CO reduction of the calcined CrO_x/silica catalyst was carried out over a range of temperatures (373-773 K) for a 15 minute duration. A Vacuum Generators SX200 quadrupole mass spectrometer multiplexed to a PC computer was used to sample the microreactor outlet via a heated fine capillary tube. For each set of experiments the whole background mass spectrum (0-200 amu) was recorded as a function of time during the CO reduction step, facilitating the identification of CO_2 (mass 44) as the only gaseous reaction product. Then, each experiment was repeated with fresh material, but on this occasion the variation in

the mass 44 peak intensity was measured directly as a function of time in order to obtain the corresponding reduction isotherm.

Polymerization activity was confirmed by the procedure described in chapter 4.

3.3 Results

Exposure of the calcined CrO_x/silica catalyst to CO gas displayed a delayed response in the mass 28(CO) intensity, Figure 1. This comprised a small dip, after which the signal increased to its saturation value with concurrent CO_2 production. This behaviour was absent if the experiment was repeated with just the SiO_2 support material.

Typical CO reduction isotherms are shown in Figure 2. Exposure of CO gas at 573 K or above was found to cause a colour change in the catalyst from bright orange to pale blue/green. The amount of CO_2 evolved at these temperatures was measured to be approximately the same in all cases. During subsequent air exposure these reduced CrO_x/silica catalysts produced a bright orange chemiluminescence to leave behind an orange/brown residue; this can be attributed to a metal $\rightarrow$ ligand charge transfer mechanism.[22]

CO reduction of the oxidised CrO_x/silica catalysts at or below 473 K exhibited no variation in colour and produced a smaller amount of CO_2. This can be taken as being indicative of incomplete reduction of the calcined CrO_x/silica material. Furthermore, it can be seen that as the reduction temperature is lowered, the induction period for CO_2 evolution and the time required to reach completion (i.e. for the CO_2 signal to return to the baseline) increases.

Ethylene polymerization activity at 383 K was checked for both the fully oxidised and CO reduced CrO_x/silica catalysts. The formation of white polymer granules was immediately evident for the latter, whereas it took approximately 90 min for the former due to its inherent induction period.

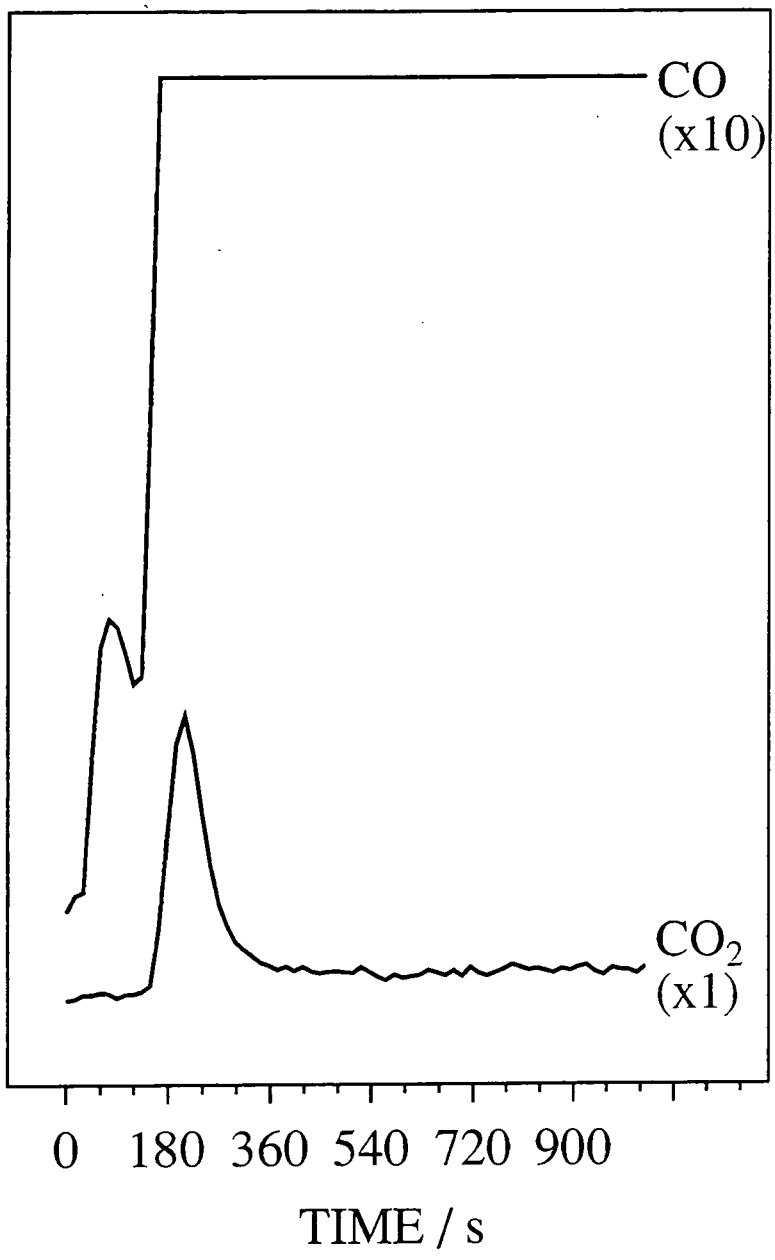

Figure 1: Profiles of mass 28 (CO) and mass 44 (CO_2) upon exposure of the calcined CrO_x/silica catalyst to CO gas. N.B. The top of the CO profile corresponds to saturation in the response of the mass spectrometer detector.

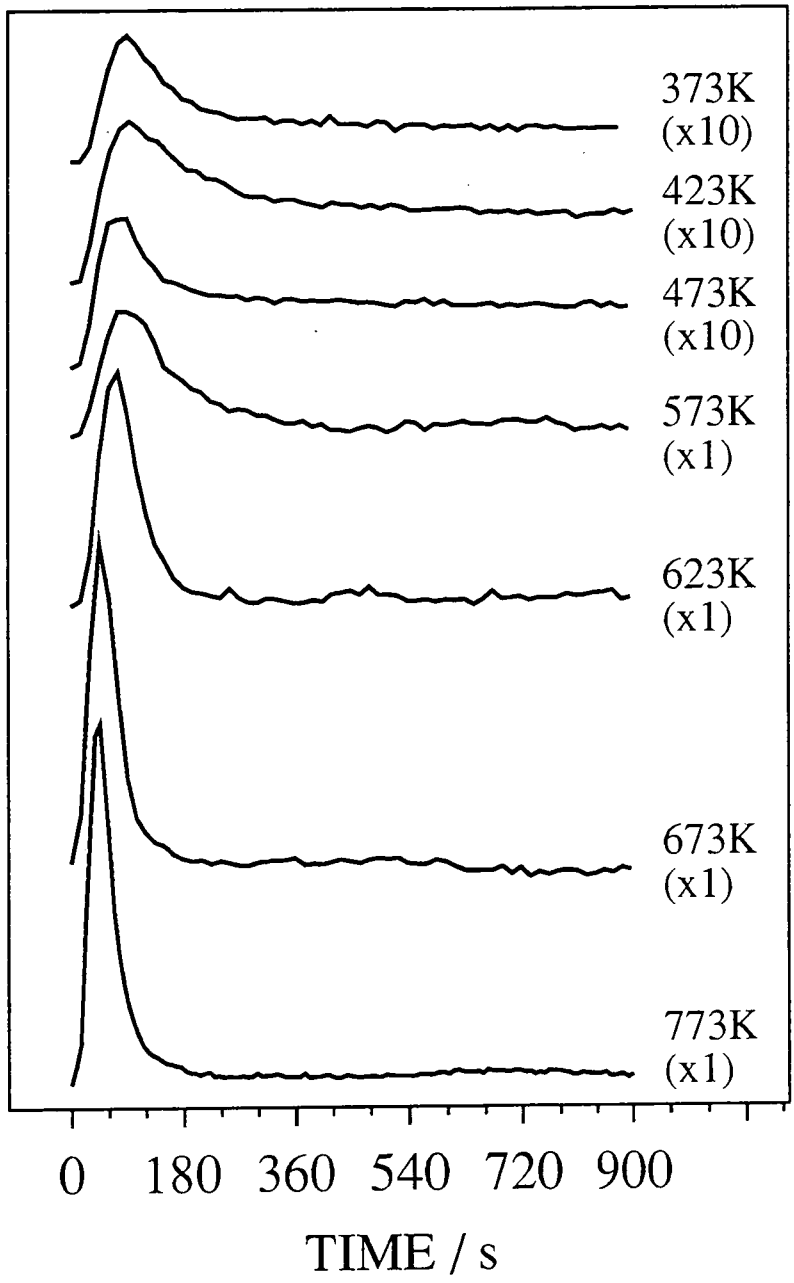

Figure 2(a): CO_2 evolution isotherms obtained by the treatment of calcined CrO_x/silica catalyst derived from chromium(III) acetate/silica precursor material.

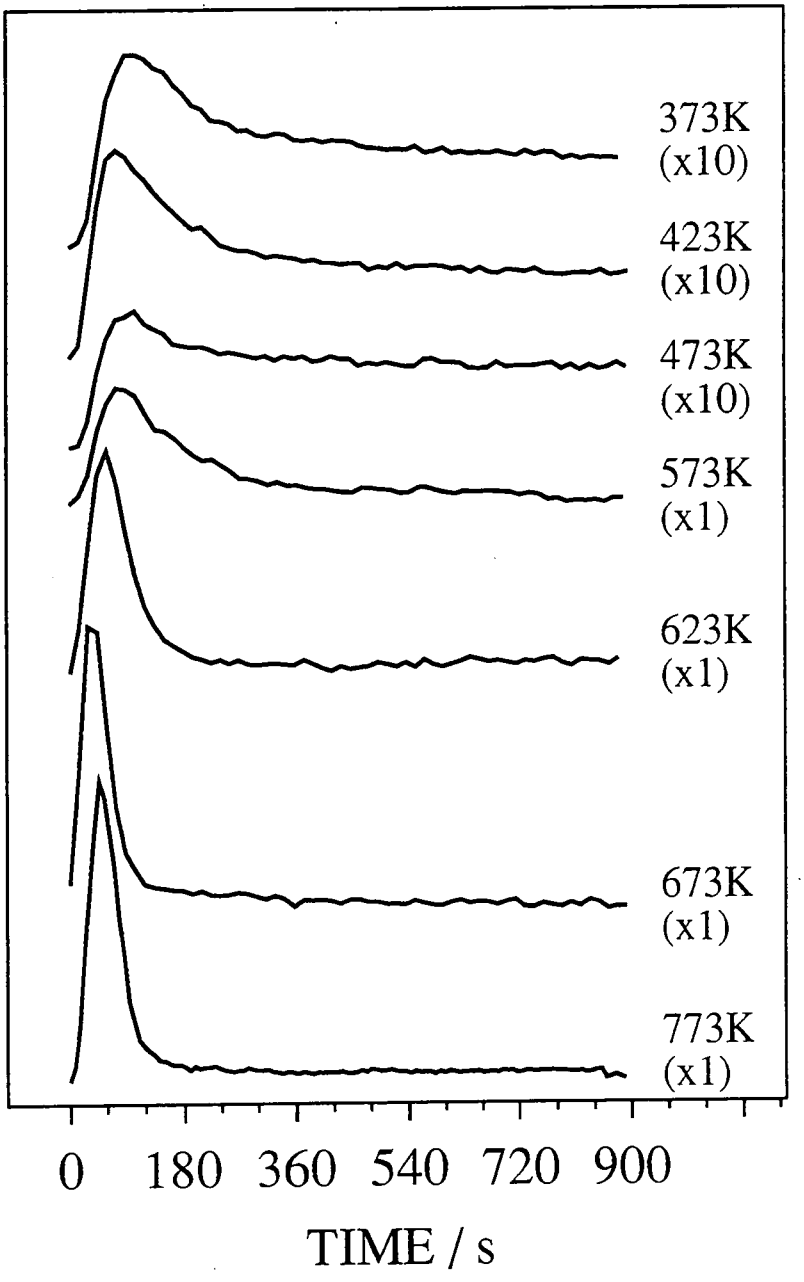

Figure 2(b): CO_2 evolution isotherms obtained by the treatment of calcined CrO_x/silica catalyst derived from chromium(III) acetylacetonate/silica precursor material.

3.4 Discussion

The very similar CO reduction behaviour of the two different types of CrO_x/silica precursor is consistent with the fact that the dry-blended $Cr(acac)_3$/silica material proceeds via a chromium acetate/silica intermediate during calcination,[23] as discussed in chapter 2. CO treatment of calcined CrO_x/silica is reported to quantitatively reduce Cr(VI) to Cr(II) centres at 623 K at 98% efficiency,[9, 10] with the remaining 2% of metal sites being incorporated as clustered α-chromia-like particles.[11] The present observation that the same amount of CO_2 is evolved for each catalyst at reduction temperatures greater than 573 K confirms that the reaction of CO with CrO_x/silica is quantitative.[8, 9, 21]

There are two possible reaction pathways which could account for the observed oxidation of CO to CO_2 by the calcined CrO_x/silica catalyst: the Eley-Rideal mechanism, which involves the reaction of gas phase CO with surface oxygen atoms:

$$CO + [O]_{surf} \rightarrow CO_2$$

or alternatively, the Langmuir-Hinshelwood mechanism, which requires both reactants to be adsorbed onto the catalyst surface prior to reaction taking place:

$$CO_{ads} + [O]_{surf} \rightarrow CO_2$$

Numerous metal single crystal modelling studies have led to a general agreement that the Langmuir-Hinshelwood mechanism is most common.[24-28] Reduction of the hexavalent CrO_x/alumina catalysts has been previously reported to proceed via a Langmuir-Hinshelwood reaction pathway.[21] In the present study, the m/e 28 (CO) profiles display a small dip prior to a rise in signal towards full intensity, Figure 1. This can be attributed to the adsorption of CO onto the CrO_x/silica catalyst surface prior to reaction, which is consistent with a Langmuir-Hinshelwood mechanism.

If the rate of CO_2 evolution is measured for the very early stages of reaction, it can be assumed that the relative decrease in oxygen coverage is negligible.[25] Arrhenius plots of ln(rate) versus 1/T can then be used to calculate the true activation energy for CO reduction of calcined CrO_x/silica catalysts.[25, 27] The initial slopes of the CO_2 evolution isotherms correspond to the rate of CO_2 production (in arbitrary rate units of counts per second). For each catalyst precursor, the respective Arrhenius plot displays two linear regimes with a discontinuity occurring between 423 and 473 K, Figure 3. The high temperature portion corresponds to activation energies of 44.7 ± 4 kJ mol^{-1} for the catalyst prepared by the impregnation of silica with aqueous chromium(III) acetate, and 43.5 ± 4 kJ mol^{-1} for the dry-blended $Cr(acac)_3$/silica catalyst. These values do not compare well with the theoretically calculated value of 95 ± 19 kJ mol^{-1} for the CO reduction of partly oxidised CrO_x/alumina catalyst.[21] This discrepancy may be explained in terms of the degree of oxidation at the catalyst surface, since only a partly oxidised surface was used in the latter case, also the CrO_x/alumina catalysts contained a much higher (10 wt%) chromium loading compared to the 1 wt% employed in the present study. Both of these factors could effect the dispersion of chromium species across the support surface and hence influence the activation energy for reaction. The difference between SiO_2 and Al_2O_3 support materials may also be a contributing factor. The observed discontinuity in the Arrhenius plots may be rationalized in terms of the broad heterogeneity of chromium sites contained in CrO_x/silica catalysts. Carbon monoxide poisoning[29] and temperature programmed reduction (TPR)[1, 30, 31] experiments have previously shown that several types of active Cr(VI) sites can exist, which differ in their reducibility. Furthermore, FT-IR studies of carbon monoxide adsorbed onto reduced CrO_x/silica catalysts have suggested the presence of at least three families of chromium(II) site.[12-16] Therefore the reduction of the various types of Cr(VI) species to each of the respective Cr(II) centres may account for the observed break in the Arrhenius plots. At temperatures greater than 573 K, it appears that there is sufficient energy for all of the Cr(VI) species to be converted to Cr(II) species, whilst at lower temperatures there may only be sufficient energy for the reduction of certain types of Cr(VI) centre. These observations fit in well with

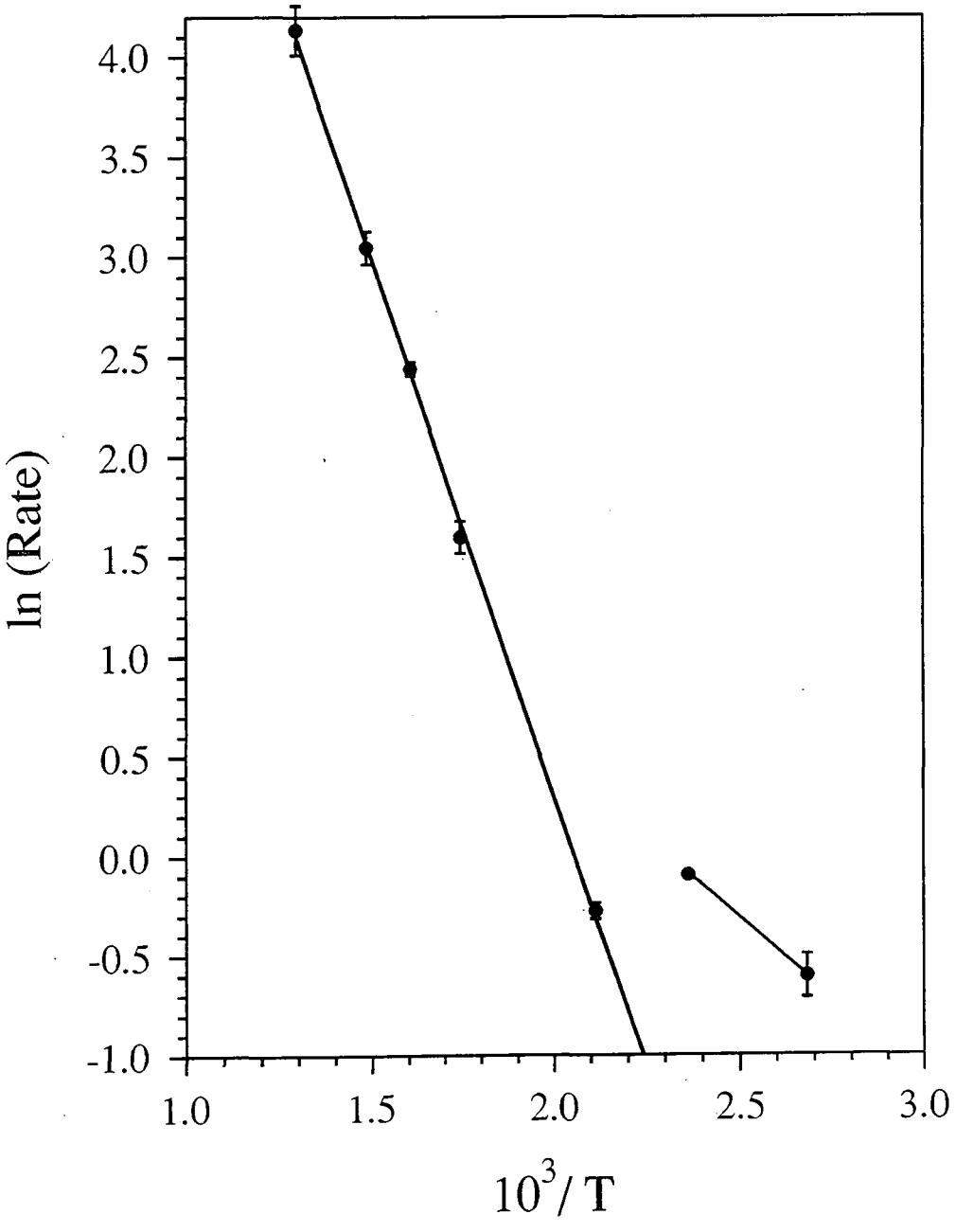

Figure 3(a): Arrhenius plot obtained by plotting ln(initial slope of CO_2 profile) (i.e. ln(rate) in arbitrary units) against 1/T for calcined chromium(III) acetate/silica.

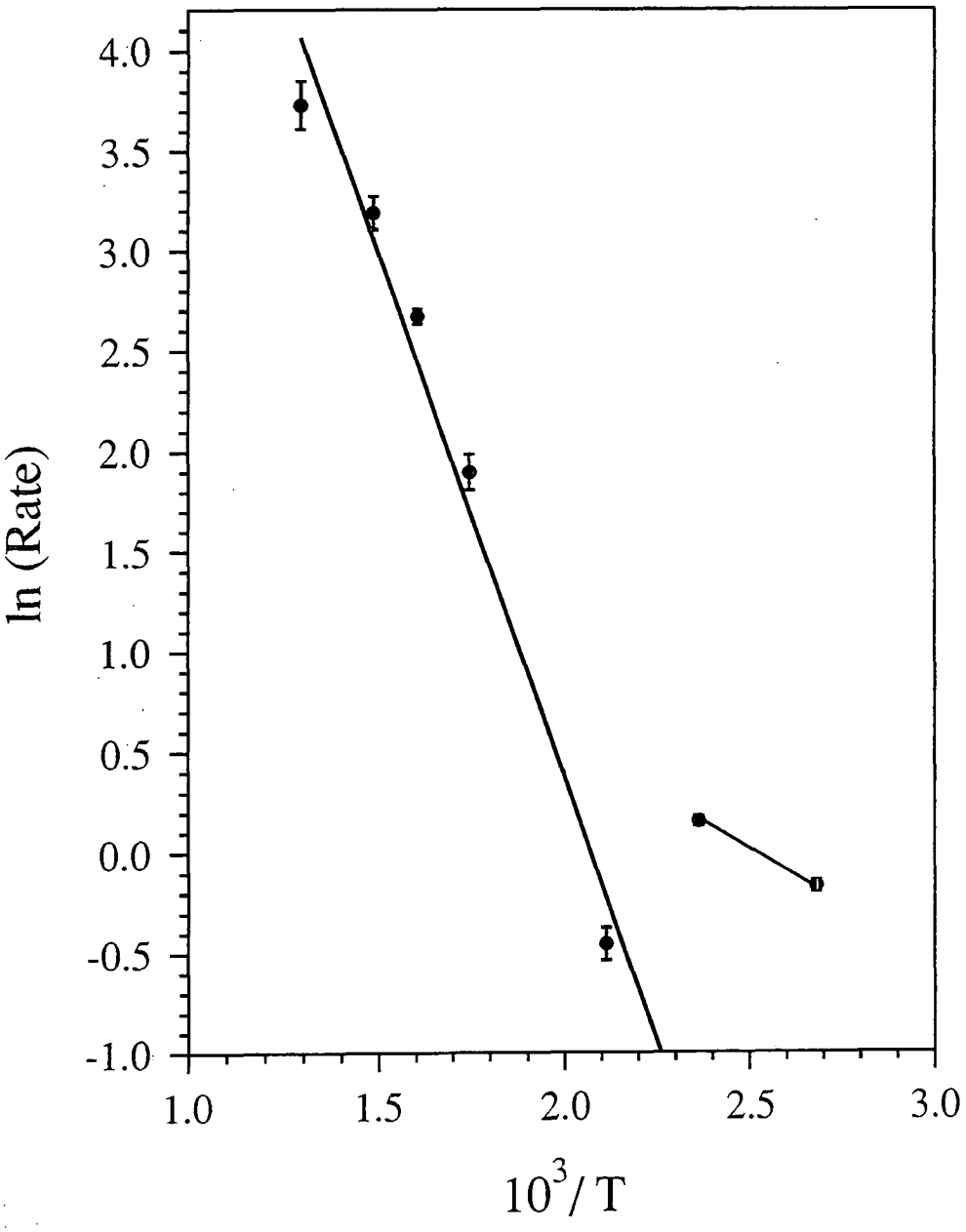

Figure 3(b): Arrhenius plot obtained by plotting ln(initial slope of CO_2 profile) (i.e. ln(rate) in arbitrary units) against 1/T for calcined chromium(III) acetylacetonate/silica.

the widely reported consensus that 623 K is the optimum CO reduction temperature,[9, 10] since this is sufficient to ensure complete reduction, but not so high as to lead to a loss in ethylene polymerization activity.[2, 14]

3.5 Conclusions

Isothermal quadrupole mass spectrometry measurements have shown that calcined CrO_x/silica undergoes CO reduction via a Langmuir-Hinshelwood type mechanism. Arrhenius plots for CO_2 formation comprise two linear portions, corresponding to the reduction of different types of chromium(VI) sites to a variety of Cr(II) centres. Complete reduction occurs at temperatures greater than 573 K, regardless of whether chromium(III) acetate/silica or chromium(III) acetylacetonate dry-blended with silica were originally used as the precursor material.

3.6 References

1. Ellison, A.; Overton, T.L., Bencze; L. *J. Chem. Soc. Faraday Trans.* **1993**, *89(5)*, 843
2. McDaniel, M.P. *Adv. Catal.* **1985**, *33*, 47
3. Clark, A. *Catalysis Reviews* **1969**, *3*, 145
4. Benham, E.A.; Smith, P.D.; Hsieh, E.T.; McDaniel, M.P. *J. Macromol. Sci.-Chem.* **1988**, *A25*, 259
5. Hogan, J.P. *J. Polym. Sci.; A-1.* **1970**, *8*, 2637
6. Marsden, C.E. *Plastics, Rubber and Composites Processing and Applications* **1994**, *21*, 193
7. Baker, L.M.; Carrick, W.L. *J. Org. Chem.* **1968**, *33*, 616
8. Xie, T.; McAuley, K.B.; Hsu, J.C.C.; Bacon, D.W. *Ind. Eng. Chem. Res.* **1994**, *33*, 449
9. Krauss, H.L.; Stach, H. *Inorg. Nucl. Chem. Lett.* **1968**, *4*, 393

10. Krauss, H.L.; Stach, H. *Z. Anorg. Allg. Chem.* **1969**, *366*, 280
11. Fubini, B.; Ghiotti, G.; Stradella, L.; Garrone, E.; Morterra, C. *J. Catal.* **1980**, *66*, 200
12. Kohler, S.D.; Ekerdt, J.G. *J. Phys. Chem.* **1994**, *98*, 4336
13. Zielinski, P.A.; Szymura, J.A.; Dalla Lana, I.G. *Cat. Lett.* **1992**, *13*, 331
14. Zecchina, A.; Spoto, G.; Ghiotti, G.; Garrone, E. *J. Mol. Catal.* **1994**, *86*, 423
15. Nishimura, M.; Thomas, J.M. *Catal. Lett.* **1993**, *21*, 149
16. Rebenstorf, B. *Acta Chem. Scand.* **1989**, *43*, 413
17. Krauss, H.L.; Rebenstorf, B.; Westphal, U. *Z. Anorg. Allg. Chem.* **1975**, *414*, 97
18. Tascón, J.M.D.; García Fierro, J.L.; González Tejuca, L. *Z. Phys. Chem. Neue Folge.* **1981**, *124*, 249
19. Little, A.H.; Amberg, C.H. *Can. J. Chem.* **1962**, *40*, 1997
20. Zecchina, A.; Ghiotti, G.; Morterra, C.; Borello, E. *J. Phys. Chem.* **1969**, *73*, 1295
21. Dekker, F.H.M.; Klopper, G.; Bliek, A.; Kapteijn, F.; Moulijn, J.A. *Chem. Engng. Sci.* **1994**, *49*, 4375
22. Morys, P.; Gerritzen, R.; Krauss, H.L. *Z. Naturforsch.* **1976**, *31b*, 774
23. Ruddick, V.J.; Dyer, P.W.; Bell, G.; Gibson, V.C.; Badyal, J.P.S. *J. Phys. Chem.* **1996**, *100*, 11062
24. Peden, C.H.F.; Goodman, D.W. *J. Phys. Chem.* **1986**, *90*, 1360
25. Engel, T.; Ertl, G. *J. Chem. Phys.* **1978**, *69(3)*, 1267
26. Campbell, C.T.; Ertl, G.; Kuipers, H.; Segner, J. *J. Chem. Phys.* **1980**, *73(11)*, 5862
27. Gland, J.L.; Kollin, E.B. *J. Chem. Phys.* **1983**, *78(2)*, 963
28. Engel, T.; Ertl, G. *Adv. Cat.* **1979**, *28*, 1
29. McDaniel, M.P.; Martin, S.J. *J. Phys. Chem.* **1991**, *95*, 3289
30. Ellison, A.; Overton, T.L. *J. Chem. Soc. Faraday Trans.* **1993**, *89(24)*, 4393
31. Kim, C.S.; Woo, S.I. *J. Mol. Catal.* **1992**, *73*, 249

CHAPTER 4. THE EARLY STAGES OF ETHYLENE POLYMERIZATION USING THE PHILLIPS CrO_X/SILICA CATALYST

4.1 Introduction

The polymerization of ethylene by CrO_x/silica catalysts has been widely studied, and a variety of different mechanisms have been put forward. The overall reaction pathway may be broken down into three separate stages: initiation, propagation, and chain termination.[1, 2] Initiation encompasses the attachment of the very first monomer unit to the catalytic site. Subsequent ethylene molecules add on during the propagation step to form alkyl chains fixed to the chromium centre. Termination involves the separation of the polymer chain away from the catalyst surface. The propagation and termination steps are well understood, and are therefore described first.

Two types of mechanism are generally accepted for the propagation of transition metal catalyzed olefin polymerization systems: these are known as the Cossee[3] and Green-Rooney[4] mechanisms after the researchers who first proposed them. The Cossee mechanism[3] requires a vacant coordination site on the metal centre in the position adjacent to the growing alkyl chain. A monomer molecule then π-bonds to the metal via this site, followed by a migratory insertion reaction which extends the growing alkyl chain by one monomer unit (thereby regenerating the vacant coordination site on the metal centre). This is summarized in Scheme 1, where [M] is the metal centre, R is the growing polymer chain, and □ is the vacant coordination site.

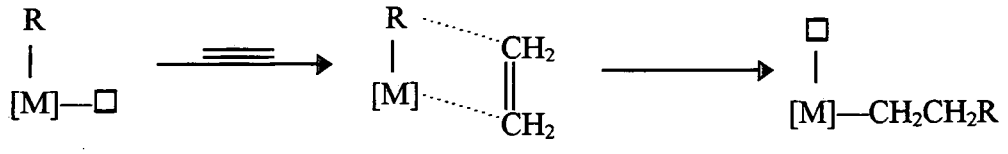

Scheme 1: The Cossee mechanism

The Green-Rooney mechanism[4] requires two vacant coordination sites at the metal centre. The growing polymer chain first eliminates an α-hydrogen to produce a metal-carbene species. An ethylene molecule then coordinates at the remaining vacant site. This is followed by addition across the metal-carbene double bond in a metathesis-type reaction to form a metallacycle species. Reductive elimination causes the ring to open, thus producing an alkyl chain which has been extended by one monomer unit along with the original two vacant coordination sites at the metal centre, Scheme 2.

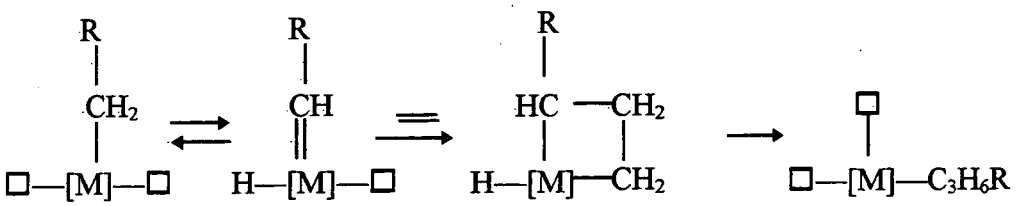

Scheme 2: The Green-Rooney Mechanism.

Termination is understood to occur via β-H elimination.[1, 5] This mechanism not only fits the known chemistry of metal alkyls, but also produces polymer containing vinyl groups at the terminating end. Infrared and NMR analysis has shown that polymer chains usually contain one vinyl and one methyl end group.[1] Quick-kill experiments have identified the presence of methyl groups during the early stages of reaction, but the absence of any vinyl centres;[1] this has been interpreted as an indication of methyl group formation upon initiation, and vinyl group production during termination.

The initiation step for the Phillips CrO_x/silica ethylene polymerization catalyst is poorly understood, and in the past has mainly been studied by infrared spectroscopy.[6-13] The present investigation employs quadrupole mass spectrometry to identify the gaseous species evolved during ethylene polymerization over CrO_x/silica catalysts which have been calcined and then reduced by CO. Using a CO reduction pretreatment has the advantage that any potential overlap with the induction period normally observed during ethylene exposure to the calcined CrO_x/silica catalyst[1] is eliminated.

4.2 Experimental

The CrO_x/silica catalyst precursor was prepared by impregnating silica with an aqueous solution of basic chromium(III) acetate and then drying, as described in chapter 2. Oxygen, argon, and carbon monoxide (BOC; 99.5%, 99.998%, and 99.9% purity respectively) were dried through a conc. H_2SO_4 bubbler, followed by a P_2O_5 drying column, and then a 3A molecular sieve (Aldrich), at a flow rate of 1.5 dm^3hr^{-1}. Ethylene (Scott Specialty Gases; 99.8% purity) was dried through a P_2O_5 drying column, followed by a 3A molecular sieve at a flow rate of 1.5 dm^3hr^{-1}. Deuterated ethylene (C_2D_4, MSD Isotopes; 99% minimum isotopic purity) was used at a flow rate of 1.5 dm^3hr^{-1} without further purification.

1 g of catalyst precursor material was loaded into a quartz microreactor tube and activated as described in chapters 2 and 3. Briefly, this comprised heating under a flow of oxygen up to 1053 K for 5 hours, and then cooling to 623 K prior to a 15 minute exposure to CO gas. The temperature of the activated catalyst was then lowered to 383 K under argon, at this point either ethylene or deuterated ethylene were introduced to make up a 50:50 mixture with argon. In the case of C_2H_4, a 15 minute exposure was used, whilst C_2D_4 was passed over the pre-reduced catalyst CrO_x/silica for 20 minutes. Upon completion of each experiment, the reactor was allowed to cool to room temperature under a flow of argon.

A Vacuum Generators SX200 quadrupole mass spectrometer multiplexed to a PC computer was connected via a heated fine capillary tube to the microreactor outlet as described in chapter 2 For each set of experiments, the whole background mass spectrum (0-200 amu) was recorded during ethylene exposure as a function of time, hence facilitating the identification of all the desorbing species during polymerization. Each experiment was then repeated using freshly activated catalyst, but this time the intensities of the previously identified mass peaks were determined with time, enabling a corresponding set of reaction profiles to be obtained.

The white powdered material produced during each experiment was mixed with potassium bromide and pressed into disks, then analyzed by infrared spectroscopy using a FTIR Mattson Polaris instrument. Typically 100 scans were acquired at a resolution of 4 cm^{-1}.

4.3 Results

CO reduction of the calcined CrO_x/silica catalyst caused a change in its appearance from bright orange to pale blue/green. Subsequent exposure of ethylene to this activated catalyst at 383 K was found to be accompanied by a delay in the m/e 28 (C_2H_4) signal intensity, followed by a small dip, prior to gradually increasing towards a saturation value (this behaviour was not observed either in the absence of activated CrO_x/silica catalyst, or in the presence of calcined silica, Figure 1). The rise after the dip coincides with a small pulse of masses 41, 42, 43 and 56 (maximum intensity ~1/3000 of the saturation value for ethylene). These mass fragments are characteristic of many different types of hydrocarbon species.[14] The presence of mass 43 suggested that the desorbing hydrocarbon molecules must contain at least 3 saturated carbon atoms, i.e. this rules out butene and propene. On comparing mass fragmentation patterns,[14] 1-hexene and 1-octene were found to be the only possible contenders. A more specific assignment was carried out by comparing the measured m/e 56:43 ratio (=1.4) with values obtained using reference hydrocarbon compounds (1-hexene =1.4, 1-octene =0.65). These observations suggest that 1-hexene is produced during the initiation step of ethylene polymerization over a CO pre-reduced CrO_x/silica catalyst.

Further experiments using deuterated ethylene were carried out in order to verify the formation of 1-hexene during the initial stages of polymerization over the pre-reduced CrO_x/silica catalyst, and also to find out whether hydrogen species from the support participate in this reaction. The major fragment for fully deuterated 1-hexene will be mass 46, or 45 if there is a hydrogen atom present (these mass fragments correspond to 41 in the case of non-deuterated 1-hexene); whilst the second largest fragment is expected to be mass 64 if fully deuterated,

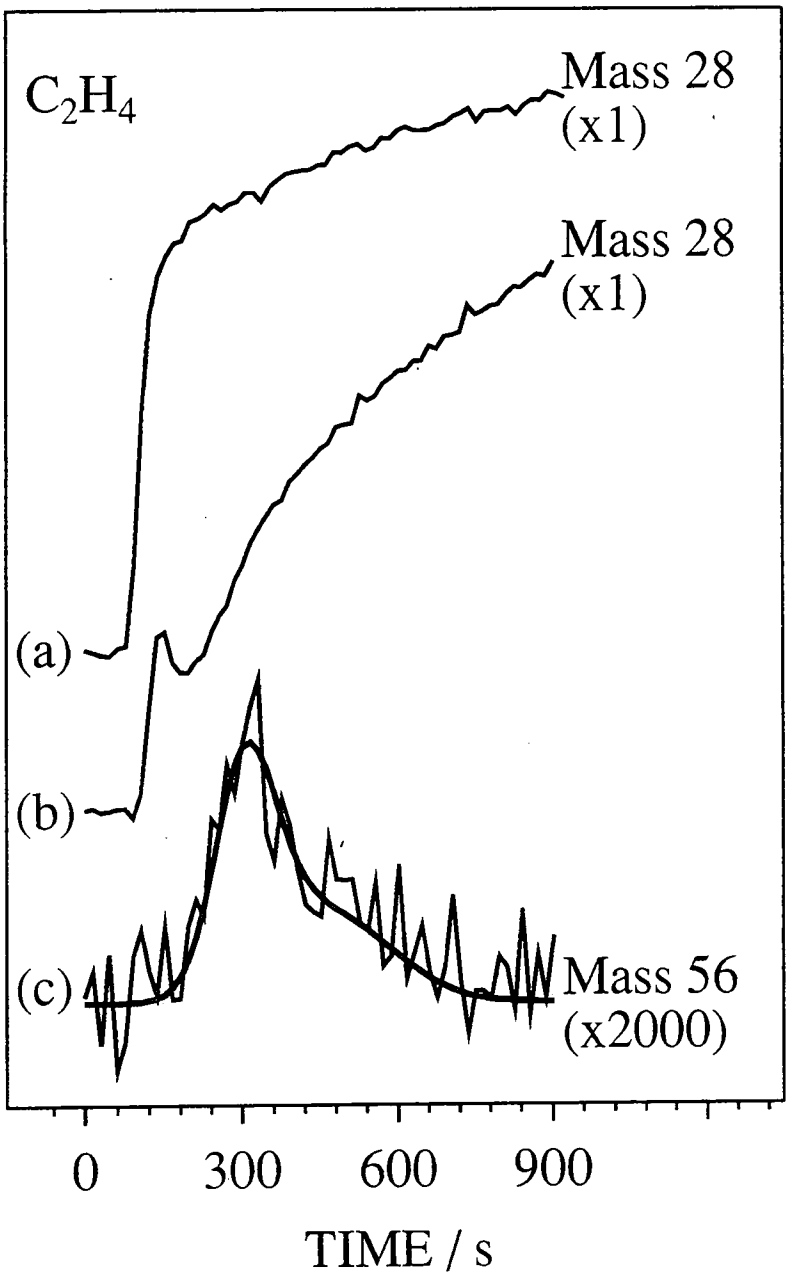

Figure 1: Mass signal intensities: (a) m/e 28 response during ethylene exposure to calcined silica; (b) m/e 28 response during ethylene exposure to calcined and pre-reduced CrO_x/SiO_2 catalyst; and (c) m/e 56 evolution for (b).

or 63 if a hydrogen atom is present (these mass fragments correspond to 56 in the case of non-deuterated 1-hexene). Exposure of the CO pre-reduced CrO_x/silica catalyst to C_2D_4 resulted in the evolution of only fully deuterated 1-hexene mass fragments, i.e. masses 46 and 64, Figures 2 and 3. This suggests that no additional hydrogen atoms are involved during the initiation step. The possibility of 1-hexene being produced via dimerization of trace amounts of propene impurity in the ethylene gas was also eliminated, since the deuterated ethylene was not found to contain any propene impurity.

For both monomers, polymerization resulted in the production of white granules, which were confirmed by FTIR to be polyethylene, Figure 4. In the case of C_2H_4, absorbances were identified at: 2920 and 2850 cm^{-1} (C-H stretches), 1469 cm^{-1} (methylene bending mode), and 719 cm^{-1} (methylene rocking mode).[15] All remaining absorbances could be assigned to the silica support material.[16] Polymer produced using C_2D_4 gave rise to the expected $\sim 1/\sqrt{2}$ shift in C-D stretching frequency (i.e. 2193 and 2083 cm^{-1}) compared to the C-H absorbances observed for C_2H_4 polymerization.[17]

4.4 Discussion

The initiation step for ethylene polymerization has primarily been studied by infrared spectroscopy in the past. Hogan[5] suggested that polymer chains were initiated by monomer insertion into a M-H bond; the resulting metal-alkyl species then propagating via a Cossee mechanism.[3] A prerequisite for this scheme is that there must be a M-H bond present prior to the onset of polymerization. Some groups have suggested that surface silanol groups provide a source of additional hydrogen atoms.[6, 18] Hydride transfer may occur between a silanol group and a supported Cr^{2+} ion to yield an O^{2-} species and a Cr^{3+}-H bond (into which the first ethylene can insert).[18] Alternatively, it has been proposed that ethylene adsorption directly onto a surface silanol group is followed by its coordination to an adjacent chromium ion along with the migration of a proton from the silanol group onto the metal centre.[6] Mechanisms such as these, which involve silanol

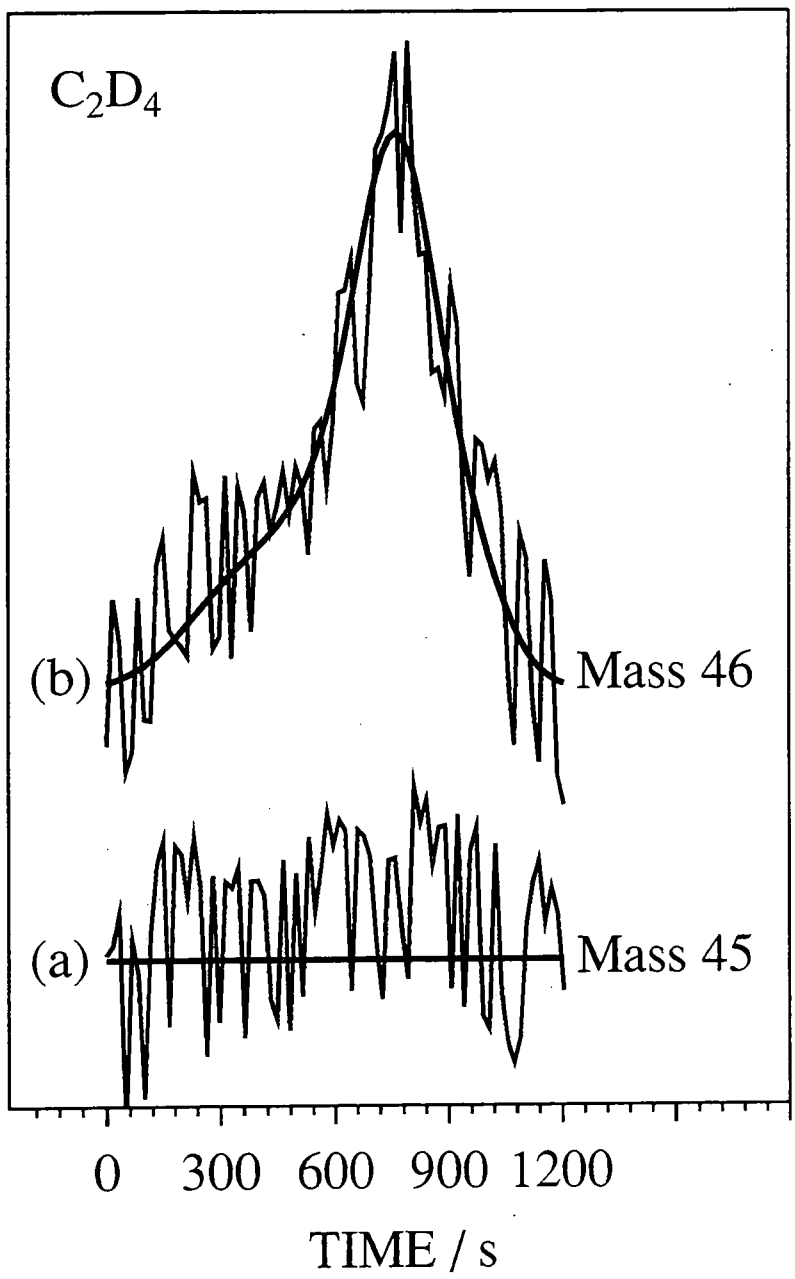

Figure 2: Mass profiles during exposure of calcined and pre-reduced CrO_x/SiO_2 catalyst to deuterated ethylene (C_2D_4): (a) m/e 45; and (b) m/e 46.

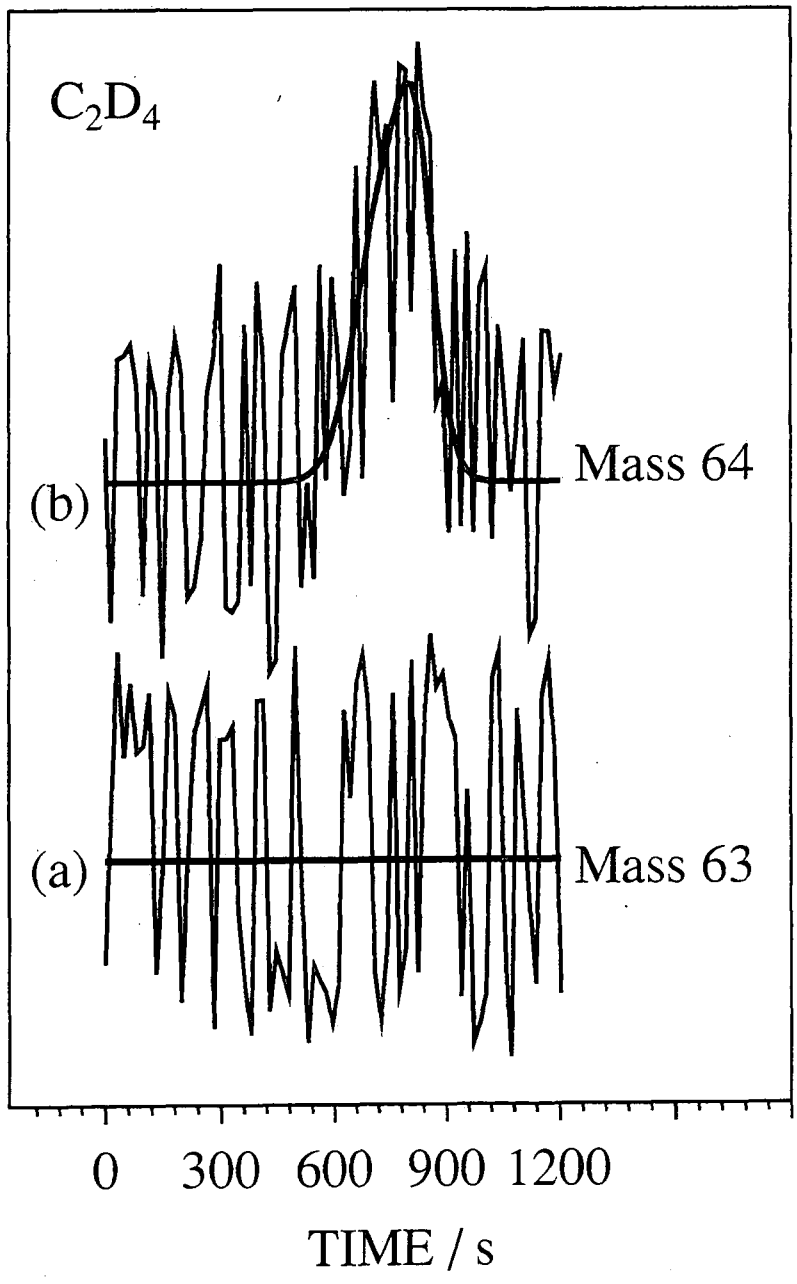

Figure 3: Mass profiles during exposure of calcined and pre-reduced CrO_x/SiO_2 catalyst to deuterated ethylene (C_2D_4): (a) m/e 63; and (b) m/e 64.

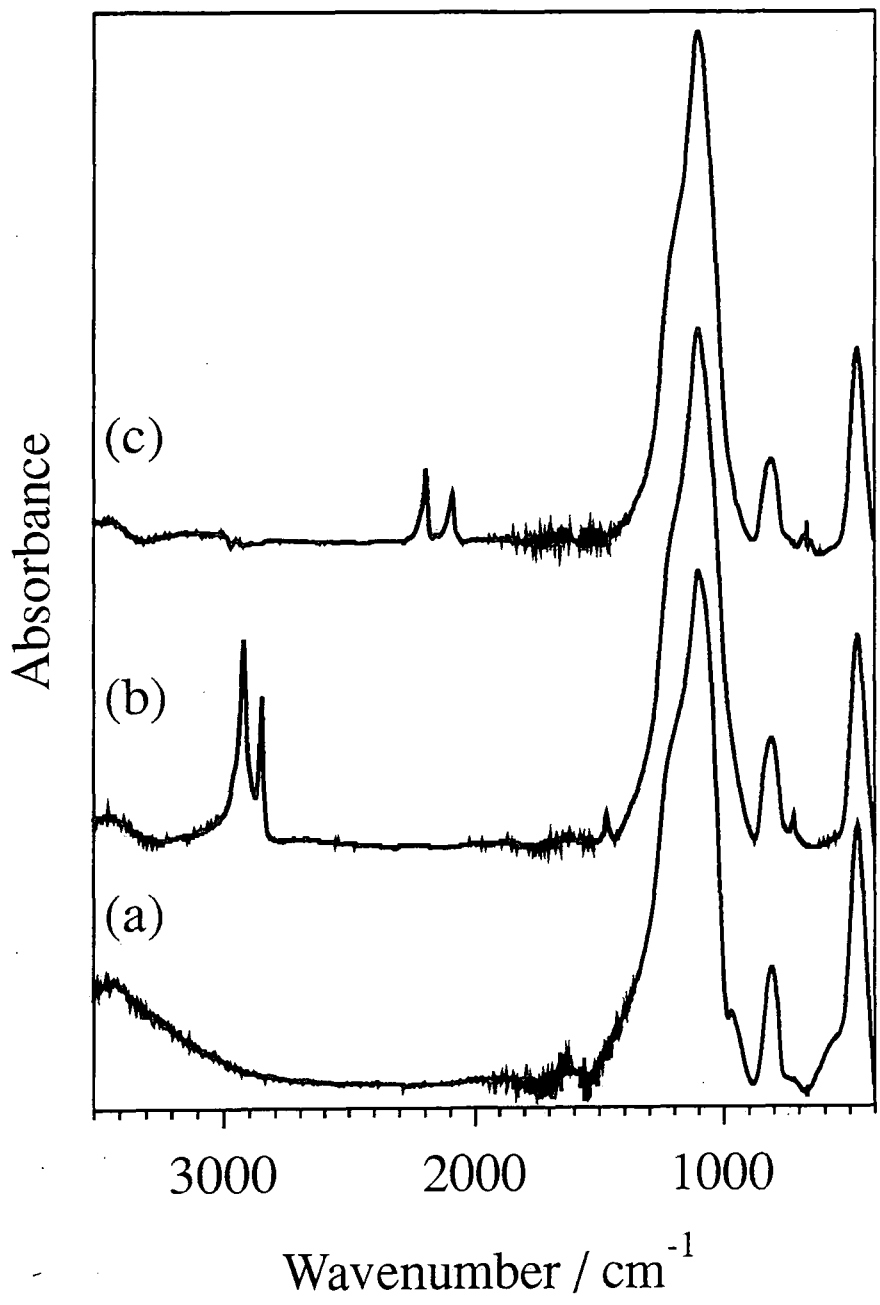

Figure 4: FTIR spectra of (a) silica support material; (b) polymer formed using ethylene (C_2H_4); and (c) polymer formed using deuterated ethylene.

species, are considered by some to be unlikely,[1] since excellent catalysts have been reported to be obtained using completely dehydroxylated precursor materials.

Metallacyclic and/or carbene reaction intermediates circumvent the prerequisite for a source of additional hydrogen atoms. For example, the interaction of two ethylene molecules coordinated to the same chromium centre can lead to the formation of a metallacyclopentane species. This can then β-eliminate to generate an allyl species[1] which may then demonstrate chain growth at either the monohapto chromium-allyl bond or at the Cr-H bond. Alternatively, the metallacyclopentane species may undergo α-hydrogen elimination onto an oxygen atom bridging between the chromium centre and the support to produce a metallacyclocarbene structure.[7] Such an intermediate can then undergo propagation via a Green-Rooney[4] type mechanism. Another possibility involves the generation of carbene species via the dissociative adsorption of ethylene on to two adjacent chromium sites.[9] A second ethylene molecule then forms an alkyl chain bridge between the two chromium sites which can subsequently propagate via either the Cossee[3] or the Green-Rooney[4] mechanism. More recently it has been suggested that adsorption of ethylene onto a chromium site to form a linear carbene species via π-complexation and rearrangement may occur.[8] Propagation is then predicted to occur via a modified Green-Rooney mechanism, where ethylene adds across the carbene double bond to form a metallacycle which then undergoes α-hydrogen elimination. Reductive elimination of this hydrogen opens up the ring to regenerate a linear carbene species which has been extended by one monomer unit.[8]

In the present study, the observed dip in ethylene signal prior to its rise towards maximum intensity during exposure to the pre-reduced CrO_x/silica catalyst occurs before there is any evolution of oligomeric mass fragments. This is consistent with ethylene adsorption onto the catalyst surface taking place first, prior to reaction at the surface. The deuterated ethylene experiments produced fully deuterated 1-hexene fragments, thereby proving that no additional hydrogen atoms are required for the initiation step (e.g. from surface silanols[6, 18]); this observation implies that a conventional linear mechanism[3, 5] is not responsible for

the 1-hexene formation since it would require a M-H bond for ethylene to insert into, Scheme 3. Also, this type of linear mechanism offers no explanation as to why the oligomeric chains terminate upon reaching 6-carbon atoms.

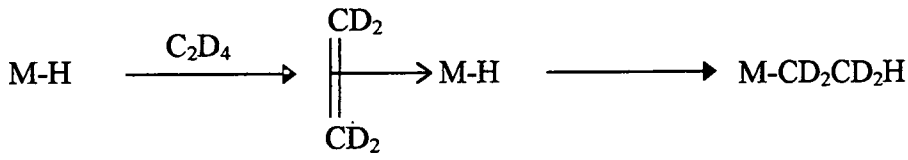

Scheme 3: Chain initiation via insertion into an M-H bond.

Selective trimerization of ethylene to form 1-hexene has previously been reported for homogeneous chromium centre catalysts, and proposed to proceed via metallacyclic intermediates.[19-21] This involves the coordination of two ethylene molecules to each chromium centre followed by rearrangement to form a chromacyclopentane species. Another ethylene molecule then inserts into the ring to create a highly reactive chromacycloheptane.[19-21] This is consistent with small rings (<7-membered) being unable to β-eliminate easily,[19, 22] and is analogous to ethylene insertion into a metallacyclobutane ring.[23] Metallacycloheptane is conformationally flexible enough to achieve the M-C-C-H planarity required for β-H elimination,[22] which will yield 1-hexene and the original chromium species if followed by reductive elimination, Scheme 4.

If 1-hexene is produced, as suggested, via a chromacyclopentane species, then it is possible that the initiation of polymerization may also proceed via this intermediate. Although β-H elimination from chromacyclopentane is inhibited, α-H elimination to either the chromium atom or to a surface oxygen atom[7, 24] could lead to the formation of a reactive cyclic carbene species, Scheme 4. In the case of the transferal of a hydrogen atom onto the chromium centre, subsequent reductive elimination of hydrogen will produce a linear carbene species, which may then propagate via a modified Green-Rooney type mechanism[8] (this involves the addition of ethylene across the carbene double bond to form a metallacyclobutane species). Alternatively, the cyclic carbene species created by hydrogen transfer to a surface oxygen atom may propagate via a modified Green-Rooney mechanism.[7, 24]

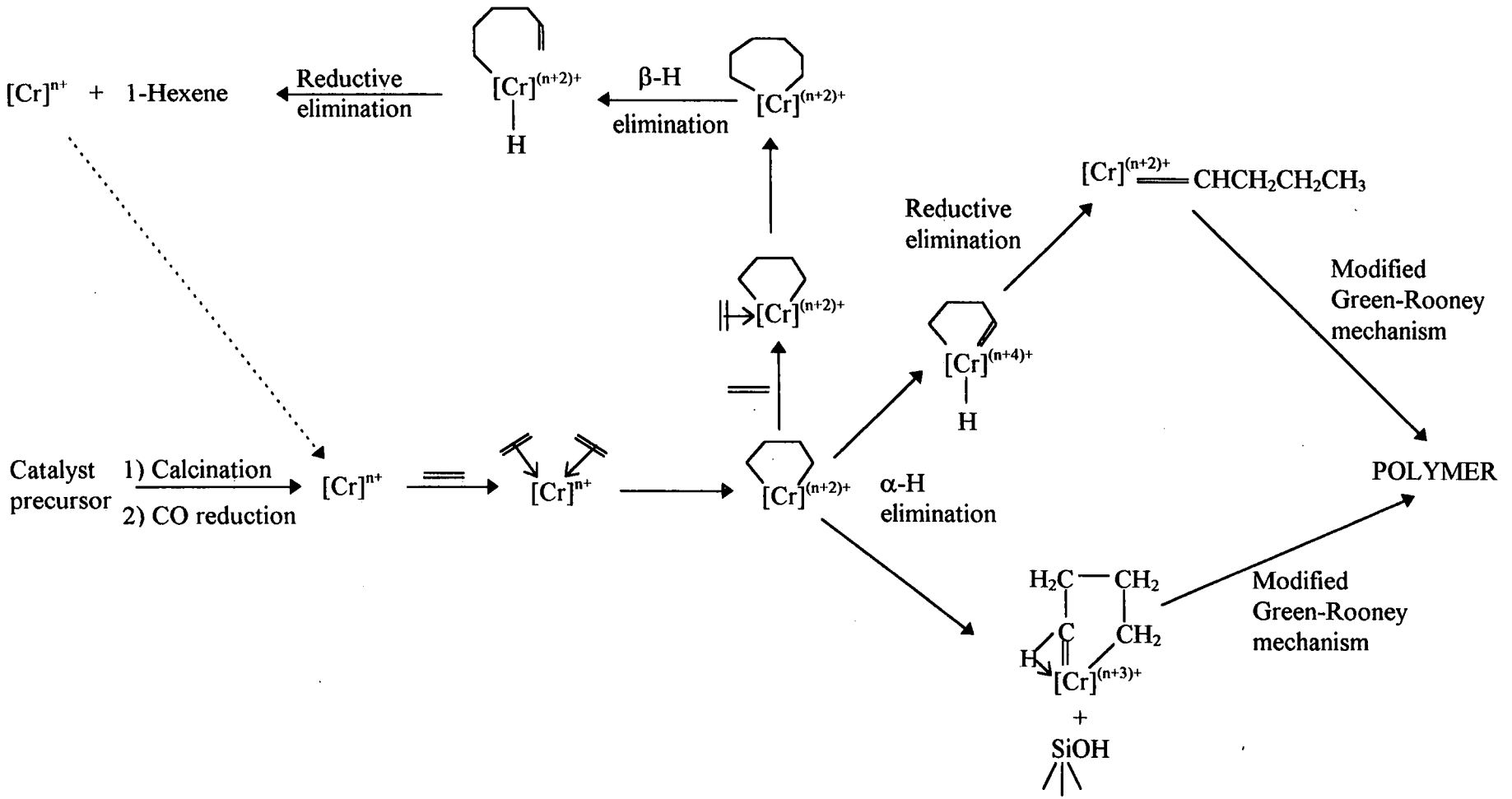

Scheme 4: Summary of the involvement of chromacyclopentane species in 1-hexene production and ethylene polymerization.

4.5 Conclusions

The initiation of ethylene polymerization over pre-reduced CrO_x/silica catalysts leads to the transient evolution of 1-hexene. This can be taken as being evidence for the formation of a chromacyclopentane intermediate species which is also capable of acting as a precursor for species involved in the propagation step of the ethylene polymerization reaction.

4.6 References

1. McDaniel, M.P. *Adv. Catal.* **1985**, *33*, 47
2. Boor, J.; *Ziegler-Natta Catalysts and Polymerizations*; Academic: London, 1979
3. Cossee, P. *J. Catal.* **1964**, *3*, 80
4. Ivin, K.J.; Rooney, J.J.; Stewart, C.D.; Green, M.L.H.; Mahtab, R. *J.C.S. Chem. Comm.* **1978**, 604
5. Hogan, J.P. *J. Polym. Sci.: A-1* **1970**, *8*, 2637
6. Jozwiak, W.K.; Dalla Lana, I.G.; Fiederow, R. *J. Catal.* **1990**, *121*, 183
7. Ghiotti, G.; Garrone, E.; Zecchina, A. *J. Mol. Catal.* **1988**, *46*, 61
8. Kantcheva, M.; Dalla Lana, I.G.; Szymura, J.A. *J. Catal.* **1995**, *154*, 329
9. Zielinski, P.; Dalla Lana, I.G. *J. Catal.* **1992**, *137*, 368
10. Zecchina, A.; Spoto, G.; Ghiotti, G.; Garrone, E. *J. Mol. Catal.* **1994**, *86*, 423
11. Ghiotti, G.; Garrone, E.; Coluccia, S.; Morterra, C.; Zecchina, A. *J.C.S. Chem. Comm.* **1979**, 1032
12. Vikulov, K.; Spoto, G.; Coluccia, S.; Zecchina, A. *Catal. Lett.* **1992**, *16*, 117
13. Nishimura, M.; Thomas, J.M. *Catal. Lett.* **1993**, *19*, 33
14. Cornu, A.; Massot, R.; *Compilation of Mass Spectral Data;* 2nd Ed., Heydon and Son: London, 1975
15. Koenig, J.L.; *Chemical Microstructure of Polymer Chains*; Wiley: New York, 1980, p199

16. Guiton, T.A.; Pantano, C.G. *Colloids and Surfaces A: Physicochemical and Engineering Aspects* **1993**, *74*, 33
17. Silverstein, R.M.; Bassler, G.C.; Morrill, T.C.; *Spectrometric Identification of Organic Compounds*; Fifth Edition; Wiley: Singapore, 1991, p93
18. Groeneveld, C.; Wittgen, P.P.M.M.; Swinnen, H.P.M.; Wernsen, A.; Schuit, G.C.A. *J. Catal.* **1983**, *83*, 346
19. Briggs, J.R. *J.C.S. Chem. Comm.* **1989**, 674
20. Meijboom, N.; Schaverien, C.J.; Orpen, A.G. *Organometallics* **1990**, *9*, 774
21. Manyik, R.M.; Walker, W.E.; Wilson, T.P. *J. Catal.* **1977**, *47*, 197
22. McDermott, J.X.; White, J.F.; Whitesides, G.M. *J. Am. Chem. Soc.* **1973**, *95*, 4451
23. Keim, W.; Mettzow, W; Chen, Z.; Huang, Z.; Shen, Z. *J. Catal.* **1992**, *137*, 423
24. McDaniel, M.P.; Cantor, D.M. *J. Polym. Sci.; Polymer Chem. Ed.* **1983**, *21*, 1217

CHAPTER 5. AN AFM STUDY OF THE BREAK-UP OF CATALYST PARTICLES DURING ETHYLENE POLYMERIZATION

5.1 Introduction

Heterogeneous polymerization catalysts require well designed support materials which are capable of undergoing fragmentation during reaction, whilst possessing the strength to withstand high temperature activation procedures (e.g. calcination).[1, 2] Fragmentation is necessary in order to maintain monomer access to actives sites located within the pores of the support.[3] Early studies of the Phillips catalyst system used high-temperature ashing of the polymer phase to leave behind fragmented support material, which was then examined by BET and mercury porosimetry methods.[4] Artefacts introduced during the ashing procedure were later shown to render the results of these studies unreliable.[5] More recently, SEM/TEM,[2, 3, 6, 7] X-ray microscopy[8, 9] and synchrotron microtomography techniques have been employed to observe the fragmentation processes occurring during polymerization, and the changing porosity of catalyst supports has been investigated using mercury porosimetry[10] and pulse solid-gas chromatography.[11] These techniques have many drawbacks, for example, SEM and TEM require the application of a conductive coating to the particle, which may influence the topography of the particles; synchrotron microtomography requires access to a synchrotron source; mercury porosimetry may itself cause the support to break-up; and pulse solid-gas chromatography is strongly dependent upon elution dynamics.

Atomic force microscopy (AFM)[12] is widely used to image the surfaces of solid materials. It works by scanning a very sharp tip across a sample surface and measuring the forces of interaction between the tip and the substrate. TappingMode™ and phase imaging[13, 14] AFM are useful variations of this technique. The former employs an etched silicon cantilever which is made to oscillate at a frequency close to its resonance frequency by a piezoelectric driver. The surface topography is imaged by measuring the drop in oscillation amplitude as the tip lightly "taps" the surface. Phase imaging AFM compares the phase of

the cantilever oscillation with that of the piezoelectric driver. The measured phase lag is dependent upon the composition of the sample; a softer sample exhibits a larger phase lag relative to a hard one.[13] TappingMode™ and phase imaging AFM can be run simultaneously, thereby offering topographical and compositional data for the same sample area. In order to be able to image small particles by AFM, certain limitations must be overcome. Firstly, the particles need to be fixed down firmly onto a substrate. Another problem arises if the feature being imaged is of comparable dimensions to the tip. If this is the case, then as the probe tip scans across the particles, the edge of the tip is imaged rather than the feature.[15] Both of these drawbacks can be overcome by partially embedding the particle in a thermoplastic adhesive;[16] the particle then appears flatter during imaging since most of its bulk is beneath the surface of the adhesive, and it is held still.

In the present study, the break-up of the Phillips CrO_x/silica catalyst during ethylene polymerization has been followed by contact mode, TappingMode™ and phase imaging AFM. Previous studies have indicated that polymer fills the support macropores first, and then causes the support to fragment in a non-uniform process, the larger particles being observed at the external surfaces of the polymer particles. The present study is aimed at investigating the surface morphology of catalyst and polymer particles without the requirement of a conductive coating, at scales inaccessible using the techniques reported previously.

5.2 Experimental

Basic chromium(III) acetate was aqueously impregnated onto silica support material (Crosfield Limited, surface area = 323 m^2g^{-1}, pore volume = 1.81 cm^3g^{-1}, prepared by the sol-gel route) and dried. 1 g of material was placed into a quartz microreactor tube and activated, reduced and reacted with ethylene as described in chapters 2 to 4. The formation of white polyethylene granules was taken as being indicative of an active catalyst, as confirmed by Fourier transform infrared spectroscopy.[17]

Sample preparation for AFM involved partially embedding particulate material into a thermoplastic adhesive.[16] Small pieces of cleaved mica (~1 cm^2) were placed onto a hotplate at 393 K. Thermoplastic adhesive (Tempfix, Agar Scientific) was spread onto the mica substrates and cooled slowly to room temperature in order to create a smooth film. The powdered sample was then dusted onto the prepared substrate and placed in a vacuum oven at 363 K for 3.5 hours. These conditions were found to partially embed the particles, thereby allowing imaging by AFM.

A Digital Instruments Nanoscope III atomic force microscope was used for contact mode, TappingMode™, and phase imaging AFM analysis of the partially embedded particles. AFM images were acquired in air at room temperature using a 100 μm x 100 μm piezoelectric scan head, and are presented as unfiltered data. Contact mode images were collected using a 200 μm wide-legged silicon nitride cantilever with a low spring constant (k = 0.12 Nm^{-1}, in order to minimise surface damage due to high contact forces). TappingMode™ and phase imaging AFM studies used a stiff silicon cantilever oscillating close to its resonance frequency.

5.3 Results

Contact mode AFM analysis of the silica support showed that the surface of each particle consisted of an aggregation of spheroids (~0.31 ± 0.07 μm diameter), with pore openings evident across the surface, Figure 1. Phase imaging AFM was used to check for the absence of any adhesive on the surface. The calcined CrO_x/silica catalyst is very similar in appearance to the silica support surface (spheroids of ~0.26 ± 0.07 μm diameter), Figure 2. This may be taken as being an indication that sintering does not occur during calcination at 1053 K. Phase imaging AFM showed only one phase to be present at the catalyst particle surface (as indicated by the absence of any significant colour contrast in Figure 3(a)).

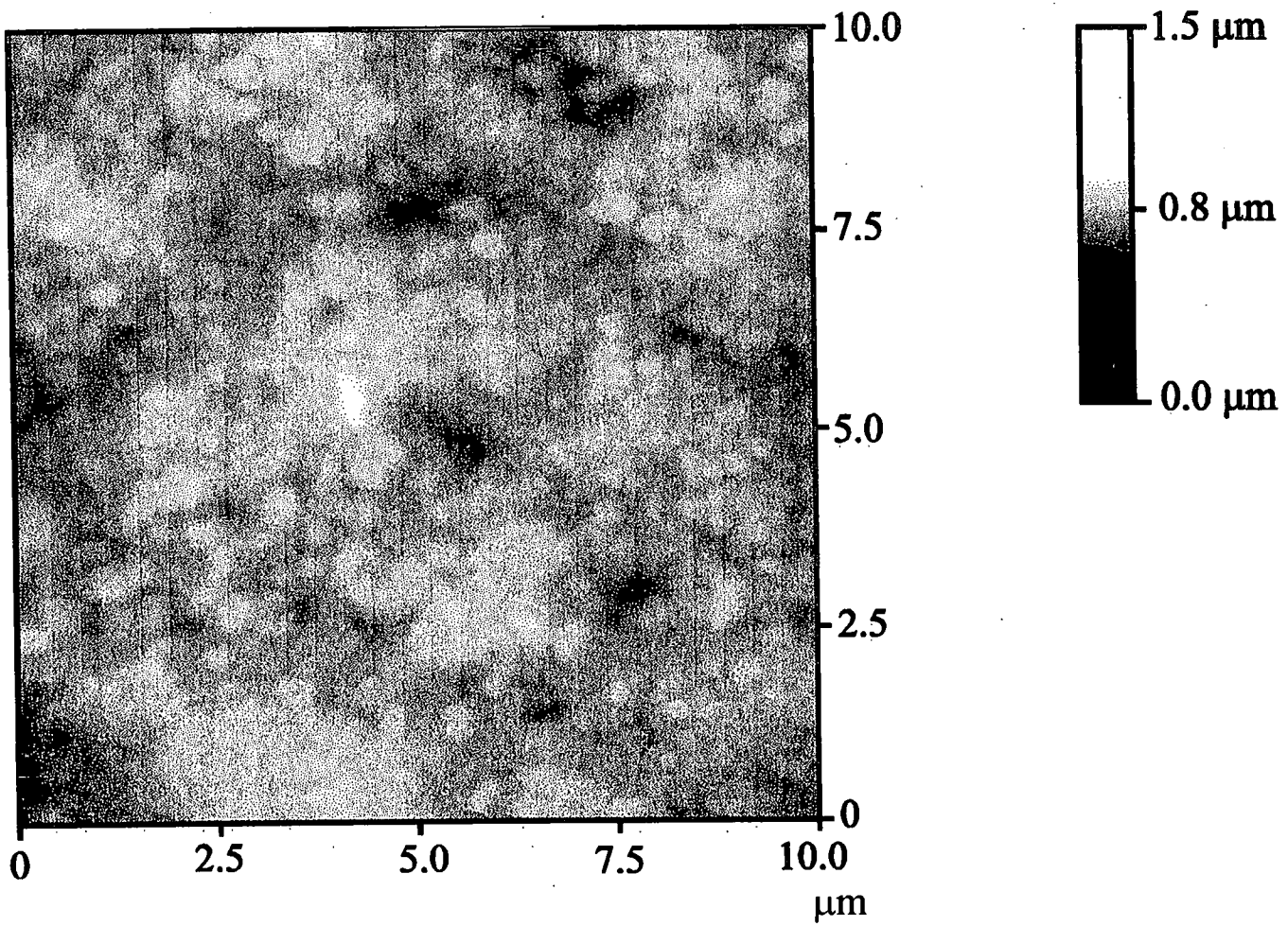

Figure 1: Contact mode AFM micrograph of as-received silica support surface.

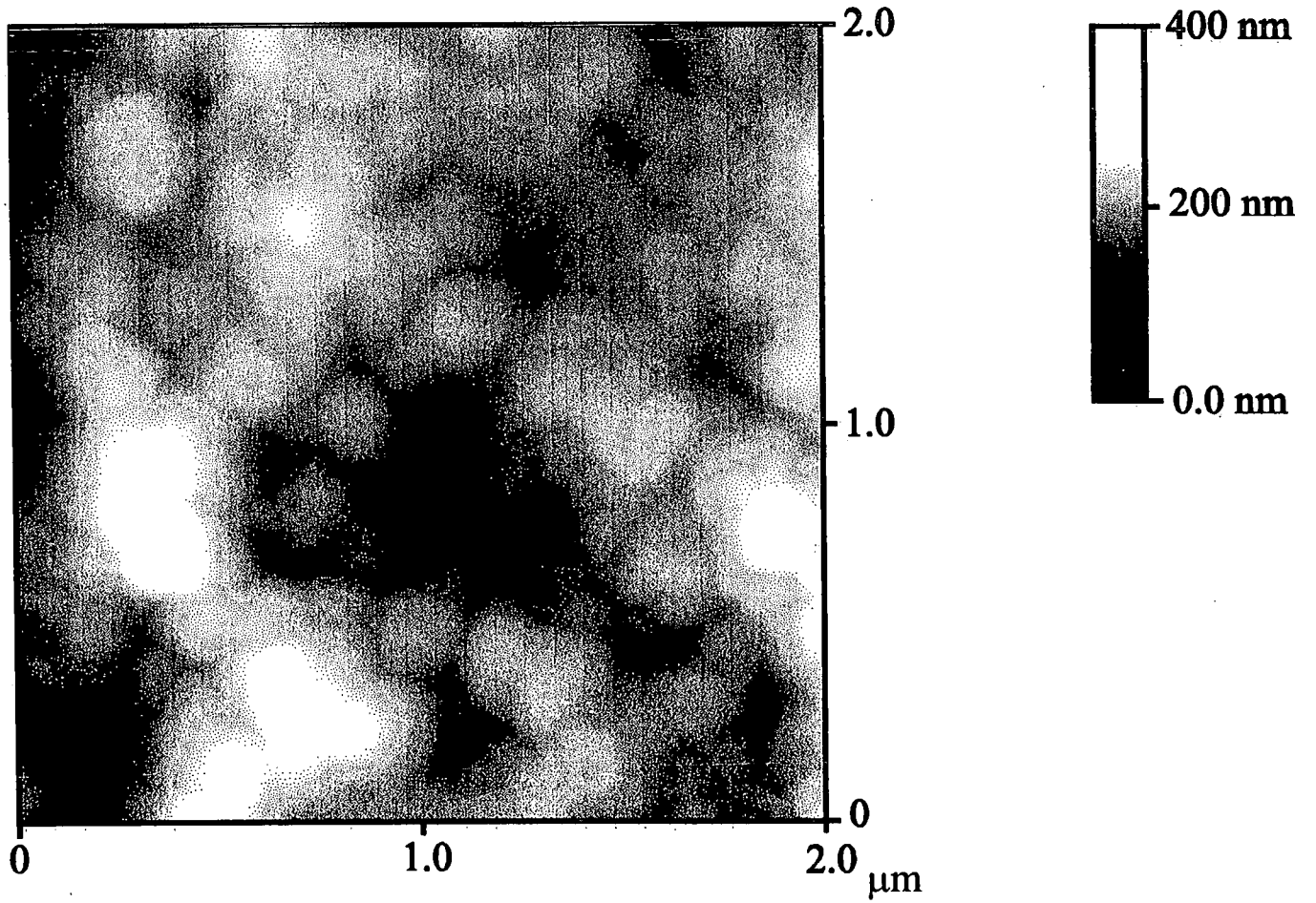

Figure 2(a): Contact mode AFM micrograph of chromium(III) acetate impregnated onto silica.

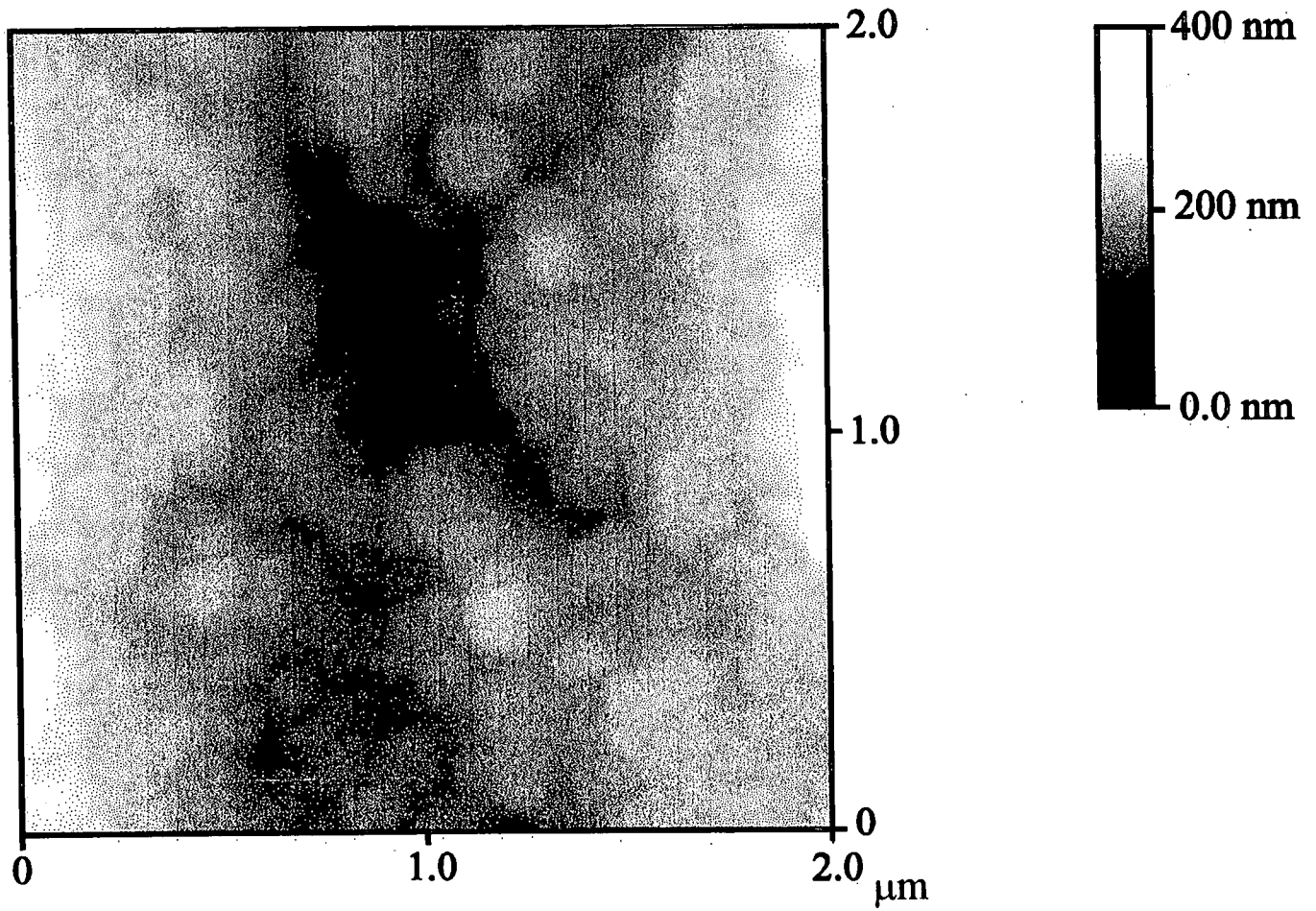

Figure 2(b): Contact mode AFM micrograph of calcined CrO_x/silica catalyst.

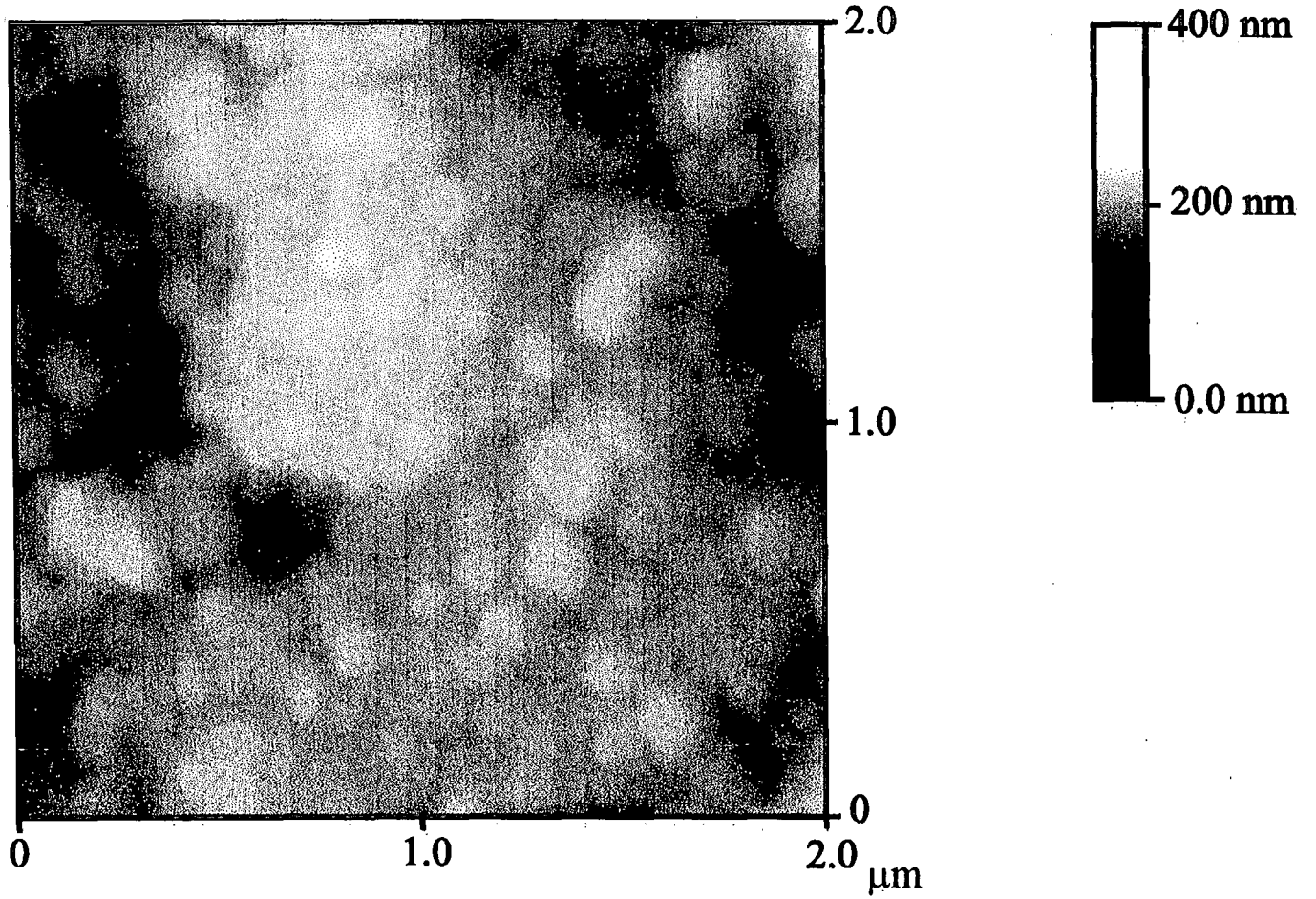

Figure 2(c): Contact mode AFM micrograph of the catalyst surface during the very early stages of polymerization.

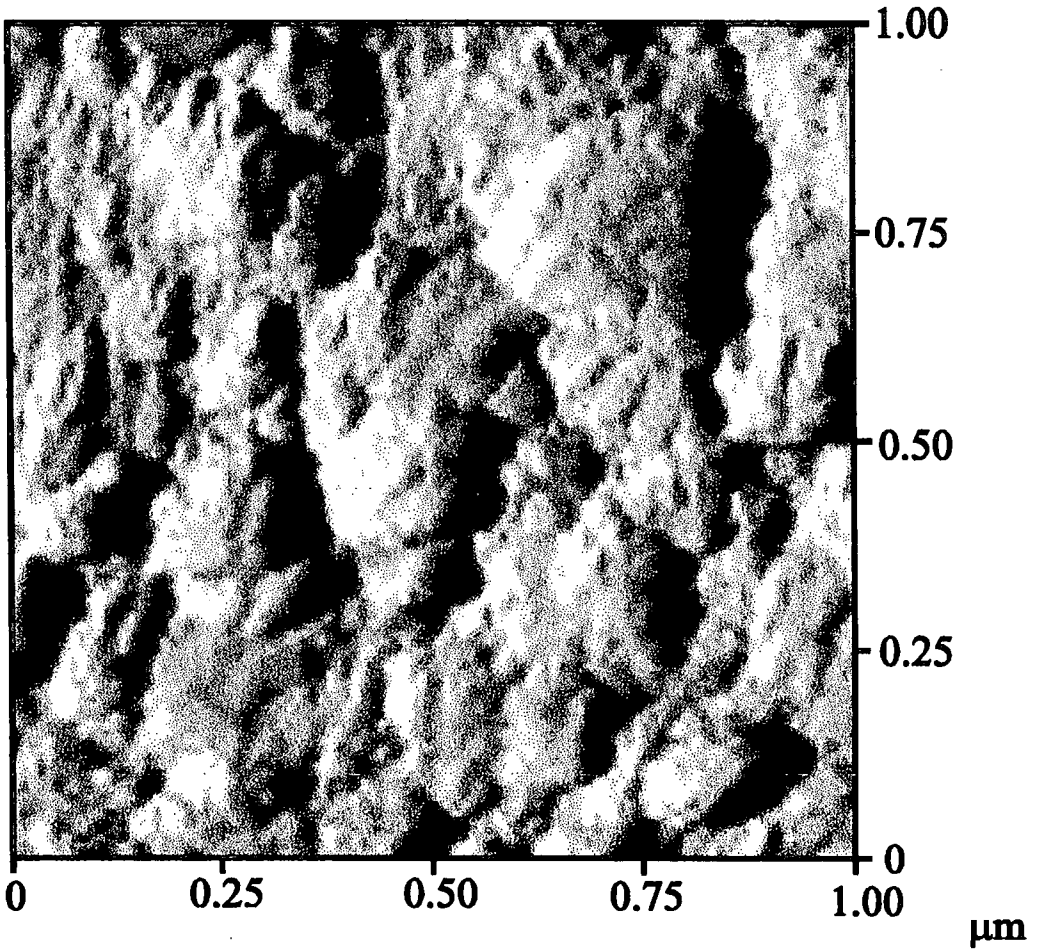

Figure 3(a): Phase imaging AFM of the calcined CrO_x/silica catalyst surface prior to ethylene exposure.

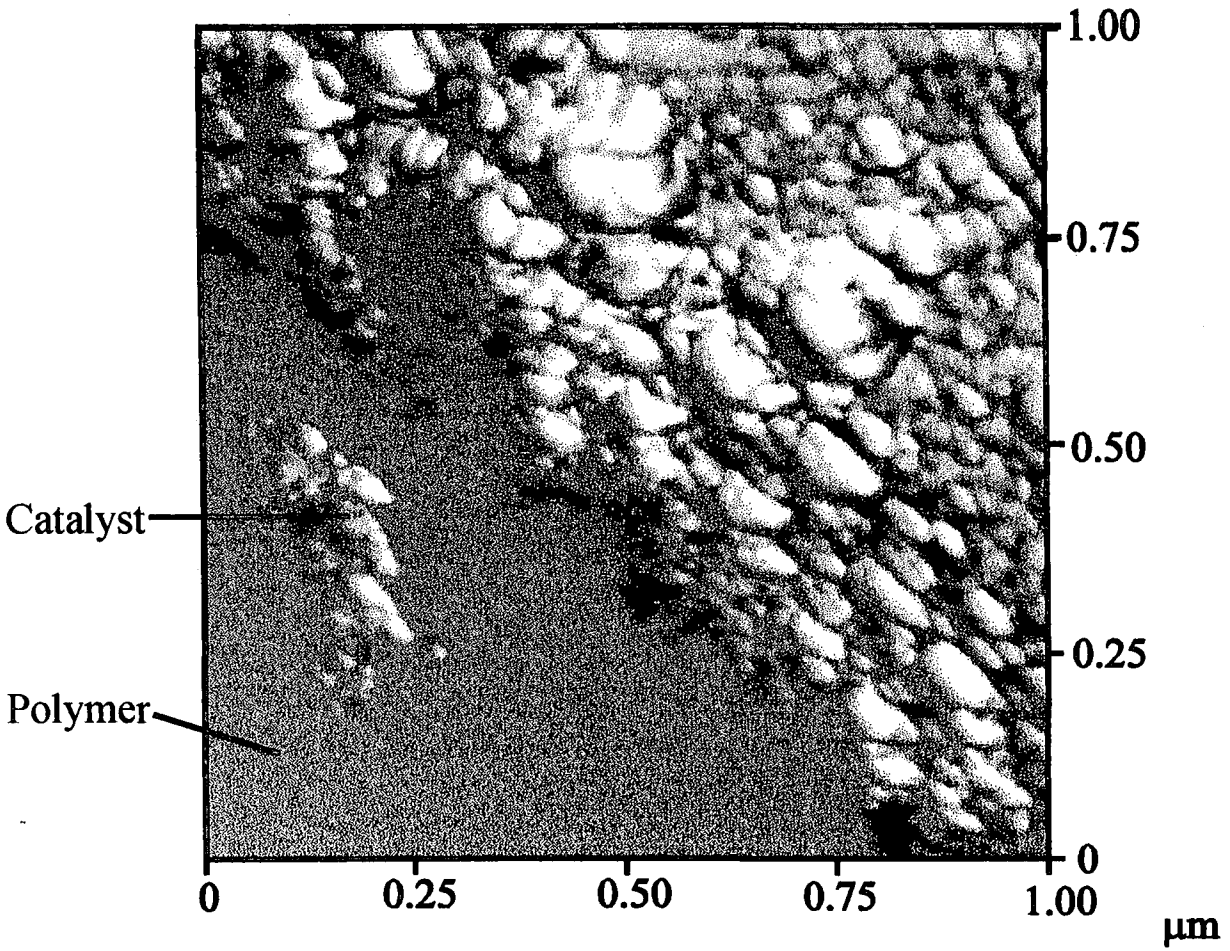

Figure 3(b): Phase imaging AFM of the calcined CrO_x/silica catalyst surface in the early stages of ethylene polymerization.

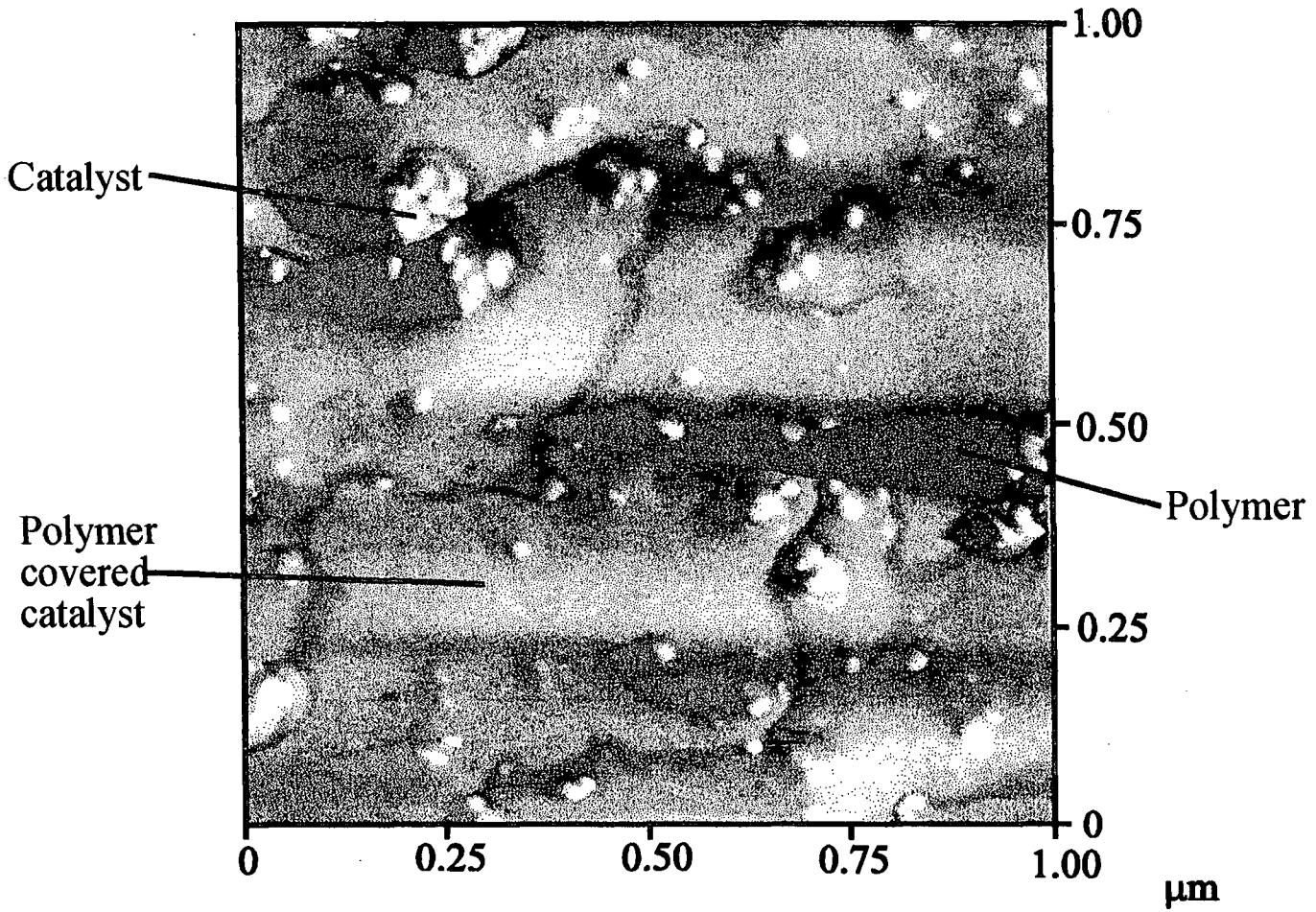

Figure 3(c): Phase imaging AFM of the calcined CrO_x/silica catalyst surface at a more advanced stage of polymerization.

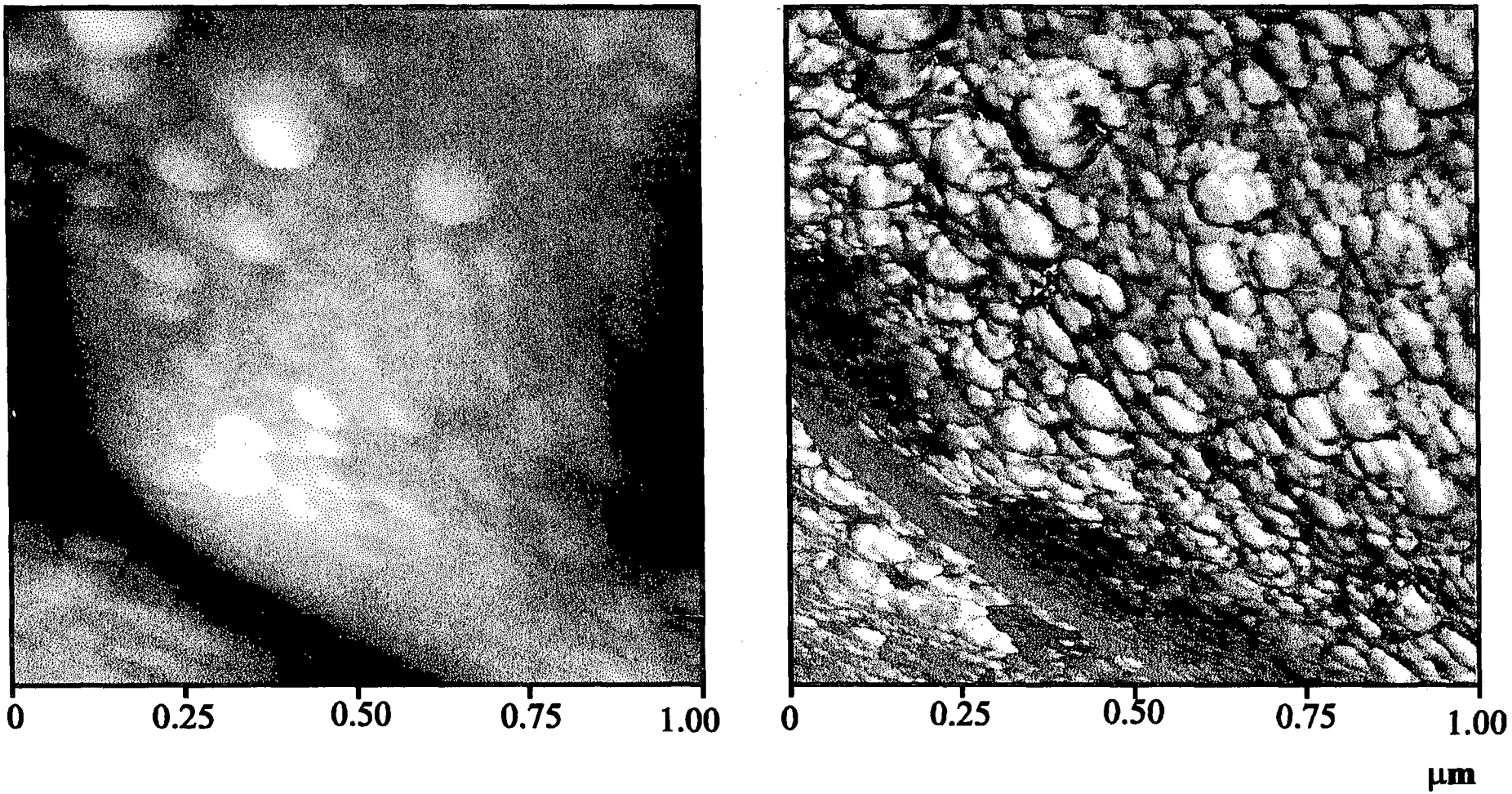

Figure 4: Polymer seeping through cracks extending from pores: (a) TappingMode ™ AFM; and (b) phase imaging AFM.

Exposure of the activated CrO_x/silica catalyst to ethylene resulted in the formation of white powder, which was identified by FTIR as being polyethylene.[17] Optical microscopy showed evidence for some agglomeration of polymerizing particles.[8, 9, 11] Contact mode AFM analysis during the very early stages of polymerization showed a surface which is very similar to that of the silica support material, except that the spheroids were smaller (~0.14 ± 0.04 μm diameter) than those observed for either the silica support or the calcined catalyst, Figure 2. Phase imaging AFM showed that the ragged appearance of the catalyst gradually breaks-up with increasing levels of polymerization (the polymer exhibits a much smoother appearance) Figure 3. Polymer starts to appear in cracks extending from pores, Figure 4. Eventually, all that remains are small fragments of catalyst dispersed within a polyethylene matrix.

5.4 Discussion

The appearance of the silica surface may be explained by taking into consideration its preparation via a sol-gel process.[1] The micelles formed during the syneresis stage of this preparative procedure vary in size from 3-50 nm depending upon the exact conditions applied during the preparation.[18] The physical similarity between the silica support material and the calcined catalyst is indicative of its high thermal stability.

Although the Phillips CrO_x/silica catalyst is known to possess a wide range of chromium sites, only a small percentage are believed to be active.[5] This helps to explain why ethylene polymerization is not homogeneous across the catalyst surface. Also the polymerization reaction is a highly exothermic process, whilst the catalyst particles are thermally insulating. This can lead to localised melting of the polymer,[8, 11] which can give rise to agglomeration of polymerizing particles (as seen by optical microscopy).[9, 11] Such agglomeration is very difficult to avoid, but can be limited via efficient cooling and fragmentation of the catalyst.[8, 11] Diluting the monomer phase with an inert gas (in this case argon) can lead an improvement in cooling efficiency.

During the early stages of ethylene polymerization, the spheroidal features appear to fragment, Figure 3. Previous solid-gas chromatography[11] and mercury porosimetry[10] studies have shown that polymerization at low yields fills the macropores of the catalyst nearest to the external particle surface with polymer until there is a sufficient build-up of pressure for fragmentation to occur, resulting in fresh catalyst surface being exposed. This serves to increase monomer transport to active sites within the pores. The fragmentation is seen to produce trough-like features at the surface, from which the polymer may then continue to grow,[19] Figure 4.

Previous studies using X-ray microscopy[8, 9] and synchrotron microtomography[9] have suggested that large fragments of catalyst are concentrated near to the external surfaces of the growing polymer particle. Three different physical models for catalyst fragmentation have been put forward: (a) a "hard-core" model in which polymerization occurs around a non-friable central catalyst particle; (b) a "uniform" site model in which small fragments are evenly distributed within the particle; and (c) an "expanding-core" model in which convection of fragments to the exterior surface is caused by internal expansion.[20, 21] The "hard-core" model is not applicable to the present study since there is evidence for catalyst fragmentation. The "uniform" model requires homogeneous break-up of the catalyst particles to reach completion during the early stages of polymerization, combined with polymer growth at roughly equal rates around each fragment (this type of mechanism is reported for Ziegler-Natta type systems, where the catalyst friability is known to be high[22, 23]). This may also be discounted in the present study since non-uniform fragmentation of the catalyst is observed, with small and large areas of the catalyst evident amongst the growing polymer, Figure 3(b). The expanding core model is therefore most applicable to the CrO_x/silica polymerization catalyst. Such non-uniform fragmentation can lead to catalyst fragments possessing differing activities; the larger fragments being less active than the smaller crystallites.[9, 19] This is because the rate of polymerization is higher at the outer shell of fragments than in the less monomer-accessible core, therefore one would expect the rate of polymerization to increase with rising levels of catalyst fragmentation since smaller fragments have a higher surface area.[5] Thus, the less active large fragments will be

convected towards the surface of the growing polymer particle via differential expansion.[8, 9] On reaching the surface, these large fragments become more accessible to monomer, which in turn leads to further build-up of polymer followed by fragmentation until eventually there are very small catalyst crystallites at the growing polymer particle surface, Figure 3(c). An intermediate shade region in the phase image at this stage can be assigned to much larger catalyst fragments which have become covered by a thin layer of polyethylene, whilst the darker phase corresponds to polyethylene expanding onto the surface from trough-like features where the larger support fragments have cracked open along a pore.

5.5 Conclusions

Phase imaging atomic force microsopy has been used to follow the different stages of ethylene polymerization over the Phillips CrO_x/silica catalyst. The catalyst undergoes continuous fragmentation during the formation of polymer, with the larger fragments being pushed out towards the surface where they undergo further fragmentation.

5.6 References

1. Marsden, C.E.; *Preparation of Catalysts V*; Eds. Poncelot, G.; Jacobs, P.A.; Grange, P.; Delman, B.; Elsevier: Amsterdam, 1991
2. Dalla Lana, I.G.; Szymura, J.A.; Zielinski, P.A. *Proceedings of the 10th International Congress on Catalysis* **1992**, 2329
3. Conner, W.C.; Laurence, R.L.; Naik, B.; Webb, S.W.; Weist, E.L. *Proceedings of the 9th International Congress on Catalysis* **1988**, 1866
4. McDaniel, M.P. *J. Polym. Sci.: Polymer Chem. Ed.* **1981**, *19*, 1967
5. McDaniel, M.P. *Adv. Catal.* **1981**, *33*, 47

6. Niegisch, W.D.; Crisafulli, S.T.; Nagel, T.S.; Wagner, W.D. *Macromolecules* **1992**, *25*, 3910
7. Szymura, J.A.; Zielinski, P.A.; Dalla Lana, I.G. *Catal. Lett.* **1992**, *15*, 145
8. Webb, S.W.; Weist, E.L.; Chiovetta, M.G.; Laurence, R.L.; Conner, W.C. *Canadian Journal of Chemical Engineering* **1991**, *69*, 665
9. Conner, W.C.; Webb, S.W.; Spanne, P.; Jones, K.W. *Macromolecules* **1990**, *23*, 4742
10. Weist, E.L.; Ali, A.H.; Conner, W.C. *Macromolecules* **1987**, *20*, 689
11. Webb, S.W.; Conner, W.C.; Laurence, R.L. *Macromolecules* **1989**, *22*, 2885
12. Binnig, G.; Quate, C.F.; Gerber, C. *Physical Review Letters* **1986**, *56(9)*, 930
13. Chernoff, D.A. *Advanced Surface Analysis* **1995**, 6
14. Babcock, K.L.; Prater, C.B. *Phase Imaging: Beyond Topography* Digital Instruments Technical Note **1995**
15. Thundat, T.; Zheng, X.Y.; Sharp, S.L.; Allison, D.P.; Warnack, R.J.; Joy, P.I.; Ferrell, T.L. *Scanning Microsc.* **1992**, *6*, 903
16. Shakesheff, K.M.; Davies, M.C.; Jackson, D.E.; Roberts, C.J.; Tendler, S.J.B.; Brown, V.A.; Watson, R.C.; Barrett, D.A.; Shaw, P.N. *Surf. Sci. Lett.* **1994**, *304*, L393
17. Koenig, J.L.; *Chemical Microstructure of Polymer Chains;* Wiley: New York, 1980, p199
18. Winyall, M.E.; *Applied Industrial Catalysis, Volume 3*; Academic, 1984, Chap. 3
19. Follestad, A.; Helleborg, S.; Almquist, V. *Studies in Surface Science and Catalysis* **1990**, *56*, 63
20. Singh, D.; Merrill, R.P. *Macromolecules* **1971**, *4*, 599
21. Schmeal, W.R.; Street, J.R. *AICHE J.* **1971**, *17(5)*, 1188
22. Kakugo, M.; Sadatoshi, H.; Yokoyama, M.; Kojima, K. *Macromolecules* **1989**, *22*, 547
23. Kakugo, M.; Sadatoshi, H.; Sakai, J.; Yokoyama, M. *Macromolecules* **1989**, *22*, 3172

CHAPTER 6. NON-EQUILIBRIUM PLASMA ACTIVATION OF SUPPORTED Cr(III) PHILLIPS CATALYST PRECURSORS

6.1 Introduction

Most supported catalyst systems conventionally require a high temperature activation procedure. In the case of the Phillips CrO_x/SiO_2 ethylene polymerization catalyst this involves heating a silica supported chromium precursor to 1073 K for several hours in a dry air or oxygen atmosphere.[1] Such thermal activation methods tend to be highly energy intensive, and can lead to sintering of the support or segregation of the active catalytic component.[2]

Low temperature activation of heterogeneous catalysts can be achieved by using non-equilibrium (non-local thermodynamic equilibrium) plasmas. Such a "cold" plasma can be considered as a partially ionized gas consisting of ions, electrons, neutrals and electromagnetic radiation, where the electron temperature (T_e) is much greater than the gas temperature (T_g). Typically T_e/T_g is of the order 10-100;[3] therefore although the bulk gas temperature is near ambient, the electrons possess sufficient energy to cause the rupture of molecular bonds. This enables conventionally high temperature thermally driven reactions to proceed at low temperatures. For example, the problems associated with high temperature segregation on zeolitic Fischer-Tropsch catalysts can be overcome by the use of oxygen or argon cold plasma treatments, leading to catalysts possessing enhanced activities compared to their thermally activated counterparts.[4] Similar improvements have also been reported for hydrogenation catalysts,[5, 6] and alkene disproportionation catalysts.[7]

It has previously been reported that air plasma activation of silica-alumina supported chromium(VI) oxide precursors can produce a high activity ethylene polymerization catalyst.[8] Current safety legislation, however, prohibits any human contact with carcinogenic chromium(VI) species, such as those involved during the production of polyethylene using the Phillips catalyst. Therefore, in the present chapter, the non-isothermal plasma oxidation of two different types of silica supported chromium(III) catalyst precursors is investigated using *in-situ*

mass spectrometry. It has been established in chapters 2 to 4 that both of the precursor materials give rise to an active ethylene polymerization catalyst via the same intermediate species during thermal activation.[9] The present study aims to establish whether low temperature plasma treatment prohibits the intermixing of the dry blended chromium(III) acetylacetonate/silica system.

6.2 Experimental

High surface area silica (Crosfield Limited, surface area=323 $m^2 g^{-1}$, pore volume=1.81 $cm^3 g^{-1}$) was used as a control sample. The CrO_x/SiO_2 catalyst precursors (Crosfield Limited) were prepared as described in chapter 2, and comprised silica aqueously impregnated with chromium(III) acetate, or a dry-blend of chromium(III) acetylacetonate and silica. In both cases, the activated catalyst contained 1 wt% chromium loading.

Plasma activation experiments were carried out in a capacitively coupled 13.56 MHz Bio-Rad E2000 plasma asher, which had been fitted with a rotating glass powder holder. Rotation of the reaction vessel was controlled by a stepper motor, as shown cross-sectionally in Figure 1. The reactor was continuously pumped by a 33 $dm^3 hr^{-1}$ Edwards E2M2 Fomblin rotary pump via a liquid air cold trap to yield a base pressure of $2x10^{-2}$ mbar. Prior to each experiment, the reaction vessel was scrubbed with detergent, rinsed with acetone, oven dried, and then cleaned *in-situ* using a 40 W air plasma at 0.2 mbar pressure (this corresponds to a plasma power density,[10] *P/p*, of 200 W $mbar^{-1}$). 0.5 g of catalyst precursor was then loaded into the reactor and evacuated down to base pressure. Oxygen gas (BOC, 99.5% purity, dried as described in chapter 2) was then introduced into the plasma chamber to a pressure of 0.9 mbar via a fine needle valve prior to the ignition of an oxygen glow discharge at 40 W (plasma power density, *P/p* =44.4 W $mbar^{-1}$) whilst rotating the vessel containing the catalyst powder. Reaction was allowed to proceed for approximately 45 min, after which time the oxygen flow was switched off and the reactor evacuated to its original base pressure.

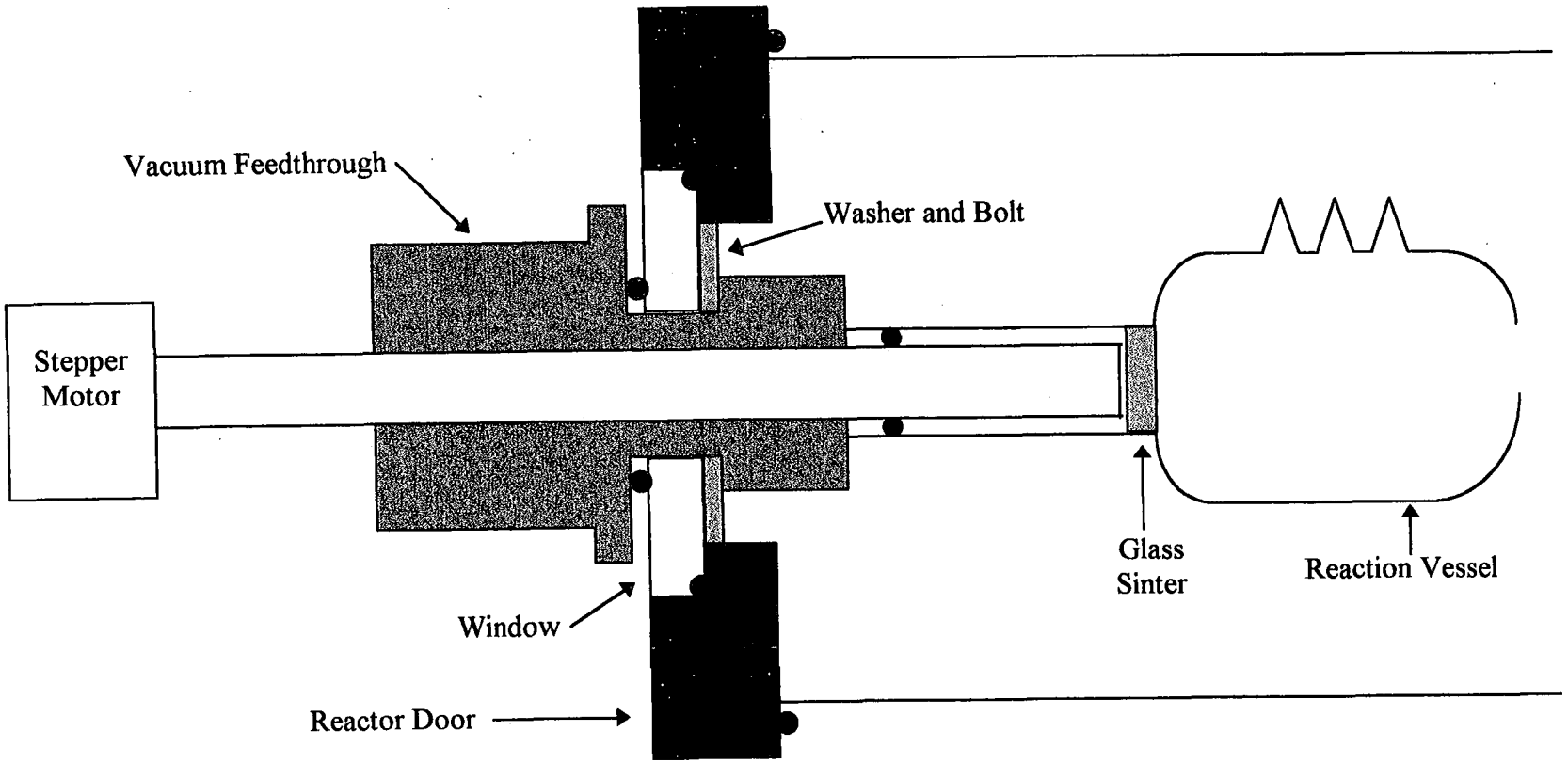

Figure 1: Cross-sectional view of the tumbler arrangement

The plasma reactor outlet was connected via a heated capillary tube to a Vacuum Generators SX200 quadrupole mass spectrometer; this was multiplexed to a PC computer, thus enabling the composition of gases within the reactor to be monitored in real time. For each set of experiments, the whole background mass spectrum was recorded as a function of time, thereby allowing all desorbing species to be identified. Each experiment was subsequently repeated using fresh material, but this time, actual reaction profiles were obtained by tuning into previously identified mass fragments. The fragmentation patterns for carbon monoxide and carbon dioxide were also measured independently using the respective gases, and normalised using the appropriate ion gauge sensitivity factors[11, 12] as described in chapter 2. The contribution from CO_2 towards the m/e 28 profile has been taken into consideration.

Ethylene polymerization activity was tested by reducing the plasma oxidized CrO_x/silica catalysts at 623 K with a 15 min exposure to carbon monoxide (BOC, 99.9% purity, dried as described in chapter 3, at a flow rate of 1.5 dm^3hr^{-1}), followed by cooling to 383 K and exposing to a 50:50 mixture of argon:ethylene (Scott Speciality Gases, 99.8%, dried through P_2O_5 and then 3A molecular sieve (Aldrich) columns). The resultant material was mixed with KBr and pressed into a disk to allow characterization by Fourier Transform Infrared Spectroscopy using an FTIR Mattson Polaris instrument. Typically 100 scans were acquired at a resolution of 4 cm^{-1}.

6.3 Results

Room temperature oxygen glow discharge treatment of the silica control samples resulted in a gradual loss of water from the surface with no observable change in the oxygen signal (mass 32), Figure 2.

Plasma oxidation of chromium(III) acetate/silica and chromium(III) acetylacetonate dry-blended with silica was accompanied by a colour change from pale blue or maroon respectively to bright orange. This is similar in appearance to the colour change observed during the thermal activation of these CrO_x/silica

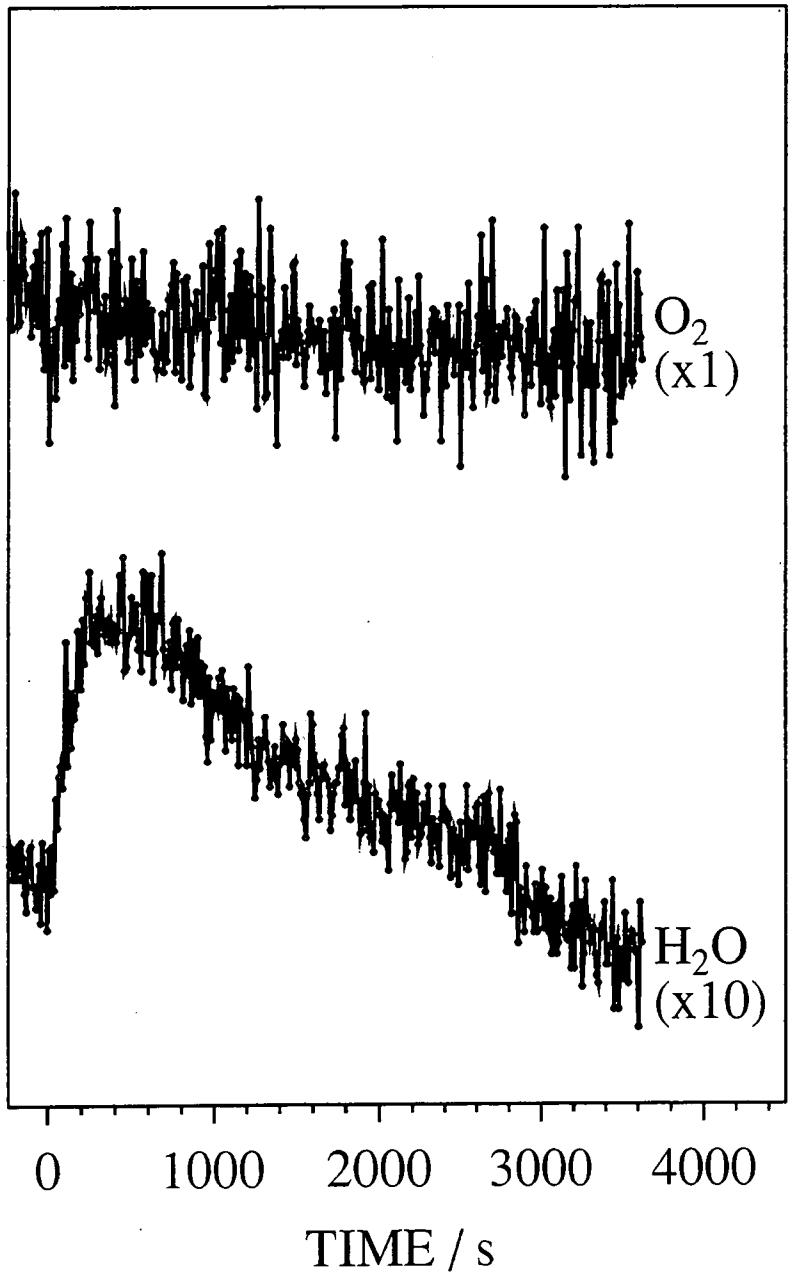

Figure 2: Change in mass signal intensity during oxygen plasma treatment of silica.

catalyst precursors[9] described in chapter 2. For both types of chromium(III) precursor, a sharp rise in CO and CO_2 evolution coincided with the onset of plasma ignition, this was followed by a gradual drop in signal intensity with treatment time, Figure 3. This trend is mirrored in the oxygen profile, demonstrating a behaviour which was absent when the silica support material was treated alone. Water loss displayed a broad peak, which was similar in appearance to that observed previously during oxygen plasma treatment of silica. The respective peak areas for the various gases detected by mass spectrometry are summarized in Table 1.

Molecule	Cr(III) acetate / silica	Cr(III) acetylacetonate / silica	Silica
CO	1.6	5.3	0
CO_2	24.3	87.4	0
H_2O†	22.4	41.3	11.7

† Uncorrected for sensitivity factor

Table 1: Summary of CO and CO_2 peak areas produced during the plasma oxidation of catalyst precursors (arbitrary units ±5%).

The plasma oxidized CrO_x/SiO_2 catalysts were then heated to 623 K (no loss of gaseous species was observed during heating) and reduced using CO gas. This was followed by cooling to 383 K and exposing the material to a 50:50 argon:ethylene gas mixture. In the case of the chromium(III) acetate aqueously impregnated onto silica precursor, the formation of white granules was observed. These were identified by FTIR analysis to be polyethylene, as evidenced by C-H stretches at 2920 and 2850 cm^{-1}, the methylene bending mode at 1469 cm^{-1} and the methylene rocking mode at 719 cm^{-1}, Figure 4.[13] All remaining peaks may be assigned to the silica support.[14] No polymer formation was detected for the starting material which consisted of a dry-blended physical mixture of chromium(III) acetylacetonate and silica.

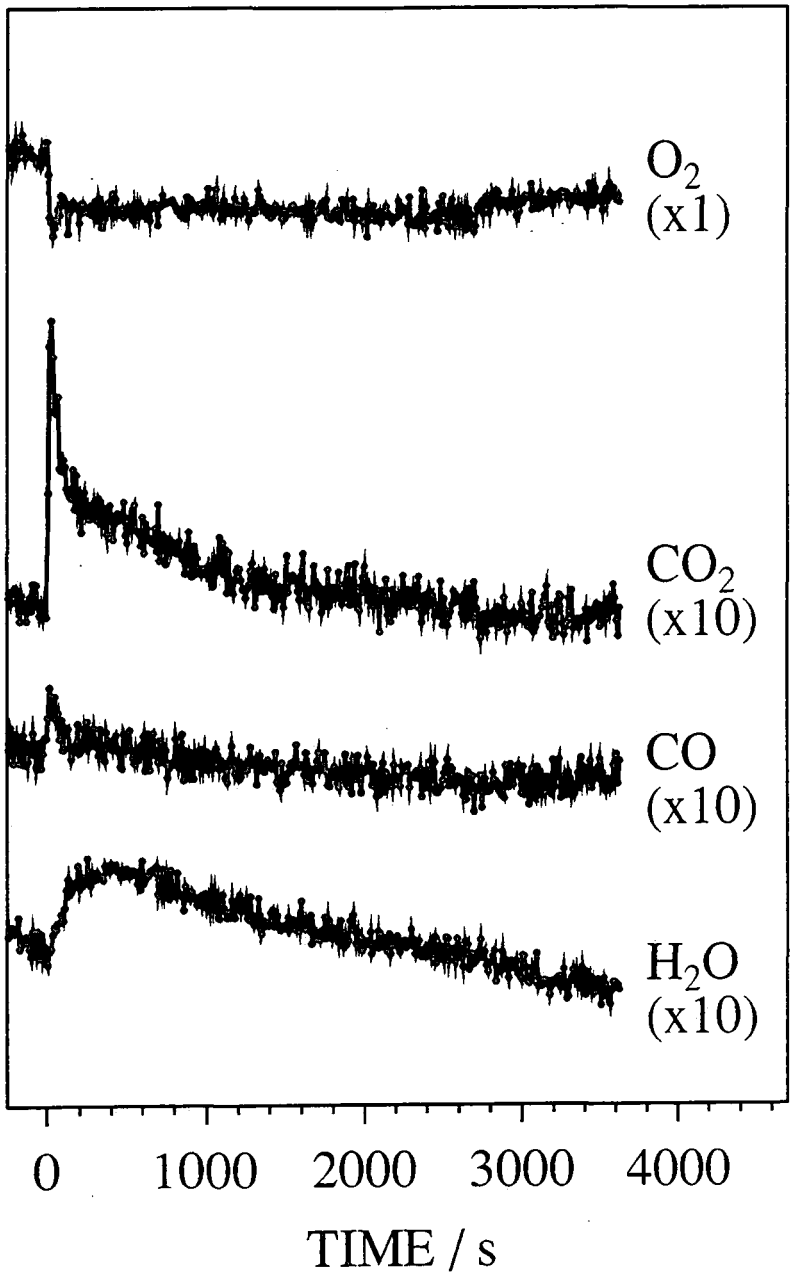

Figure 3(a): Change in mass signal intensity during oxygen plasma treatment of chromium(III) acetate aqueously impregnated onto silica.

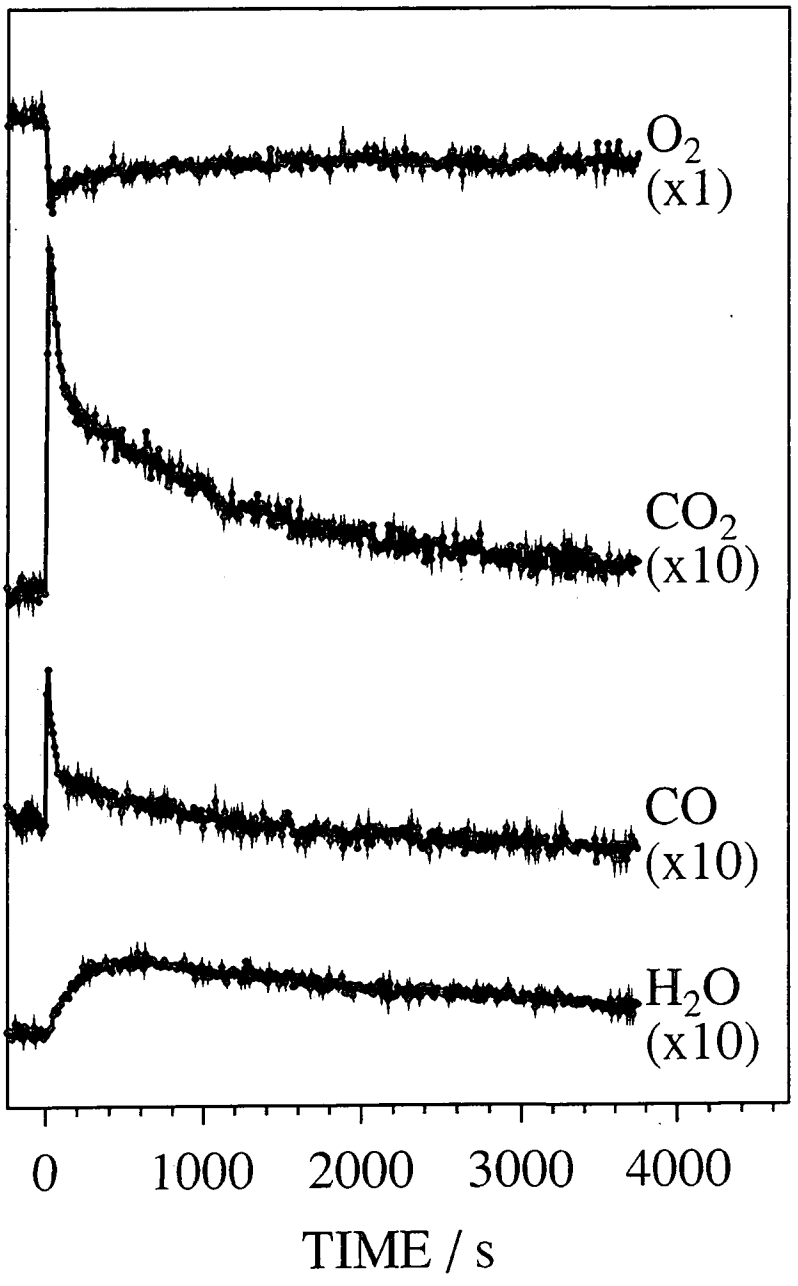

Figure 3(b): Change in mass signal intensity during oxygen plasma treatment of chromium(III) acetylacetonate dry-blended with silica.

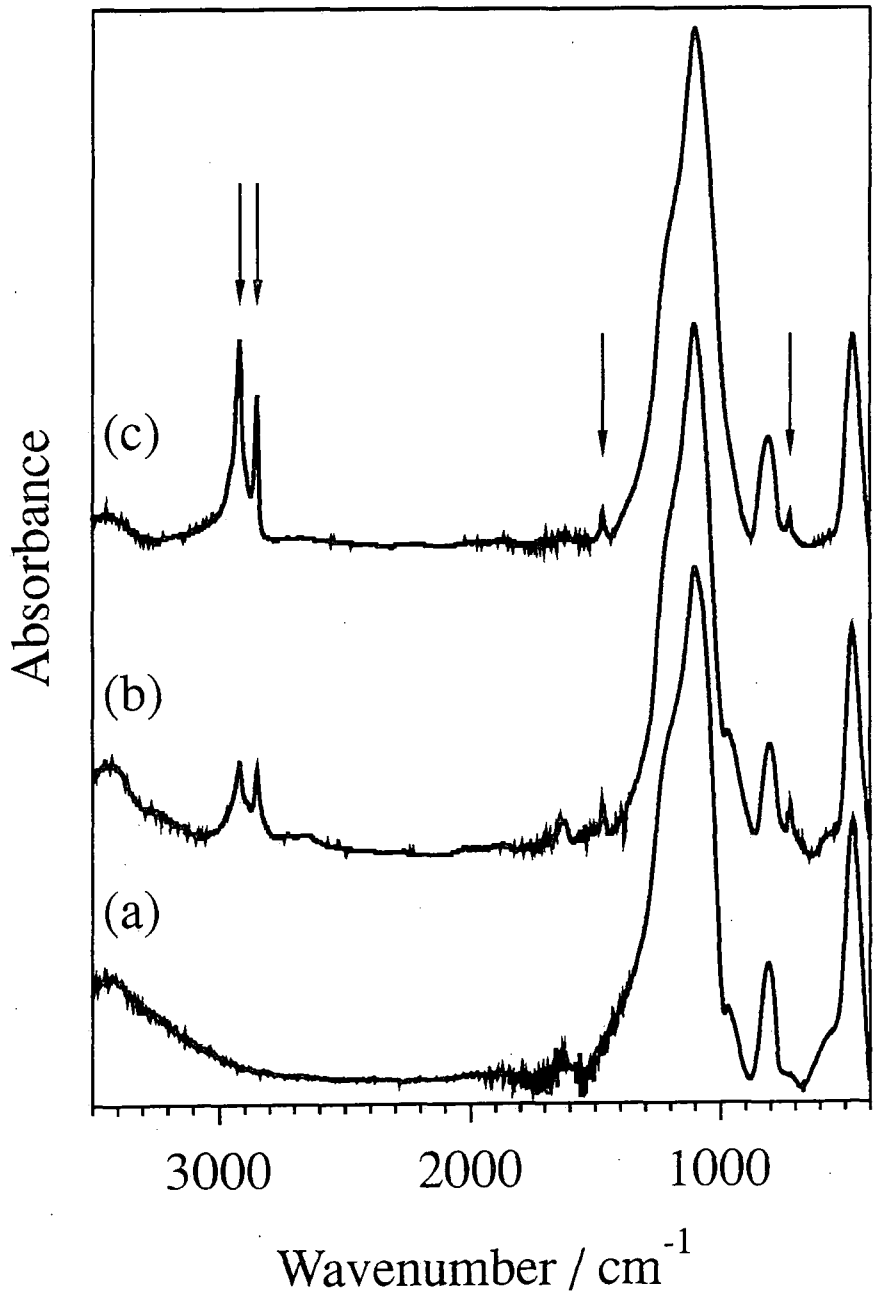

Figure 4: FTIR spectra of (a) the silica support material; (b) plasma activated chromium(III) acetate/silica following exposure to ethylene; and (c) thermally activated chromium(III) acetate/silica following exposure to ethylene.

6.4 Discussion

The excitation of a gas into the plasma state can greatly enhance its chemical reactivity. Application of an electric field causes free electrons to gain energy, which is subsequently lost via electron-neutral or electron-ion collisions.[15] A wide variety of reactants are generated by these processes in an oxygen plasma, including neutral ground-state (e.g. O, O_2 and O_3) and metastable (e.g. $O_2(a^1\Delta_g)$) species, positively charged (e.g. O^+, O_2^+, O_3^+, O_4^+) and negatively charged (O^-, O_2^-, O_3^-, O_4^-) ions,[3, 16, 17] alongside electrons and electromagnetic radiation. The most abundant neutral species is ground-state O_2, whilst atomic oxygen is the predominant reactive constituent.[16]

Water loss from the silica support surface must be initiated via interaction with one of the reactive constituents of the oxygen glow discharge. The absence of a dip in the oxygen profile during oxygen plasma treatment of the silica support material rules out the involvement of any oxygen containing species, thereby leaving electrons and UV/VUV radiation as contenders. The negative charge associated with the plasma sheath region adjacent to a particle surface means that incident electrons will be retarded as they approach the silica surface, hence electron bombardment is minimal. UV/VUV radiation must therefore be responsible for the elimination of water from the silica support surface. This deduction is consistent with previous UV/VUV exposure studies which have shown that silanol groups undergo a condensation reaction in the presence of water to form siloxane bonds along with the concomitant loss of water from the surface.[18-21]

The peak profiles of the gaseous products evolved during plasma oxidation of the supported chromium(III) catalyst precursors can be explained in terms of the various types of electrical discharge - substrate interactions which can potentially occur during treatment. CO and CO_2 formation coincides with ignition of the glow discharge and rapid consumption of oxygen; therefore this corresponds to straightforward oxidation of the organic ligands by excited oxygen species. The intensity of these oxidised carbon moieties diminishes with reaction time. It is found that approximately 3.6 times more carbon species are evolved

from the Cr(III) acetylacetonate/silica precursor compared to the Cr(III) acetate/silica precursor, Table 1. This may be rationalised by taking into consideration that in $Cr(acac)_3$ there are fifteen carbon atoms for every chromium atom, whereas in chromium(III) acetate ($Cr_3(OH)_2(CH_3COO)_7$) there are only 4.7 carbon atoms per chromium atom. The overall theoretical ratio is therefore 3.2, which makes the experimentally measured value of 3.6 seem reasonable. The water profile does not follow the behaviour seen for CO and CO_2. Instead a broad peak which is similar in appearance to that observed during oxygen plasma treatment of just the silica support material is obtained. This difference can be attributed to the water by-product of oxidative decomposition being initially adsorbed onto the silica support at the low temperatures involved in the plasma oxidation reaction, and then desorbing in a UV/VUV induced process.

It should be noted that the plasma oxidation procedure employed in the present study requires approximately 0.1% of the total energy input and takes ~1% of the time required for the corresponding thermal activation procedure investigated in chapter 2. Low temperature glow discharge treatment gives rise to a much faster rate of oxidation than the thermal activation procedure, as evidenced by the relative proportion of CO_2 loss, Table 2. This is consistent with an oxygen plasma being a more reactive medium compared to conventional thermal oxidation.

Activation Procedure	$(CO_2 / (CO + CO_2)) \times 100$	
	Cr(III) acetate/silica	**$Cr(acac)_3$ /silica**
Thermal	84.6%	84.3%
Plasma	93.8%	94.3%

Table 2: The relative proportion of CO_2 in the oxidized carbon species produced during plasma and thermal activation procedures (±2%).

The absence of any ethylene polymerization activity following plasma oxidation and CO reduction of the dry blended chromium(III) acetylacetonate/silica precursor system indicates that no migration of the

chromium species onto the silica support occurs, as previously observed during conventional thermal treatments[9] described in chapter 2.

6.5 Conclusions

The plasma oxidation of silica supported chromium(III) catalyst precursors results in the instantaneous breakdown of the organic ligands into CO, CO_2 and H_2O. The immediate adsorption of water onto the support surface is implied by the peak shapes. Subsequent UV/VUV radiation from within the electrical discharge leads to the gradual desorption of water from the silica surface. Non-equilibrium glow discharge oxidation proceeds at near-ambient temperatures in a matter of just a few minutes, and is a factor of approximately 1000 times more efficient in terms of energy consumption than the conventional thermal procedure. Chromium(III) acetate aqueously impregnated onto silica gives rise to an active ethylene polymerization catalyst, whereas a physical mixture of chromium(III) acetylacetonate with silica does not. This difference can be attributed to the lack of dispersion of the oxidized chromium species across the silica support surface during low temperature plasma oxidation of the latter.

6.6 References

1. McDaniel, M.P. *Adv. Catal.* **1985**, *33*, 47
2. Dadashova, E.A.; Yagodovskaya, T.V.; Beilin, L.A.; Shpiro, E.S.; Lunin, V.V. *Kinetics and Catalysis* **1991**, *32*, 1350
3. Bell, A.T. in *Techniques and Applications of Plasma Chemistry*; Eds. Hollahan, J.R. and Bell, A.T.; Wiley: New York, 1974
4. Dadashova, E.A.; Yagodovskaya, T.V.; Shpiro, E.S.; Beilin, L.A.; Lunin, V.V.; Kiselev, V.V. *Kinetics and Catalysis* **1993**, *34*, 670
5. Nogier, J.P.; Bonardet, J.L.; Fraissard, J.P. *Studies in Surface Science and Catalysis* **1983**, *17*, 233

6. Tiep, V.L.; Thoang, H.S.; Bureau-Tardy, M.; Djega-Mariadassou, G.; Che, M. *Tap Chi Hoa Hoc* **1985**, *23*, 1
7. Blecha, J.; Dudáš, J.; Lodes, A.; Derco, J. *J. Catal.* **1989**, *116*, 285
8. Horvath, B. U.S. Pat. 3,485,771 (filed Dec. 1966, issued Dec. 1969)
9. Ruddick, V.J.; Dyer, P.W.; Bell, G.; Gibson, V.C.G.; Badyal, J.P.S. *J. Phys. Chem.* **1996**, *100*, 11062
10. Yasuda, H.; *Plasma Polymerization;* Academic: London, 1985, p304
11. Barteau, M.A., Bowker, M., Madix, R.J. *Surf. Sci.* **1980**, *94*, 303.
12. Ko, E.I., Benziger, J.B., Madix, R.J. *J. Catal.* **1980**, *62*, 264.
13. Koenig, J.L.; *Chemical Microstructure of Polymer Chains;* Wiley: New York, 1980. p199
14. Guiton, T.A.; Pantano, C.G. *Colloids and Surfaces A: Physicochemical and Engineering Aspects* **1993**, *74*, 33
15. Friedel, P.; Gourier, S. *J. Phys. Chem. Solids* **1983**, *44*, 353
16. Ichikawa, Y.; Wu, R.L.C.; Kaneda, T. *J. Appl. Phys.* **1990**, *67*, 108
17. Shibata, M.; Nakano, N.; Makabe, T. *J. Appl. Phys.* **1995**, *77*, 6181
18. Debauche, C.; Licoppe, C.; Flicstein, J.; Dulac, O.; Devine, R.A.B. *Appl. Phys. Lett.* **1992**, *61*, 306
19. Fominski, V.Y.; Markeev, A.M.; Naumenko, O.I.; Nevolin, V.N.; Alyokhin, A.P.; Vyukov, L.A. *Appl. Surf. Sci.* **1994**, *78*, 437
20. Van de Leest, R.E. *Appl. Surf. Sci.* **1995**, *86*, 278
21. Parada, E.G.; González, P.; Serra, J.; León, B.; Pérez-Amor, M.; Flicstein, J.; Devine, R.A.B. *Appl. Surf. Sci.* **1995**, *86*, 294

CHAPTER 7. CONCLUSIONS

This thesis has investigated the activity of two different chromium(III) Phillips catalyst precursors, both of which are used commercially. The two precursors are prepared via different routes by Crosfield Limited. The first comprises a high surface area silica support which has been aqueously impregnated with basic chromium(III) acetate ($Cr_3(OH)_2(CH_3COO)_7$) and then dried to produce a free-flowing, pale blue catalyst precursor. The second is prepared by physically mixing the same silica support material with chromium(III) acetylacetonate, and is maroon in appearance. Both of these precursors contain a 1 wt% chromium loading.

In order to produce an active Phillips catalyst, it is necessary to heat a catalyst precursor under dry air or oxygen to 673-1073 K in a process known as calcination. The catalyst precursor comprising chromium(III) acetate supported on silica undergoes a single step reaction which occurs at the same temperature (~563 K) as the decomposition of bulk basic chromium(III) acetate. This result indicates that the impregnation of silica with chromium(III) acetate leaves chromium(III) acetate species dispersed across the silica surface. The oxidation of both bulk and supported chromium(III) acetate is believed to occur via attack of oxygen at the methyl group of the acetate ligand, followed by C-C and C-H bond scission to produce carbon dioxide, carbon monoxide and water as gaseous products. The chromium(III) acetylacetonate catalyst precursor reacts in a two step process when heated under an oxygen atmosphere. The first stage is observed close to the melting point of chromium(III) acetylacetonate (489 K). The chromium species become mobile and disperse across the catalyst support, whilst undergoing a cycloaddition reaction with molecular oxygen. This is followed by C-C and O-O bond cleavage to create acetate-like structures supported on the silica. These acetate moieties subsequently react by the same pathway as observed for the impregnated precursor. The catalysts produced during calcination of both precursors are active for the polymerization of ethylene.

Following calcination, Phillips catalysts exhibit an induction period prior to the onset of polymerization when exposed to ethylene. This induction period is

due to the reduction of the hexavalent chromium species by ethylene, and may be eliminated by pre-reduction of the catalyst using carbon monoxide. Both calcined precursors undergo CO reduction via a Langmuir-Hinshelwood type mechanism, involving the reaction of adsorbed CO molecules with surface oxygen atoms. Arrhenius plots for the formation of CO_2 exhibit two linear portions, which correspond to the reduction of different Cr(VI) centres to a variety of Cr(II) species. Complete reduction is observed to occur at temperatures greater than 573 K, with an activation energy of ~44 kJ mol^{-1}, regardless of the precursor used.

Exposure of the CO-reduced catalysts to ethylene leads to the formation of polyethylene, with the transient evolution of 1-hexene during the early stages of reaction. 1-hexene production is believed to proceed via the formation of a chromacyclopentane intermediate species, which may also act as a precursor for species involved during the propagation stage of the polymerization.

During ethylene polymerization, the catalyst support material must fragment in order to sustain monomer access to the active sites located within the pores. Phase imaging atomic force microscopy shows the fragmentation of the catalyst to be a continuous, non-uniform process. Pores may be seen to crack open, forming trough-like features, from which polymer may flow onto the surface.

Treatment of both catalyst precursors in a non-equilibrium oxygen plasma leads to immediate oxidation of the organic ligands to create gaseous carbon dioxide, carbon monoxide and water. The water is adsorbed onto the silica support, and is subsequently lost in a UV/VUV induced condensation process. The oxidation reaction takes place within a few minutes, and requires approximately one thousandth of the energy necessary for the conventional calcination procedure, however, an active polymerization catalyst is only obtained from the precursor prepared by aqueous impregnation of chromium(III) acetate on silica. This difference from the thermal procedure is attributed to the inability of a low-temperature plasma to disperse the chromium species across the support surface during treatment of the physically mixed chromium(III) acetylacetonate/silica precursor.

APPENDIX

University of Durham - Board of Studies in Chemistry
Colloquia, Lectures and Seminars from Invited Speakers

1993

October 4th — Prof. F.J. Feher, University of California
Bridging the Gap Between Surfaces and Solution with Sessilquioxanes

October 27th — Dr. R.A.L. Jones, Cavendish Laboratory
Perambulating Polymers

November 10th — Prof. M.N.R. Ashfold, University of Bristol
High Resolution Photofragment Translational Spectroscopy: A New Way to Watch Photodissociation

November 17th — Dr. A. Parker, Rutherford Appleton Laboratory
Applications of Time Resolved Resonance Raman Spectroscopy to Chemical and Biochemical Problems

1994

January 26th — Prof. J. Evans, University of Southampton
Shining Light on Catalysts

February 2nd — Dr. A. Masters, University of Manchester
Modelling Water Without Using Pair Potentials

February 16th Prof. K.H. Theobald, University of Delaware
Paramagnetic Chromium Alkyls: Synthesis and Reactivity

February 23rd Prof. P.M. Maitlis, University of Sheffield
Across the Border: From Homogeneous to Heterogeneous Catalysis

October 19th Prof. N. Bartlett, University of California
Some Aspects of Ag(II) and Ag(III) Chemistry

November 23rd Dr. J.M. Williams, University of Loughborough
New Approaches to Asymmetric Catalysis

December 7th Prof. D. Briggs, ICI and University of Durham
Surface Mass Spectrometry

1995

January 18th Dr. G. Rumbles, Imperial College
Real or Imaginary Third Order Non-Linear Optical Materials

March 1st Dr. M. Rosseinsky, Oxford University
Fullerene Intercalation Chemistry

April 26th Dr. M. Schroder, University of Edinburgh
Redox-active Macrocyclic Complexes: Rings, Stacks and Liquid Crystals

May 3rd Prof. E.W. Randall, Queen Mary and Westfield College
New Perspectives in NMR Imaging

October 11th Prof. P. Lugar, University of Berlin
Low Temperature Crystallography

November 17th Prof. D. Bergbreiter, Texas A&M
Design of Smart Catalysts, Substrates and Surfaces from Simple Polymers

November 22nd Prof. I. Soutar, Lancaster University
A Water of Glass? Luminescence Studies of Water Soluble Polymers

November 29th Prof. D. Tuck, University of Windsor
New Indium Coordination Chemistry

1996

January 10th Dr. B. Henderson, Waikato University
Electrospray Mass Spectrometry-A New Sporting Technique

January 17th Prof. J.W. Emsley, Southampton University
Liquid Crystals: More Than Meets the Eye

January 31st Dr. J. Penfold, Rutherford Appleton Laboratory
Soft Soap and Surfaces

March 6th Dr. R. Whitby, University of Southampton
New Approaches to Chiral Catalysts: Induction of Planar and Metal Centred Asymmetry

March 12th Prof. V. Balzani, University of Bologna
Supramolecular Photochemistry

Conference Attended

June 30th - July 5th 1996 — 11th International Congress on Catalysis, Baltimore, USA

Examined Lecture Courses

General Laboratory Techniques (Dr. Hampshire)

Spectroscopies (Dr. Halliday)

Electron Microscopy (Dr. Durose)

Synthetic Methodology in Organometallic and Coordination Chemistry (Prof. Gibson and Prof. Parker)